



Republic of Iraq  
Ministry of Higher Education and  
Scientific Research  
University of Misan/College of  
Engineering  
Department of Electrical Engineering



# **Droop Control in Microgrid for Enhanced Efficiency and Stability**

Prepared By

**Ruqaya Majeed Kareem**

B.Sc. electrical engineering, 2021

A thesis submitted in Partial Fulfillment of the Requirements for  
the Master of Science degree in Electrical Engineering

The University of Misan

2025

Thesis Supervisor: **Assist. Prof. Dr. Mohammed Kh. Al-Nussairi**

2025 A.D.

1446 A.H

بِسْمِ اللَّهِ الرَّحْمَنِ الرَّحِيمِ

﴿فَرِحِينَ بِمَا آتَاهُمُ اللَّهُ مِنْ فَضْلِهِ وَيَسْتَبْشِرُونَ بِالَّذِينَ

لَمْ يَلْحَقُوا بِهِمْ مِنْ خَلْفِهِمْ أَلَّا خَوْفٌ عَلَيْهِمْ وَلَا هُمْ

يَحْزَنُونَ﴾

Rejoicing in what Allah has bestowed upon them of His bounty  
and they receive good tidings about those [to be martyred]  
after them who have not yet joined them – that there will be  
no fear concerning them nor will they grieve

صدق الله العلي العظيم

آل عمران ﴿170﴾

## ABSTRACT

A microgrid (MG) is a small power system with one or most distributed generating (DG) units. Frequency and voltage control are stages of network-independent operation. It is a difficult problem and important to provide reliability and stability. Thus, the operating control problem is one main issue for the microgrid that must be addressed during operation. However, load variations and switching processes in the microgrid between islanded mode and grid connection cause the frequency and voltages to deviate from their nominal values and lead to disturbances in microgrids and dynamic behavior, which calls for developing an optimal control method. Among these methods, droop control is a common method because of the lack of critical communication links among parallel linked inverters to regulate the DG units inside a microgrid. Unfortunately, this strategy isn't accurate in keeping the system frequency and voltage near their nominal values. As a result, the parameter values must be carefully selected utilizing the optimization techniques. This work aims to improve the droop controller based on optimized PI controller parameters to control the frequency and voltage of microgrids under various conditions by using three efficient metaheuristic optimization algorithms, Slime Mould Algorithm (SMA), Sine Cosine Algorithm (SCA), and Sparrow Search Algorithm (SSA). Finally, to evaluate the effectiveness of the suggested control strategies, the study's results are compared with those of conventional droop control methods. The simulation results demonstrated the significant superiority of the proposed methods, including the SMA, in frequency stability, voltage response, load-sharing balance, overshoot reduction, and improvement in settling time and rise time. Moreover, it proved its ability to reduce oscillations and enhance response accuracy based on error metrics such as integral time absolute error (ITAE), integral time square error (ITSE), integral absolute error (IAE), and integral square error (ISE). The SMA method demonstrated its superiority in all

tested and simulated cases, showing a faster rise time to reach stability (0.3956s), the lowest overshoot (0.2247%), and a settling time of (0.497060s) when switching between operating modes in the microgrid.

## **STATEMENT OF AUTHORSHIP**

This thesis was completed as part of the MSc. (**Electrical Engineering**) at **the College of Engineering -University of Misan**. It is my own unaided work. Where the work of others has been used or drawn on, it has been fully attributed to the relevant source.

Signature:

Name: Ruqaya Majeed Kareem

Date:    /    /2025

## **SUPERVISOR CERTIFICATION**

I certify that the preparation of this thesis entitled "**Droop Control in Microgrid for Enhanced Efficiency and Stability**" was presented by "**Ruqaya Majeed Kareem,**" and has been prepared and written under my supervision at The University of Misan / College of Engineering as a partial fulfillment of the requirements of the degree of the Master of Science in Electrical Engineering.

Signature:

Supervisor: **Assist Prof. Dr. Mohammed Kh. Al-Nussairi**

Date: / / 2025

In view of the available recommendations, I forward this thesis for discussion by the examining committee.

Signature:

Name: **Assist Prof. Dr. Mohammed Kh. Al-Nussairi**

Head of Electrical Engineering Department

Date: / / 2025

## CERTIFICATION OF THE EXAMINING COMMITTEE

We certify that we, the examining committee, have read the thesis titled **(Droop Control in Microgrids for Enhanced Efficiency and Stability)** which is being submitted by **Ruqaya Majeed Kareem**, and examined the student in its content and what is concerned with it, and that in our opinion, it meets the standard of a thesis for the degree of Master of Science in Electrical Engineering.

Signature:

Name: **Assist. Prof. Dr. Mohammed Kh**

**AL-Nussairi**

(Supervisor)

Date: / /2025

Signature:

Name: **Assist. Prof. Dr. Sadeq D.**

**AL-Majidi**

(Member)

Date: / /2025

Signature:

Name: **Assist. Prof. Dr. Osama Yaseen  
Khudair Al-Atbee**

(Member)

Date: / /2025

Signature:

Name: **Assist. Prof. Dr. Jabbar  
Raheem Rashed**

(Chairman)

Date: / /2025

Approval of the College of Engineering

Signature:

Name: **Prof. Dr. Abbas Oda Dawood**

Dean of the College of Engineering

Date: / /2025

## DEDICATION

To my God, Allah Almighty, my creator, my strong pillar, my source of inspiration, wisdom, knowledge, and understanding.

To the Prophet of God “Mohammed” and his pure immediate family. I would be honored to dedicate this dissertation to “Al-Imam Al-Mahdi” (May God Almighty hasten his honorable return).

To the one whose presence is sufficient to light my way even if it is in the darkest darkness, to the one who surrounds me with safety at all times, to the one who strengthens my resolve if it is shaken at any moment, to the one who was my shadow and my source of pride...my father.

To the good heart, whom God placed heaven under her feet, to the lady of my heart, to the light of my eyes and the light of my path, to whom her prayers and words were the companions of excellence...my mother.

To my brothers and sisters, who have been a constant source of support and encouragement.

To my friends, who believe in me even when I feel frustrated and disappointed, and to their support and kindness. To everyone who taught me a word... and to everyone who supported me.

I dedicate this thesis to all of them, hoping to God Almighty that it will be a window of knowledge, a source of knowledge, and a benefit to us all.

Finally, to myself... I dedicate as a reward for her hard work, appreciation of her effort, and love for her. Every effort I made was out of love for me and my family.

## ACKNOWLEDGEMENTS

First, I praise and am deeply grateful to Allah for the enormous graces he bestowed upon me to achieve this thesis.

I extend my thanks to the Dean of the College of Engineering and the head of the Department of Electrical Engineering. I would like to express my deep gratitude, thanks, appreciation, and respect to my supervisor, “**Asst. Prof. Dr. Mohammed Khalaf Juma**” for all the guidance, support, and instruction he provided me during this study.

I would like to extend my full thanks and appreciation to my family for their unlimited support and all their efforts on my behalf. Without them, I would not have arrived here.

I would like to express my deepest gratitude and appreciation for my big brother, “**Mustafa**” who has surrounded me with his support and love throughout my time studying for my master's degree. He never hesitated to give me all he could of his time and effort, leaving his interests aside to be my helper and supporter.

I would also like to thank everyone who helped and supported me, even with just one word, and all who helped me somehow. Special thanks go to “**Asst. Prof. Dr. Hasanain A. H. Al-Behadili**” and “**Asst. Prof. Dr Ameer Latif Saleh.**” I will never forget the help of “**Eng. Dalal Kareem Attwan**” and “**Eng. Murtada Majeed Kareem**” for helping me with this thesis.

## **DEDICATION TO THE ESTEEMED EXAMINATION COMMITTEE**

I express my sincere gratitude and deep appreciation to "**Assist. Prof. Dr Jabbar Raheem Rashed,**" the esteemed examination committee chair, for his invaluable efforts and insightful guidance, which have significantly contributed to elevating this research to higher academic standards. I also extend my heartfelt thanks to the examination committee members, "**Assist. Prof. Dr. Sadeq D. AL-Majidi**" and "**Assist. Prof. Dr. Osama Yaseen Khudair Al-Atbee**", for their valuable feedback that has enriched and enhanced this work academically.

I pray for your continued success and prosperity in your academic journey and your service to knowledge and scholarship.

The researcher

# TABLE OF CONTENTS

ABSTRACT .....	IV
STATEMENT OF AUTHORSHIP .....	VI
SUPERVISOR CERTIFICATION .....	VII
CERTIFICATION OF THE EXAMINING COMMITTEE .....	VIII
DEDICATION .....	IX
ACKNOWLEDGEMENTS .....	X
Dedication To the esteemed examination committee .....	XI
TABLE OF CONTENTS .....	XII
LIST OF TABLES .....	XV
LIST OF FIGURES .....	XVI
LIST OF abbreviations .....	XVIII
LIST OF SYMBOLS .....	XX
LIST OF PUBLICATIONS .....	XXIII
CHAPTER One:.....	2
Introduction .....	2
1.1 Background .....	2
1.2 Description of Microgrids .....	3
1.2.1 Structure of microgrids .....	3
1.2.1.1 Distributed generators .....	3
1.2.1.2 Energy storage systems .....	6
1.2.1.3 Loads .....	7
1.2.1.4 Control units .....	7
1.2.1.5 Point of coming coupling .....	7
1.2.2 Classification of microgrids.....	8
1.2.2.1 Classification of microgrids according to power supply .....	8
1.2.2.2 Classification of microgrids according to location .....	11
1.3 Control of Microgrids .....	12
1.3.1 Centralized control.....	13
1.3.2 Decentralized control strategies for efficient operations and management .....	13
1.3.3 Master-Slave control.....	14
1.4 Enhancing Performance in Microgrids .....	15
1.5 Enhancing Stability in Microgrids .....	16
1.6 Literature Review .....	17
1.6.1 Adaptive droop control methods.....	17
1.6.2 Virtual impedance droop control .....	20
1.6.3 Artificial intalligent.....	21

1.6.4	Artificial intelligence by using algorithm optimization .....	25
1.6.5	Different methods of droop control .....	28
1.7	Motivation .....	53
1.8	Significance of Research .....	55
1.9	Problem Statement.....	55
1.10	Aim and Objective of the Thesis.....	56
1.11	The Thesis Structure .....	57
CHAPTER Two:	.....	59
Microgrid Modeling	.....	59
2.1	Power Electronic Converter .....	59
2.2	Microgrid Modeling With The Proposed Control.....	59
2.3.1	Power control used to optimize droop control.....	63
2.2.1.1	Voltage and frequency control.....	64
2.2.1.2	Current control .....	64
2.2.2	Inverter .....	64
2.2.3	LC filter.....	65
2.2.4	dq Frame .....	66
2.3	Power Sharing .....	67
2.4	Fitness Function .....	67
CHAPTER Three:	.....	70
Droop Control Based on Optimization Techniques	.....	70
3.1	Concept of Droop Control .....	70
3.1.1	Classification of droop control technique.....	71
3.1.2	Advantages and disadvantages of droop control .....	85
3.2	Proportional-integral .....	86
3.3	Concept of Optimization.....	87
3.3.1	Classification of optimization algorithm .....	88
3.3.1.1	Metaheuristic optimization algorithms .....	89
3.3.1.2	Swarm intelligent .....	90
3.4	Optimization Techniques .....	91
3.4.1	Slime Mould Algorithm.....	91
3.4.1.1	Mathematical model of SMA .....	91
3.4.2	Sine Cosine Algorithm.....	96
3.4.2.1	Advantages and disadvantages of SCA .....	96
3.4.2.2	Mathematical model of SCA .....	97
3.4.3	Sparrow Search Algorithm .....	103
3.4.3.1	Mathematical model SSA .....	103
Summary	.....	109
CHAPTER Four:	.....	111
Results & Discussion	.....	111
4.1	Case Studies and Proposed Test System.....	111
4.1.1	Results of change in microgrid operation mode.....	111
4.1.1.1	Analysis of voltage and frequency regulation .....	111

4.1.1.2	Analysis of active power and reactive power .....	115
4.1.2	Results of islanded microgrid operation mode .....	118
4.1.2.1	Analysis of voltage and frequency regulation .....	118
4.1.2.2	Analysis of active power and reactive power .....	122
4.2.3	Results of load change (equal load) .....	124
4.2.3.1	Analysis of voltage and frequency regulation .....	124
4.2.3.2	Analysis of active power and reactive power .....	128
4.2.4	Results of load change (increase load) .....	132
4.2.4.1	Analysis of voltage and frequency regulation .....	132
4.2.4.2	Analysis of active power and reactive power .....	136
	Summary .....	141
	CHAPTER Five: .....	143
	Conclusion & Recommendations .....	143
5.1.	Conclusion .....	143
5.2.	Recommendations .....	145
	Reference .....	146
	Appendix .....	154

## LIST OF TABLES

Table 1-1 The Summary of The Previous Studies.....	36
Table 2-1 Details Parameters Microgrids. ....	63
Table 3-1 Comparison between SMA, SCA, and SSA. ....	109
Table 4-1 PI control parameters.....	111
Table 4-2 Optimization of objective functions in different modes. ....	118
Table 4.3 Optimization of objective functions in different modes for error percentage .....	140
Table 4-4 Evaluation of Control Methods for Frequency and Voltage Stability in Microgrids.....	141

## LIST OF FIGURES

Figure 1-1 Description of Microgrids.....	3
Figure 1-2 Classification of DG Unit Operations in a Microgrid; .....	5
Figure 1-3 Control Strategies of DG Unit Operations in a Microgrid.....	6
Figure 1-4 Components of a Microgrid. ....	8
Figure 1-5 AC Microgrid Structure .....	9
Figure 1-6 DC Microgrid Structure .....	10
Figure 1-7 Hybrid Microgrid Structure .....	11
Figure 1-8 Block Structure for Master/Slave Control .....	15
Figure 2-1 Structure of Microgrid.....	61
Figure 2-2 Structure internal of microgrid (Proposed controller) .....	62
Figure 2-3 LC Filter Scheme .....	65
Figure 3-1 Details for Droop Control with Voltage Formation.....	71
Figure 3-2 DG connected to the grid (AC Bus).....	72
Figure 3-3 Conventional droop characteristics .....	73
Figure 3-4 Conventional droop control. ....	74
Figure 3-5 Reverse droop control curve. ....	76
Figure 3-6 Virtual Droop Control. ....	78
Figure 3-7 Robust Droop Control. ....	80
Figure 3-8 DG connected by VSC to a microgrid. ....	84
Figure 3-9 PI Control Structure Diagram .....	87
Figure 3-10 Optimization Algorithms Classification. ....	89
Figure 3-11 Flowchart Slime Mould Algorithm.....	95
Figure 3-12 The Effect Function of The Sine Cosine.....	99
Figure 3-13 Flowchart Sine Cosine Algorithm.....	102
Figure 3-14 Flowchart Sparrow Search Algorithm .....	108
Figure 4-1 System Frequency Response During Change MG Operation Mode. .....	113
Figure 4-2 System Voltage Response During Change MG Operation Mode. .	115
Figure 4-3 Analysis of Active Power and Reactive Power During Change MG Operation Mode. ....	117
Figure 4-4 System Frequency Response During Islanded MG Operation Mode. ....	120
Figure 4-5 System Voltage Response During Islanded MG Operation Mode.	121
Figure 4-6 Analysis of Active Power and Reactive Power During Islanded MG Operation Mode. ....	124
Figure 4-7 System Frequency Response during equal loads. ....	126
Figure 4-8 System Voltage Response During Equal Loads. ....	127
Figure 4-9 Analysis Active Power and Reactive Power During equal loads ....	131
Figure 4-10 System Frequency Response During Increased Loads. ....	134

Figure 4-11 System Voltage Response During Increase Loads. .... 136  
Figure 4-12 Analysis Active Power and Reactive Power During Increase loads  
..... 140

## LIST OF ABBREVIATIONS

Abbreviation	Full From
ANN	Artificial neural network
AI	Artificial Intelligence
AO	Aquila optimizer
BB-BC	Big Bang-Big Crunch
BELBIC	Brain Emotional Learning-Based Intelligent Controller
BESS	Battery Energy Storage Systems
BOA	Butterfly Optimization Algorithm
BTB	Back-to-Back Converter
CC	Conventional Control
CDC	Conventional Droop Control
C/DC	Centralized/Decentralized Control
CFNN	Cascade -Forward Neural Networks
CL	Communication link
CSI	Current source inverter
DCIMG	DC Islanded Microgrid
DG	Distributed Generation
DERs	Distributed Energy Resources
DR	Demand Response
DRL	Deep Reinforcement Learning
ESS	Energy Storage System
EVs	Electric Vehicle
FC	Fuel Cell
FF	Fitness Function
FIS	Fuzzy Inference System
FLC	Fuzzy Logic Control
FNN	Fuzzy-Neural Network
GDC	Generalized Droop control
GOA	Grasshopper Optimization Algorithm
GA	Genetic Algorithm
HBB-BC	Hybrid Big Bang-Big Crunch
HMG	Hybrid Microgrid
IAE	Integral Absolute Error
IMG	Islanded Microgrid
ISE	Integral Square Error
ITSE	Integral Time Squared Error
ITAE	Integral Time Absolute Error
LFC	Load Frequency Control
MBO	Monarch Butterfly Optimization
MGs	Microgrids

MMG	Multiple Microgrids
MOHBB-BC	Multi-Objective Hybrid Big Bang-Bing Crunch
OF	Objective Function
PCC	Point of Common Coupling
PID	Proportional-Integral-Derivative
PI	Proportional-Integral
PSO	Particle Swarm Optimization
PV	Photovoltaic
PVG	Photovoltaic Generation
RES	Renewable Energy source
SCA	Sine Cosine Algorithm
SCMBO	Sine Cosine-Based Monarch Butterfly Optimization
SI	Swarm Intelligent
SMA	Slime Mold Algorithm
SM	Sliding Mode
SOC	State-of-Charge
SSA	Sparrow Search Algorithm
SSA	Salp Swarm Algorithm
SSIA	Salp Swarm Inspired Algorithm
SS	Static Switch
SVPWM	Space Vector Pulse Width Modulation
THD	Total Harmonic Distortion
VCS	Voltage-Control Source
VSG	Virtual Synchronous Generator
VSI	Voltage Source Inverter
WOA	Whale Optimization Algorithm

## LIST OF SYMBOLS

Symbol	Definition	Unit
$A^+$	Represents a $1 \times d$ matrix with every element selected at random 1	-
$\alpha$	Is a random number $\in (0,1]$	-
arctanh(.)	The inverse hyperbolic function	
$bf$	The optimum fitness obtained during the current iterative process	-
$\beta$	The random number that follows the conventional normal distribution	-
$D_i$	The coefficient of the droop	-
DF	This shows the fitness value of the optimum solution obtained in the current iteration.	-
E	The inverter's output voltage amplitude	Volt
$E_{rated}$	The nominal voltage and phase angle of DG	-
f	The reference frequency	HZ
$f_n$	The frequency characteristics' constant coefficients	HZ
$\Delta f$	variations of the inverter's frequency	HZ
$Fx$	Indicates the individual's fitness value	-
$f_i$	Is the current sparrow individual's fitness value	-
$f_g$	Is the best fitness value for the present area	-
$f_w$	Is the worst fitness value for the present area	-
$Fx$	Indicates the individual's fitness value	-
$I_0$	The rated the value of the current	Amp
$I_a, I_b, I_c$	Are the per-phase currents	Amp
$I_{od}$	The output current on the d reference frame	Amp
$I_{oq}$	The output current on the q reference frame	Amp
iter <sub>max</sub>	Represents the maximum number of iterations	-
K	Is a random number $\in [-1,1]$	-
$K_e$	The amplifier	-
$K_p$	proportional gain	-
$K_i$	integral gain	-
$k_i$	The coefficient of the adaptive virtual impedance	-
L	The inductance	
L	Represents a $1 \times d$ matrix with all elements equal to 1	-
L <sub>b</sub>	The lower search range	-
m	The droop coefficient of the frequency	-
$m_{Qi}, m_{pi}$	The coefficients of the droop	-

MAX <sub>t</sub>	The maximum iteration number	
n	The droop coefficients of the voltage	
$n_{qi}$	The reactive droop coefficient	-
P	The active power before the filter	Watt
$P_i^t$	Represents the destination point's location in the $i_{th}$ dimension	-
Q	Is a random number that follows a normal distribution	-
Q	The reactive power before the filter	
$Q_i$	The reactive power output	-
$r_i$	The feeding resistance	-
r	The random number in [0,1]	-
R <sub>2</sub>	Is the warning threshold [0,1]	-
S	The operator of the Laplace transform	Volt
$S(i)$	The fitness value of $\vec{X}(t)$	-
ST	Is the safety threshold $\in[0.5,1]$	HZ
Smell-Index	A sorted series of fitness functions (ascending from the lowest value problem)	-
t	The current iteration number	-
T	Represents the maximum number of iterations	-
tanh(.)	The tangent function is hyperbolic	-
U <sub>b</sub>	The upper of the seek range	-
V	The voltage amplitude for the common AC bus	Volt
$V_n$	The voltage characteristics' constant	Volt
$V_0^*$	The rated value of the voltage	Volt
$\Delta V_s$	variations of the inverter's voltage	Volt
$v_{od}$	The output voltage on the d reference frame	Volt
$v_{oq}$	The output voltage on the q reference frame	Volt
$vc$	The parameter that minimizes a linear from 1 to 0	-
$vb$	Is the parameter with a range between [-a, a]	-
$\omega_c$	The cutoff frequency of the high-pass filter	rad
$\omega_c$	The frequency of the filter cutoff	rad
$\vec{W}$	The weight of a slime mould	-
$x_i$	The reactance	ohm
$\vec{X}(t)$	Slime bacteria's position vector at iteration time t	-
$\vec{X}_B(t)$	The individual's position vector has the highest focus.	-
$\vec{X}_a(t)$ & $\vec{X}_b(t)$	It describes two individuals randomly selected based on the slime mould	-
$X_{i,j}^t$	Indicates the sparrow's position and that of the $i_{th}$ sparrow in the $j_{th}$ dimension	-
x	Indicates the iteration time	-

$X_{\text{worst}}^t$	Shows the worst location of the t-generation sparrow populations	
$X_P^{t+1}$	Represent the optimal position held by the producer	
$X_{\text{best}}^t$	Represents the optimum position of the sparrow population	
$y$	Indicates the range of value fluctuation for the finder's position	
$Z$	The line impedance	ohm
$Z_v$	The virtual impedance	ohm
$z$	The variable that allows values between [0,0.1]	
$\varphi$	The phase angle differential between the PCC and Inverter output voltage	-
$\theta$	The line impedance phase angle	-
$\delta_{\text{rated}}$	The phase angle of DG	-
$\varphi$	Is a lower number that prevents the denominator from becoming zero	-

## LIST OF PUBLICATIONS

- [1] M. Ruqaya, M. K. Al-nussairi, and R. Bayindir, “Optimal Operation of Droop Control in Microgrids Using Different Techniques Optimization : Review,” vol. 3, no. 2, pp. 48–95, 2024.
- [2] M. Ruqaya, M. K. Al-nussairi, “Droop Control Optimization Based on Gray Wolf Optimizer for AC-Microgrid”

# CHAPTER ONE: INTRODUCTION

---

---

**CHAPTER One:****Introduction****1.1 Background**

A microgrid is a small-scale distribution network that is low voltage consisting of various DG units whether it is renewable (wind turbines, microturbines, fuel cells, photovoltaic, etc.), conventional (gas microturbines, biomass boilers, etc.), or a combination of the two, and electrical loads that are either connected to the utility grid at the PCC or separated. Interconnecting power systems is essential for maintaining an efficient power flow supply and improving the system's reliability. Renewable energy has become a significant source of power systems, replacing conventional sources[1][2]. DG has increased dramatically in recent decades, and the demand for electrical energy has risen as it has become a profitable supplementary service in our lifestyle[3]. DG units provide the following advantages over conventional centralized power generation: higher energy efficiency, less pollution, lower power transmission losses, and a more flexible installation site[4]. The microgrid can operate in grid-connected, islanded, and transition modes. During islanded mode, it is essential to maintain the frequency and voltage within the nominal range, which is the primary concern in a microgrid application; in the grid-connected mode, a controller's primary function is to manage energy. The microgrid connects to the utility grid via a bus bar called the PCC. In this mode of operation, the utility grid provides stability to the microgrid. The controller maintains voltage and frequency stability in islanded mode while fulfilling local energy demands. The microgrid regulates this stability via the instrumentation of the electronic converters that connect the parallel generators[5]. Different approaches have been proposed to achieve this, and among them, the most commonly applied and

simple control method is droop control. It allows multiple sources to generate at different frequency values and maintain the voltage magnitude. However, the droop-controlled system will alter the load sharing due to operating frequency variations. It is intended to analyze the effects of droop-controlled microgrids for different parameters and operating conditions[6].

## 1.2 Description of Microgrids

This section provides a general description of microgrids in terms of structure, classification, and control. Figure (1-1) illustrates the description of microgrids.

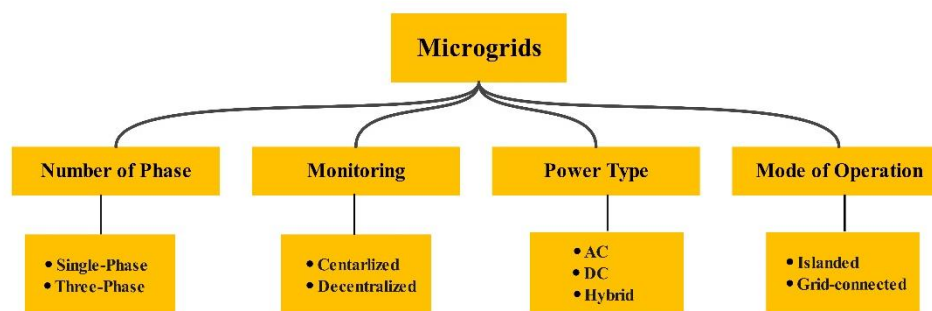


Figure 1-1 Description of Microgrids[7].

### 1.2.1 Structure of microgrids

In general, the elements that constitute a microgrid are defined as follows[8]:

#### 1.2.1.1 Distributed generators

Electrical microgrids are an excellent choice for integrating various DG forms since they take advantage of the available resources in each area (wind, sun, biomass, etc.). DGs can operate in two methods: as power sources or current, in compliance with power regulations, or as voltage sources that determine the frequency and voltage of the microgrid. Current sources classify the main techniques into nonlinear and linear controllers. When power converters act as

---

---

voltage sources, their regulation usually depends on a voltage loop cascaded with an inner power loop.

### ❖ **Distributed generator operation**

Inverter-based microgrids can operate as an autonomous system in island mode. However, the inverters are divided into three control categories as follows[9]:

- 1. Grid-feeding units:** Grid-feeding units in the DG in this class are designed to regulate current/power output that has synchronization frequency with the primary AC bus, creating an ideal current source see Figure (1-2a). It doesn't contribute to the MG's power balance. This control technique is commonly employed for wind and PV integration applications, particularly in grid-connected mode. The voltage output control isn't an aim because it is constantly controlled by another grid or forming unit.
- 2. Grid-forming units:** DGs in this class are designed for stand-alone operation and represent a perfect AC voltage source with constant output frequency, as seen in Figure (1-2b). It consists of a closed-loop controller to ensure effective disturbance rejection and steady-state values. Grid-forming units balance load demands and generation power in microgrids operating in island mode, regulating system frequency and voltage. In grid-connected units, the grid-forming units become grid-feeding units due to the presence of voltage and frequency references. Control mechanisms for grid-forming units should be compatible with both microgrid operation modes to ensure smooth transitions during the MGs mode changes.
- 3. Grid-supporting units:** These have a controlled voltage source (DG) that can manage and share power in both microgrid operating modes by adjusting its output voltage and frequency. Figure (1-2C) illustrate an output impedance with a voltage source, where the frequency and voltage

are contingent upon the necessary reactive and active output power are no longer constant. This category can also function as a current or voltage source depending on the control system. It combines the grid-feeding and grid-forming unit features for smooth operation switching and transfer.

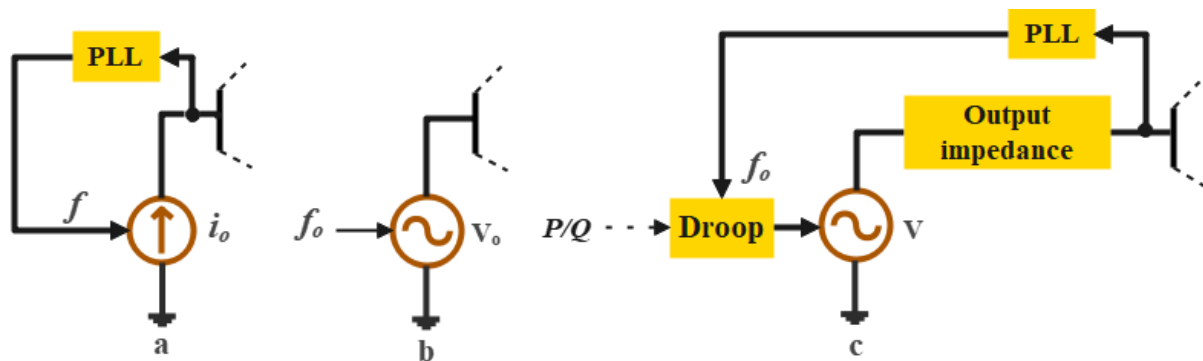


**Figure 1-2 Classification of DG Unit Operations in a Microgrid;**  
**(a) Grid - feeding; (b) Grid - forming; (c) Grid - supporting units[9].**

Figure (1-3) shows several control methods developed to enhance power quality, voltage/current tracking, and disturbance rejection of the inverter output.

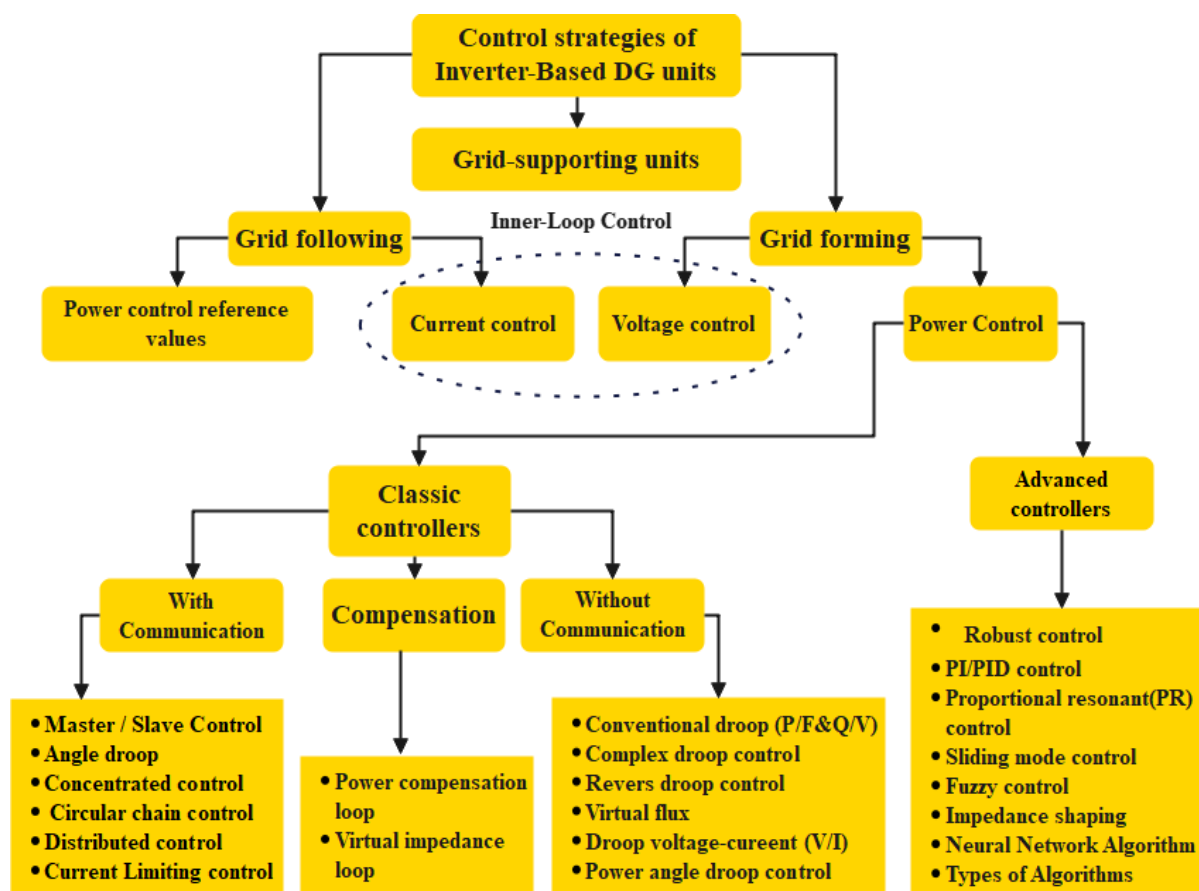


Figure 1-3 Control Strategies of DG Unit Operations in a Microgrid.

### 1.2.1.2 Energy storage systems

Energy storage systems increase power quality and stability. Furthermore, they improve the general performance of microgrids in three methods: DGs can operate at the stable and constant output or optimally follow the control reference notwithstanding load variations; they give ride-through ability when there is dynamic variability in primary energy; and they allow DGs to run smoothly as dispatchable units. If the MG exclusively employs RESs, ESSs will need to exist. Storage can reduce generation costs and ensure energy exchange with the

---

---

electrical grid. ESSs can also be beneficial in cushioning the effect on the system as it transitions from islanded to grid-connected mode[10].

### **1.2.1.3 Loads**

Microgrids can provide electrical power to various loads (industrial, residential, etc.). These loads are categorized as critical/sensitive or noncritical to achieve the intended operation. This operation includes improved power quality for specific loads, priority service to critical loads, and increased reliability for predefined load classifications. Local generation with quick and precise protection measures can keep disturbances from impacting sensitive loads[11].

### **1.2.1.4 Control units**

Control units are composed of control converters operating island-based or connected to the grid. In grid-connected mode, phase and grid frequency computation are crucial. The grid current is regulated in both modes by controlling the fast inner-current loop. The DC link voltage is managed by outer-voltage loop control, which is slower than the inner-current control loop. The main objective of current and voltage loop controller design is to maintain system stability under dynamic conditions[11].

### **1.2.1.5 Point of coming coupling**

Microgrids incorporate distributed energy resources as a grid that may connect to or disconnect from the main grid at the PCC[11].

### **1.2.1.6 Protection elements**

Protection schemes are important issues in microgrids. In general, a protection system consists of protection devices, protective relays, measurement equipment, and grounding.

Figure (1-4) represents the components of microgrids.

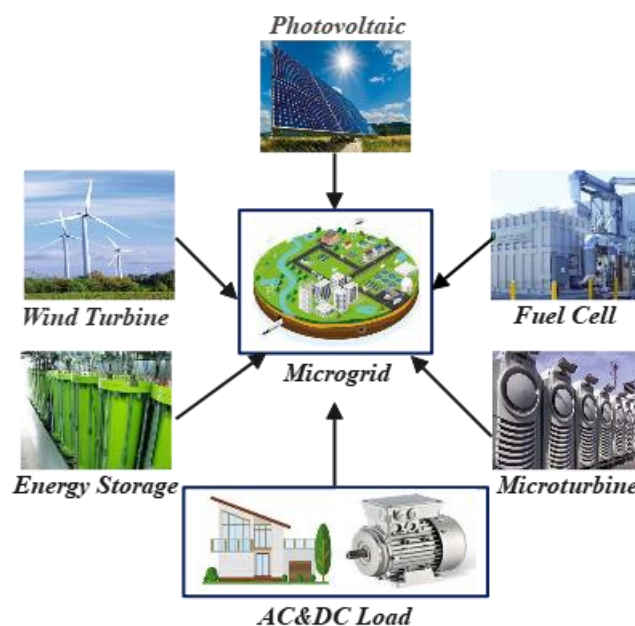


Figure 1-4 Components of a Microgrid[12].

## 1.2.2 Classification of microgrids

This section describes the types of Microgrids, which are classified into several types based on the distribution system type and location. Below is an explanation of each type.

### 1.2.2.1 Classification of microgrids according to power supply

1. **AC microgrids:** AC distribution systems are a famously utilized structure for MG implementations. The constructed AC structure, including protective devices, transformers, and distribution systems, is popularly used in the AC MG, and the AC MG is a more reliable system due to its ease of deployment[11]. Moreover, most loads in the distribution networks are of AC-based power, making it more sensible to adopt AC microgrids as bases for innovative grid expansion. Despite the many benefits of the AC system compared to the DC system, the inherent problem of frequency synchronization for separate DG units and imprecise reactive power sharing made planning and managing AC microgrids

difficult. The impact of poor reactive power sharing may be evident in higher thermal losses in distribution networks, while frequency regulation problems necessitate the employment of more AC/DC converter equipment. Conversion systems will complicate microgrid control and protection due to increased unwanted voltage, current harmonics, and nonlinear loads. Furthermore, the control and protection activities become more challenging during islanded operations because too few disturbances can generate significant stability problems in the islanded MG[1].

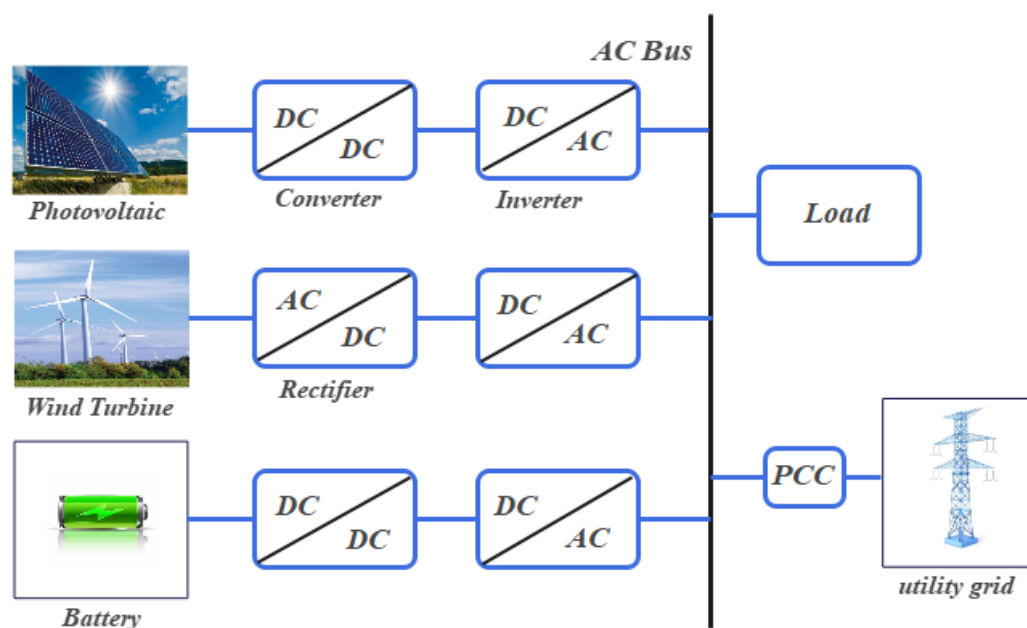


**Figure 1-5 AC Microgrid Structure**

2. **DC microgrids:** DC microgrids are a collection of DC-based generation units, including fuel cells and photovoltaic (PV) linked to a shared DC bus that serves DC loads. In this system, DG units connect to the shared voltage-regulated DC bus by AC/DC rectifiers or DC/DC converters aided by power electronics. The DC MG uses a converter interface to convert existing AC power from wind power into DC. However, it might also be coupled to the primary AC grid via DC/AC inverters. The key advantage of this kind of microgrid is increased energy storage efficiency and reduced conversion losses due to fewer AC/DC/AC conversions. Furthermore, the simplicity or removal of frequency synchronization

concerns is another advantage[1]. DCMGs provide several benefits, including increased efficiency and simplicity of integration and optimization of DERs[10].

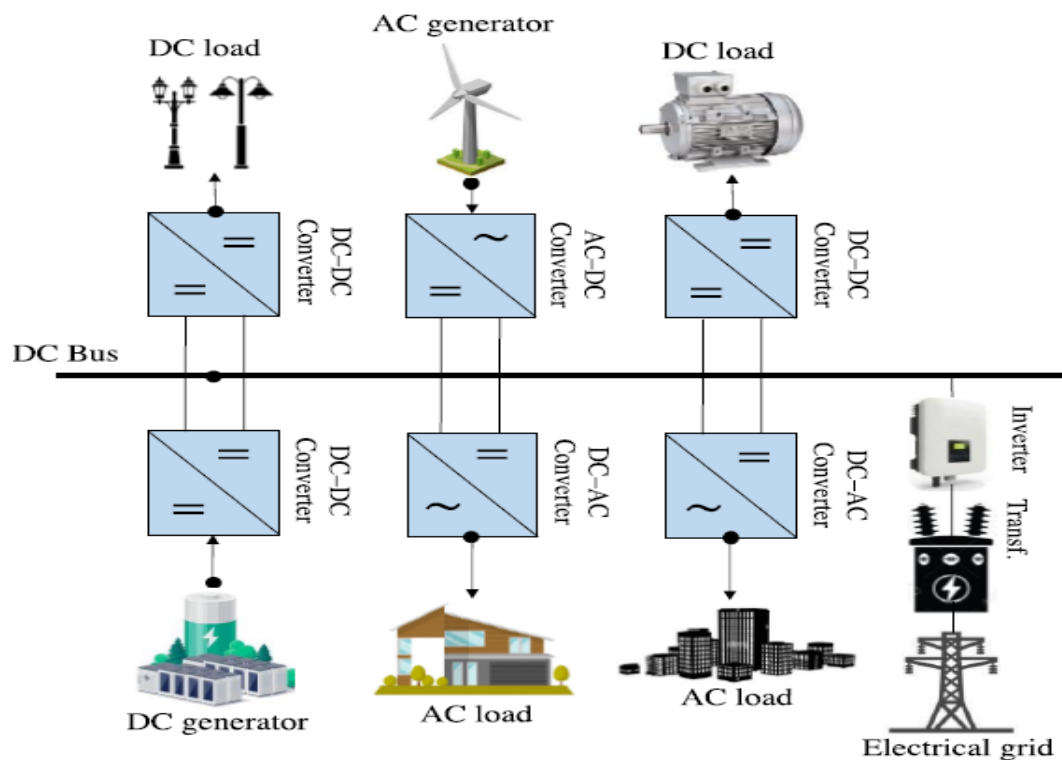


Figure 1-6 DC Microgrid Structure[10]

**3. Hybrid microgrids (AC/DC):** This construction combines the benefits of the two types of AC and DC microgrids, allowing for using both AC and DC loads in a single microgrid[1]. This hybrid MG enables sensible loads on the DC bus while more robust loads are installed on the AC bus. The hybrid MG's key issues include controlling bus voltages and complicated power management. Furthermore, the hybrid MG is divided into two groups:

- ❖ Coupled AC configuration.
- ❖ Decoupled AC configuration.

The AC bus connects directly to the utility grid in a coupled AC structure. Nevertheless, if additional AC-DC or DC-AC converters are employed to connect the utility grid, this type of coupling is referred to as a decoupled AC

structure[11]. The main benefits of this design are improved voltage transformation. Despite a hybrid AC/DC configuration for microgrids that improves conversion efficiency and energy storage, the rising complexity in design, protection, and stability of AC/DC networks act as the key impediments to the continued spread of this type of microgrids[1]. The key benefits of an HMG are as follows[13].

Integration of new generating or consuming points, Additional ESS, and PVs can be connected directly to the DC bus without synchronization, voltage transformation is greatly minimized, and reduced converters and losses are for economic feasibility.

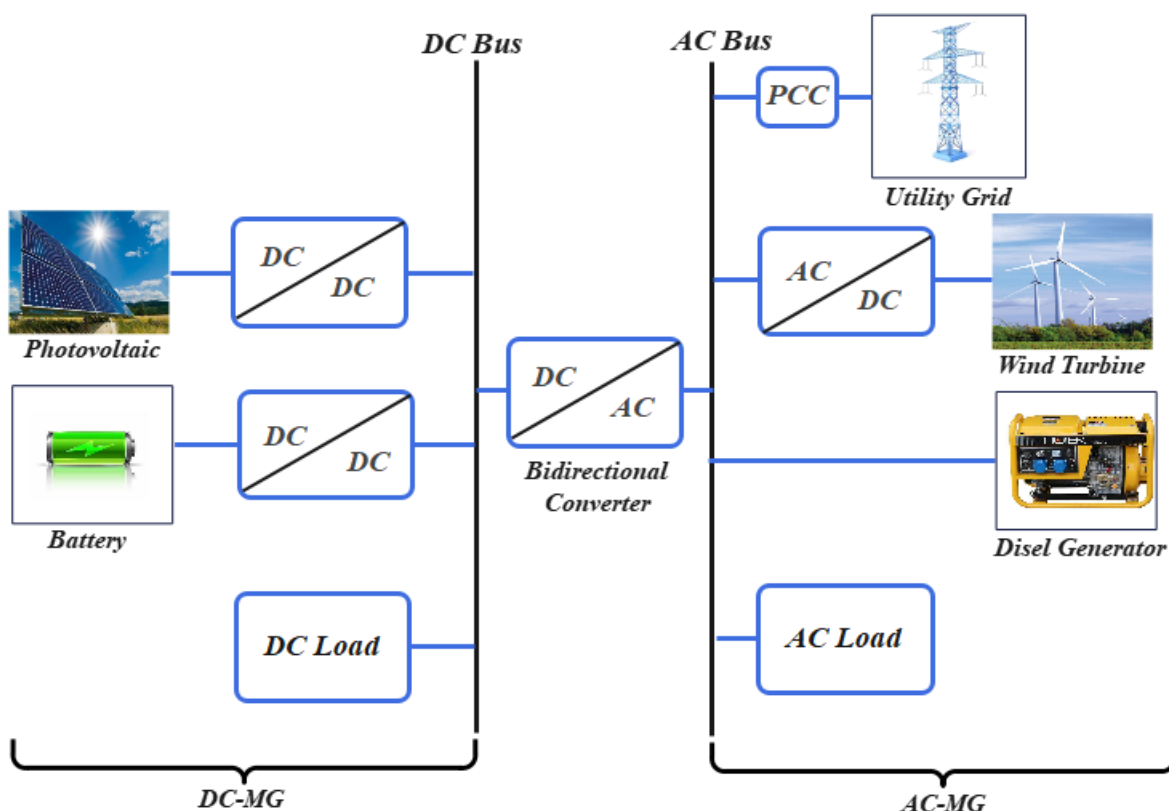


Figure 1-7 Hybrid Microgrid Structure

### 1.2.2.2 Classification of microgrids according to location

- 1. Urban microgrids:** These are typically linked to a utility grid and can exchange power with the grid across PCC. These microgrids, also called grid-connected microgrids, can operate as islanded microgrids in

---

---

uncommon circumstances such as poor power quality, failures on the primary grid, and grid maintenance. To keep the grid's power quality and the microgrids' validity for the grid's stability, these microgrids adhere to all laws and regulations, including extensive control strategies. These kinds of microgrids can be established in commercial and residential settings, including shopping centers, hospitals, data centers, communities, and campuses of universities[14].

- 2. Remote microgrids:** These are established in remote locations, such as military bases, islands, and hilly regions where the utility grid cannot reach due to topographical constraints. urban microgrids, these microgrids, also called islanded MGs, aren't linked to the grid supply. For political, economic, and technological reasons and a lack of investment, they are less prevalent than urban microgrids, with remote and island settlements being their ideal settings[14].

### 1.3 Control of Microgrids

Microgrids provide significant benefits, including enhanced power quality and reliability for sensitive loads and increased utilization of different energy resources, such as renewable energy. Furthermore, because of their proximity to energy end consumers, microgrids are expected to benefit customers and service providers significantly. To improve control performance, DGs are typically connected to microgrids via power inverters[15]. Many control methods have been widely used worldwide to operate parallel-connected inverters for load sharing in DG grids, including:

- ❖ Centralized / Decentralized.
- ❖ Master-slave control.
- ❖ Average current-sharing control.
- ❖ Current power-sharing technique.
- ❖ Peer-to-peer control.

In this thesis, only the centralized, decentralized, master-slave methods have been illustrated, as they are considered the most common approaches. Additionally, the droop control method is classified as a centralized control approach.

### **1.3.1 Centralized control**

The distinction between centralized and decentralized control is essential for further understanding this topic. A conventional power grid is considered a centralized control system, where the balance between generation and demand is managed by several large-scale generation units whose information is gathered and processed in control centers that supervise the distribution of active and reactive power via transmission and distribution networks. On the other hand, a microgrid is considered a decentralized control system: generation and consumption units, storage devices, and other controllable components must coordinate the exchange of active and reactive power among them locally, respecting their operational limits[16]. The fundamental elements forming the system to be controlled must be previously defined. These elements usually comprise a power system that includes generation, consumption, storage, and other devices that can participate in the active/reactive power exchange. The control objectives must also be defined during the formulation of a control scheme[17].

### **1.3.2 Decentralized control strategies for efficient operations and management**

Decentralized control strategies provide as an alternative to centralized control strategies. In their most general form, they allow each generator unit in the microgrid to determine its output power without considering the power output of other units. Droop control is a widely used and better-known decentralized

---

---

control strategy that can be implemented through primary control. There are different vertical arrangements for droop control. Still, the widely spread one combines P-f and Q-V droop control, where the active power frequency and the reactive power voltage droop control methods are used for distributed generator units. Recent developments have enabled the implementation of droop control for several inverter-connected distributed generator unit types[16]. Such systems can achieve stable operation in a grid-forming configuration, even if losses and/or unknown disturbances are acting on the system[17].

### 1.3.3 Master-Slave control

Each inverter includes a parallel control unit function based on the master/slave control scheme. The first module, in parallel, acts as the master inverter, responsible for parallel control, while the rest serve as slave inverters via a mode-selecting switch or software option. Figure (1-8) illustrates the "master/slave" control mechanism. The master module controls the output voltage and defines the current reference for the other slave modules. Slave units use the master's current reference to ensure equitable distribution. However, the system isn't redundant because it has a single point of collapse. If the master unit fails, or loss of a malfunction or the communication link in the master block might cause the entire system to fail. Thus, this system must include some redundancy to avoid or lessen the likelihood of failure. In summary, master/slave control can provide good power-sharing performance while being simple to implement. If the master inverter collapses, the enhanced control strategy switches to another standard inverter that serves as the new master. Thus, parallel operation would be unaffected. However, one clear difficulty with each master-slave control technique is that the current of high-output overshoot can happen during transients because the master current output isn't controlled, resulting in poor transient performance[18].

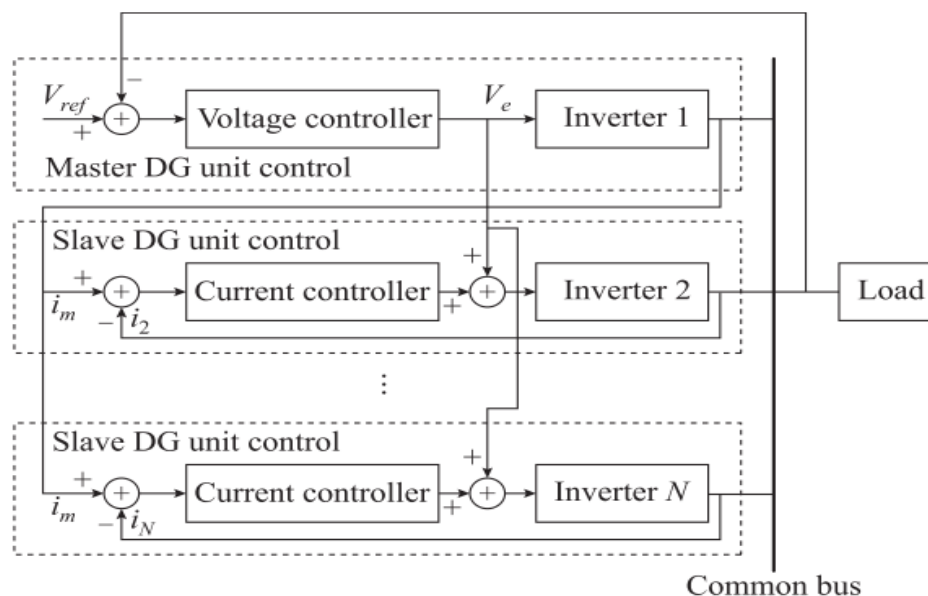


Figure 1-8 Block Structure for Master/Slave Control[18]

## 1.4 Enhancing Performance in Microgrids

In many distribution or transmission system designs, secondary control is required to improve microgrids' efficiency. Among the numerous routines or power flow optimization algorithms proposed for microgrids, a simple control technique applied in the generation interfacing with the grid shall also be considered, as it impacts overall system stability. It is not solely based on dynamics or transient responses. Still, it can also directly impact steady-state power-sharing discrepancies due to the power export from sources on the load incongruity between multiple generators in the microgrid. Here, a control technique, namely droop control, used in voltage source inverters for the islanded operation of the microgrid is taken up for study[19]. The average properties of droop-based generations, like the combined frequency and voltage control or load speed control inertia, shall be considered electrical inertia enhancement in a microgrid islanded from a utility grid. The droop control technique also helps mitigate power-sharing discrepancies and load incongruity, promoting a smoother, more reliable microgrid operation. Incorporating droop control into

---

---

microgrid designs enables seamless integration of renewable energy sources, facilitating the transition towards a cleaner and sustainable energy future. With its versatile capabilities and significant impact on microgrid stability, droop control represents a crucial aspect of secondary control in modern power systems and microgrid implementations. It plays a pivotal role in ensuring microgrids' overall efficiency and reliability, paving the way for a more sustainable and resilient energy infrastructure [20].

## **1.5 Enhancing Stability in Microgrids**

Microgrids represent small-scale power systems composed of DER with localized loads that can operate independently from the grid. DG growth has mainly increased interest in microgrids. However, the intermittent nature of renewable energy resources poses challenges to microgrid stability and control [21]. Power system stability is defined as the ability of a power system to regain a state of equilibrium after being subjected to a disturbance. Increasing renewable energy resources in a microgrid can lead to potential issues related to stability, such as a decrease in the system of damping. Microgrid stability can be classified as small-signal stability or transient stability. Microgrid frequency and voltage control are similar to the control method used in conventional grids, with frequency and voltage as two significant control variables. In a microgrid, controllable DGs are operated to maintain the adequacy of active and reactive power balance while operating within their generation limits. However, droop-based control methods of synchronous machines may also find limitations in microgrids with high levels of inverter-based resources. Stability is classified as a 'small signal' if the disturbances are small. The power system is subjected to constant small disturbances on occasion. Power systems with tightly interconnected connections and many interconnected machines can exhibit small-time electromechanical oscillations. These oscillations may persist for a long time and become significant because the system cannot dampen them. This makes

---

---

small signal stability of the power system deteriorate, leading to an uncontrollable system. Voltage stability deals primarily with the ability of a power system to maintain steady voltages at all buses in the system after being subjected to a disturbance, which can also be classified into short-term and long-term voltage stability. Droop control used in voltage regulation of DG units may inadvertently increase the system's operating range, making them more prone to voltage instability[20].

## 1.6 Literature Review

Concerns about environmental pollution, global climate change, and dramatic growth in energy consumption have prompted energy suppliers to look for a faster and more cost-effective way to expand the capacity of electricity delivered to loads. These loads must be power-sharing equally, so the droop control strategy is used for this purpose.

This section presents works related to this research. The literature review includes an introduction of the key topics and a review of related works. These studies were divided into five groups based on different methods. The first group studied research that used adaptive droop control methods. The second group studied research that dealt with the technique of adding virtual impedance. The third group reviewed research based on artificial intelligence, such as (neural networks, fuzzy systems, and deep reinforcement). The fourth group was based on a group of algorithms. The fifth group included a group of different methods. Finally, a summary of these methods' advantages and drawbacks was presented, as shown in Table (1-1).

### 1.6.1 Adaptive droop control methods

**The researchers in [22]** investigate the difficulty of stability analysis for droop-controlled, inverter-based microgrids with meshed topology. Following that, a use port Hamiltonian description is developed for local stability for a

---

---

lossless microgrid, from which suitable stability criteria are supplied for general loss microgrids. This method, the conventional voltage droop control, does not guarantee proportional reactive power-sharing.

**The paper**[23] has introduced a novel approach to addressing uncertainties stemming from the intermittent nature of distributed generating resources and regulating the frequencies and voltage of the controller based on a multi-agent-based distributed adaptive controller specifically designed for microgrids. To assess the proposed distributed adaptive controllers' performance, the suggested control's effectiveness is compared with a controller's faster convergence content than the DG units without adaptive control.

**In reference** [24] has proposed an adaptive droop control technique to enhance microgrid efficiency under different load profiles. The efficiency model is analyzed, and the Lagrange Multiplier Method is used to derive the optimal conditions. The strategy improves efficiency while retaining conventional advantages. The verification findings demonstrate that the suggested efficiency analysis model can find optimal points and examine the time-variant efficiency feature. Therefore, the proposed adaptive control technique can increase the microgrid's overall efficiency under various load profiles.

**The paper**[25] presented a novel adaptive droop control and unified power management strategy for inter-microgrid power sharing in a hybrid AC-DC MMG system, which dynamically adjusts the droop coefficients of the VSCs to ensure optimal utilization of available resources in each microgrid under different operating conditions. The results show that the adaptive droop control method allows for reduced power exchange within the microgrid and the need to import energy from the utility grid.

**In the study**[26] to compensate for power unbalance and support primary frequency in MGs, the authors proposed a novel hybrid energy storage system that

---

---

comprises an FC as the primary power source and a battery as a complementary power source based on adaptive droop control. The FC can compensate for fast power transients and effectively coordinates with the battery through a dynamic droop-based control strategy. This control strategy's objective is to prioritize power sharing between the FC and the battery in the hybrid energy storage system, ensuring effective support of the primary frequency in the MG. The method significantly reduces the number of cycles and the charging/discharging rate, thereby improving the battery's lifespan.

**M. Ghazzali, M. Haloua, and F. Giri in**[27] addresses the control and power distribution issue among distributed generators in AC-islanded microgrids by presenting an adaptive control. The proposed approach offers several advantages, including ensuring accurate power sharing and voltage and frequency regulation. The developed adaptive control law can be expressed in a simple mathematical form, making it easily implementable and requiring minimal computational performance compared to other adaptive controllers for microgrids, such as adaptive neural network-based controllers and adaptive fuzzy logic controllers. The results of the simulations demonstrated that the proposed adaptive controllers exhibit greater robustness to disturbances than the conventional hierarchical control.

**The paper**[28] has been presenting an adaptive novel droop control strategy that allows for the simultaneous regulation of frequency and voltage at the output of inverters in isolated microgrids. The approach is based on the conventional Droop control (P-f) and (Q-V) structure. This controller is simple, easily implementable, and applicable to various systems and voltage regulation devices. It can effectively mitigate the impact of significant disturbances, such as generation loss, and enhance system stability against small perturbations. The simulation results demonstrate the controller's efficacy, showcasing its ability to

---

---

respond to load variations swiftly, facilitate active power-sharing among the inverters, and ensure stable and secure microgrid operation.

### 1.6.2 Virtual impedance droop control

**This Study**[29] investigates an efficacious power-sharing method between paralleled inverters in microgrid applications. This study aims to determine the virtual impedance value to mitigate power-sharing errors. A fuzzy logic controller is proposed, relying on the instantaneous reactive power and active power demands. The fuzzy logic controller allows for accurate reactive power sharing and enhances dynamic performance.

**The paper**[30] has proposed a novel VSG control strategy incorporating improved governor control and coupling compensation. Experimental results confirm the efficacy of the proposed strategy, which increases the angular frequency inertia, minimizes the difference in governor control between the novel VSG control strategy and the diesel generator, and enhances the AC microgrid performance.

**As present in** [31] implementing a complex virtual impedance to address feeder mismatching, compensate for reactive power-sharing errors, achieve precise power-sharing among DG units, and reduce active power oscillations. Simulation results demonstrate that the proposed controller exhibits accurate power-sharing capabilities and surpasses conventional droop control in minimizing active power oscillations.

**The paper**[32] has been proposing a coordinated virtual impedance control technique for DGs. Within this strategy, both virtual resistance and virtual inductance are concurrently adjusted to compensate for the mismatched line impedance among DGs, thereby enhancing the stability of the microgrid system. Consequently, the transient condition exhibits a 50% reduction in active

---

---

power oscillation compared to conventional control methods, and the system's dynamic performance is enhanced with a reactive power-sharing error of less than 0.15%.

**This study**[33] proposes a centralized controller to enhance the stability margins of microgrids. Firstly, the apparent impedance of the MG is periodically determined. Subsequently, the matrix fitting method is utilized to compute the system eigenvalues according to the estimated apparent impedance. This controller employs a recursive modification of the coefficient of droop of DGs, ensuring that the system's eigenvalues remain within an acceptable range.

**The paper**[34] has proposed a novel C/DC control method that eliminates errors in case of a CL and when the Q-V droop curve cannot accurately share reactive power due to different bus voltages in the microgrids. To achieve this objective, we employ a centralized Adaptive virtual impedance control method for precise reactive power-sharing in normal situations.

### 1.6.3. Artificial intelligent

**The researcher**[35] proposes a control strategy based on the dynamic droop coefficient for transmission lines with different impedances by multi-objective optimization problem for droop control in microgrid inverters, considering bus voltage and reactive power distribution deviations. The optimization problem is solved using DRL. The strategy successfully meets load requirements and solves uneven reactive power distribution problems without voltage drop. The study is better than virtual impedance.

**In reference**[36] the purpose of this paper is to overcome disturbances in the electric grid, such as power imbalance and inertia in the grid's response. So, the researchers proposed an SM robust droop control scheme assisted by an ANN algorithm for an islanded PVG integrated microgrid. When the droop response's performance is compared to fixed-gain PID, the controller operates constantly,

---

---

resulting in minimal voltage and power errors in the steady state for photovoltaic generation (PVG).

**The paper**[37] has been introducing a method that combines neural networks with fuzzy control to detect the load power at the AC bus terminal and generates an adaptive power coefficient to adjust the amplitude voltage and address the reactive power distribution. Simulations and experimental results demonstrate that the adaptive compensation control strategy exhibits accurate power sharing, desirable dynamic characteristics, and robustness

**This study**[38] introduces a CFNN droop control approach. This method manages inverter-based microgrids operating in grid-connected and islanded modes to enable accurate tracking of reference power and demand under various operating instances for innovative grid applications. Thus, the system's voltage and frequency are maintained in islanded and grid-connected modes. The experimental results substantiate the effectiveness of the developed control technique in both operating modes.

**This paper**[39] presents an online droop-based demand response DR, known as GDC, based on An ANN employed for the online adjustment of droop coefficients. The results demonstrate a significant reduction in power-frequency fluctuations and the voltage variations and frequency deviations resulting from different faults staying within an acceptable range compared to CCs and (GDC-based only DR + CC) methods

**S. A. Shezan et al. in**[40] offer a comprehensive investigation into the control and optimization of a solar-wind-standalone hybrid microgrid using optimization algorithms and a fuzzy logic controller. The proposed approach was implemented in MATLAB Simulink alongside a comprehensive standalone hybrid microgrid system model. The simulation results demonstrate that the proposed FLC keeps

---

---

voltage and frequency within acceptable ranges during various operational conditions.

**The paper**[41] has been presented as a distributed intelligent secondary control approach for a power electronic-based AC microgrid using a BELBIC. The suggested controller can regulate frequency deviations and voltage amplitude, ensuring minimal steady-state variations with broader bandwidth and enabling precise power-sharing through the droop mechanism.

**M. Srikanth and Y. Venkata Pavan Kuma in**[42] a novel method is presented to enhance the microgrid's stability and transient response when faced with the connection/disconnection of high inductive loads called the (SMDCM). The proposed technique is characterized by its simplicity, speed, and robustness and is based on identifying an infeasible range of droop coefficients. The effectiveness of the proposed strategy is demonstrated by comparing it with the traditional constant droop coefficient and fuzzy logic-based droop control technique. Simulation results reveal. The simulation results reveal that this method outperforms other methods due to the SMDCM showcasing satisfactory frequency values of 50.02 Hz and 49.8 Hz under the same conditions, respectively.

#### **1.6.4 Artificial intelligence by using algorithm optimization**

**The researcher in**[43] proposes an optimal control strategy for regulating PV frequency and voltage according to MG systems operating in islanding mode. The methodology employs the GOA to optimize the PI controller parameters, thereby improving the power quality and dynamic response of the MG system. The simulation results verify that the GOA presents a faster and superior alternative to PSO and WOA, resulting in minimal voltage and frequency overshoot, lower output current, and THD.

**In reference** [20] introduces an optimized load-sharing approach based on a droop control strategy for parallel batteries operating in a DC microgrid and control algorithm SSA utilization to prevent non-matching conditions when including the actual battery capacity, which its lifecycle can influence. Consequently, power-sharing will be proportionate to the actual capacity. So, the lifecycle of the batteries will be extended, and power-sharing will be optimized. The simulation demonstrates the capability of the proposed control strategy to manage these situations effectively.

**This paper**[44] investigates how to effectively govern a DG inverter's output voltage to enhance microgrids' performance during island conditions and load fluctuations. The proposed method dynamically adjusts the parameters of the PI controller after a load change in a standalone microgrid by using the HBB-BC. This proposed method ensures a more stable microgrid in terms of voltage and frequency. The outcomes of the case study are that it is observed that the HBB-BC algorithm offers a superior solution compared to the PSO and BB-BC algorithms.

**The paper**[45] has proposed an algorithm called SCMBO to improve the performance of the energy management system by achieving an economically optimal schedule for the generation units and battery storage while ensuring the microgrid's stability. The proposed algorithm's effectiveness is verified by comparing its outcomes with MBO and PSO. The results demonstrate that the proposed method effectively minimizes fuel costs while maximizing the efficiency of the photovoltaic and wind turbine systems. This confirms that the proposed controller enhances system reliability and efficacy.

**This paper**[46] aims to bridge gaps such as mitigating emissions from power generation activities and the uncertainties associated with load and renewable generation forecasting by presenting a methodology for determining the optimal droop settings by employing fuzzified PSO. Its efficacy is assessed

using a 33-bus DCIMG test system, and the results obtained demonstrate its effectiveness.

**The reference**[47] introduces a novel iteration of the SSIA with the updating characteristics of the PSO for the optimization of the microgrid droop controller. To address the uncertainties associated with microgrid droop control, like inaccuracies in controller gains, degradation of system parameters, challenges in energy sharing among multiple sources, and system dynamics. Simulation results demonstrate the enhanced performance of the improved SSIA compared to the original SSIA and PSO.

**The authors**[48] introduces a novel methodology using FL-based fine-tuning and a BOA-based (PID) controller implemented for frequency secondary control to enhance the LFC islanded multi-source (MG). The simulation and the presented outcomes show improvement and enhancement of the MG's frequency stability while also addressing the issues of overshooting and undershooting to meet the load demand and ensure the system's resilience.

**The authors**[49] proposed a method for improving droop control in islanded microgrids with multiple DGs by employing an enhanced improved PSO. The method evaluates the microgrid structure and line parameters. It introduces a FIS, resulting in correct active and reactive power allocation while maintaining stability systems such as bus voltage and frequency, improving dynamic performance and transient stability.

**The paper**[50] has been presented the utilization of the AI Optimization, AO technique to enhance the efficiency of the droop control mechanism on a DC microgrid. The simulation results indicate that the AO-PI method performs better than the traditional and PSO-PI methods. It can mitigate the settling time by 0.028% and achieve better final power by 0.798%.

**The authors**[51] propose a method to improve the dynamic characteristics of an inverter-based microgrid by developing a precise small-signal state-space model that encompasses the droop controller, network, and loads by using a GA to optimize the operational characteristics of the microgrid.

### 1.6.5 Different methods of droop control

**The authors**[52] proposed a supplementary loop around a conventional droop control of each DG converter to solve the problem of the system's stability for range operation mode while ensuring satisfactory load distribution by using high gain angle droop gain. This ensures efficient load sharing in island microgrids through angle droop control.

**This paper**[53] examines the potential of two isolated microgrids to provide mutual support during connected emergencies; one microgrid utilizes conventional frequency droop control. On the other hand, the second microgrid solely relies on converter-interfaced DGs. A BTB converter facilitates the connection between these two microgrids. The back-to-back converter system enables bidirectional power transmission between the microgrids. However, if there is an overload in one of the microgrids, the other microgrid can provide power to assist, if feasible.

**The paper**[54] has presented a novel approach to self-adjusting nominal voltage-based modification in the  $Q-V$  to enhance reactive power distribution amongst distributed generation sources in an isolated microgrid. The proposed method integrates nominal voltage calculation with system frequency, improving voltage references for all distributed generators. Utilizing an adaptive nominal voltage instead of a fixed nominal voltage substantially improves reactive power sharing.

**The paper**[55] has proposed a droop control strategy for multi-objective optimization based on Lagrange multipliers, where three objective functions are

constructed to enhance system performance and stability in the IMG. These objective functions pertain to (i) accurate sharing of real power, (ii) sharing of reactive power, and (iii) regulation of load-bus voltage. The suggested technique can significantly enhance the voltage profile of the load bus while achieving accurate proportional power sharing.

**The paper**[56] has introduced a decentralized control method to achieve generation-storage coordination by utilizing DC bus voltage signaling. Initially, a novel droop control strategy based on SOC is developed for storage. This strategy supports the DC bus voltage and ensures a balanced SOC for storage. An adaptive power control technique is employed for PV generators, enabling seamless output power adjustment by the DC bus voltage. Integrating these two strategies across DC bus voltage signaling effectively achieves the coordination between generating and storage.

All the previous studies are summarized in Table (1-1).

Table 1-1 The Summary of The Previous Studies.

Research's	years	Method	Type of controller	Type of control area	Comparative study
Schiffer et al. [22]	2014	Adaptive droop control	Droop control	Inverter-based microgrids	---
Yuan et al. [24]	2019	Adaptive droop control-based Lagrange Multiplier Method.	Droop control	Autonomous Microgrid	Conventional droop control
Sinha, Ghosh, and Bajpai [25]	2021	Adaptive droop control	Droop control	Hybrid multiple microgrids	More than one microgrid (ACMG1, ACMG2) was compared in terms of PV, FC, VSC, and BB.
Marzebali, Mazidi, and Mohiti [26]	2020	Adaptive droop-based control technique based on hybrid energy storage	Droop control	Stand-alone microgrids	FC and battery
Ghazzali, Haloua, and Giri [27]	2020	Adaptive one-layer control	Droop control	AC islanded microgrids	Conventional secondary control
Alexandre and Belém [28]	2021	Conventional structure of the Droop control (P-f) and (Q-V)	Droop control	Isolated microgrids	---
Abdalfatah, E. El-kholy, and Awad [29]	2023	FLC and adaptive virtual impedance	Droop control	paralleled inverters in microgrid	The proposed method with virtual impedance is compared to the method without virtual impedance.
Peng et al. [30]	2019	VSG	VSG	AC microgrid	Experimental results validate the effectiveness of the proposed VSG control strategy.
Pham and Lee [32]	2021	Virtual impedance control technique	Virtual impedance	Islanded Microgrid	The feasibility and effectiveness of the proposed control strategy were validated by simulations and experiments with a 1.3-kVA prototype microgrid composed of three DGs.

Gothner et al. [33]	2021	centralized controller based on apparent impedance	Droop control	Microgrid	Simulation and experimental results for an MG based on DGs rated at 60 kVA are included to validate the proposed control scheme.
Lai et al. [35]	2023	Droop control technique-based (DRL)al-nussiri	Droop control	Microgrid	Droop control with virtual impedance
Kanwal et al. [36]	2023	ANN	Droop control, PID		SM control performance is compared with various PID
Alzayed et al[38]	2022	CFNN	Droop control-based CFNN	Inverter-Based Microgrid	Conventional droop control
Habibi, Shafiee, and Bevrani [39]	2019	ANN	Droop control	Islanded microgrids	CC, GDC-based DR+CC ANN-GDC
Shezan et al. [40]	2023		PID, FLC	Islanded hybrid microgrid systems	Simulation results show that by using PID and FLC and comparing them
Q. Q. Zhang and Wai [57]	2022	AFNN-DSC	Droop control	Islanded microgrid	The effectiveness of the proposed control method is verified by numerical simulations for real scenarios.
Yeganeh et al. [41]	2023	BELBIC	Droop control, PI	Islanded AC Microgrids	conventional PI controller, ANN-PI
Srikanth and Venkata Pavan Kumar [42]	2023	SMDCM, FLC	PI	Microgrids	The two proposed methods were compared with each other
Jumani et al. [43]	2018	GOA	PI		PSO, WOA
Sedighzadeh, Esmaili, and Eisapour-Moarref[44] and [58]	2017	HBB-BC	PI	Autonomous microgrids	PSO, BB-BC
Naik, Dash, and Bisoi [45]	2021	SCMBO	Droop control	Stand-alone microgrid	MBO and PSO

Maulik and Das [46]	2018	PSO	Droop control	Islanded DC Microgrids	Multi-objective GA
Ebrahim et al.[47]	2020	Hybrid SSIA - PSO	Droop control, PI	Microgrid	SSIA and PSO
Djema and Boudour [48]	2022	FLC, BOA	PID	Islanded Multi-Area AC Microgrid	Conventional method
Zhang et al. [49]	2020	Adaptive Droop Control with PSO	Droop control	Islanded Microgrid	Conventional method
Aribowo, Suryoatmojo, and Pamuji [50]	2022	AOA	Droop control, PI	DC Microgrid	Conventional method
Ferahtia et al. [20]	2022	SSA	Droop control	DC microgrid	---
Majumder et al.[52]	2010	supplementary loop around a conventional droop control	Droop control	Autonomous Microgrid	conventional droop control
Dheer, Gupta, and Doolla [54]	2020	modification in the Q-V	Droop control	Islanded Microgrid	simulation studies and experimental validation on a laboratory prototype
Arabpour and Hojabri [34]	2023	(C/DC) control without CL		AC microgrids	C/DC with CL
Arunima and Subudhi [23]	2023	Adaptive controller	Droop control	Microgrid	---
Dawoud, Megahed, and Kaddah [59]	2021	Modified droop control angle	Droop control	Multi-microgrid	Various simulation studies are executed and compared with the related works

## 1.7 Motivation

Droop control is one of microgrids' most widely used frequency and voltage regulation strategies. Its widespread adoption is due to its numerous advantages, such as easy implementation, simplicity in control design, and low control damping requirements. This control strategy is essential when a microgrid is connected to the distribution system, operating as droop control. The droops are carefully selected to ensure that the power developed by the generation sources closely resembles that of the distribution system's synchronous generators. When there is a reduction in voltage or a decrease in speed, the load on the microgrid increases. This increase is intended to share the generation sources between them, guaranteeing sufficient response and guiding the generators with nonrenewable sources to contribute more. In doing so, the available capacity for voltage regulation is increased. However, traditional droop control may present certain challenges that need to be addressed through extensive research. It is crucial to apply an appropriate amount of research to overcome these challenges effectively.

Simple droop control might not always deliver the desired enhanced efficiency and stability due to the potential existence of an inverted structural relationship between voltage and power. Therefore, seeking and controlling the system's stored energy becomes crucial in applying droop control. By optimizing trading and utilizing the principles of control, a prudent selection of energy combinations can be made, resulting in an economical approach. Consequently, microgrids can operate efficiently through comprehensive analysis and innovative mechanisms. Microgrids can benefit from advanced droop control techniques with careful analysis and implementation. These advanced strategies consider various factors, including power source characteristics, load demands, and system constraints. The aim is to ensure optimal performance and reliability while adapting to the varying conditions of power distribution. This can be

achieved by incorporating sophisticated algorithms and intelligent decision-making processes into the droop control system. Such advancements further enhance energy utilization efficiency, ultimately contributing to sustainable development. The exploration of new possibilities and solutions in droop control continues, with researchers and industry professionals pushing the boundaries of this technology. The ongoing advancements and innovations in droop control hold immense potential in shaping the future of microgrid technology.

These advancements facilitate the seamless integration of renewable energy sources into existing power systems, enabling the transition towards a greener and more sustainable future. The deployment of droop control in microgrids is crucial for achieving energy efficiency, grid stability, and environmental preservation, by investing in continuous research and development, the capabilities of droop control can be expanded even further. This continuous improvement empowers microgrids to play a pivotal role in the global energy transition, contributing significantly to a sustainable future. With each advancement, droop control strengthens its position as a crucial tool, driving the efficient operation of microgrids and supporting renewable energy integration. As the world embraces a greener future, droop control remains at the forefront of technological advancements, cementing its importance in pursuing a sustainable and environmentally conscious world.

The novelty of this thesis lies in the application of two swarm-based optimization algorithms, the SMA and the SSA, which have not been previously used for optimizing PI controller parameters in droop control for microgrids and reducing voltage and frequency variations during islanding and load changes. These methods were specifically chosen for their ability to handle complex, nonlinear optimization problems efficiently, provide strong exploratory capabilities to reach a wide range of potential solutions, refine the discovered solutions, and reduce the time required to achieve the optimal solution, While the

---

---

SCA has been used in similar applications, our study provides a comparative analysis of SMA, SSA, and SCA to demonstrate the strengths of each approach and their suitability for enhancing the stability and efficiency of droop control in microgrids.

This thesis presents an ideal droop controller designed to ensure that distributed generators (DGs) can operate in proper operation of parallel-connected inverters in microgrids. It includes a controller based on a set of swarm algorithms droop controllers, such as SMA, SCA, and SSA. The controller reduces voltage and frequency variations that arise during islanding or load changes connected to the microgrid using the PI controller.

## **1.8 Significance of Research**

The significance of this thesis is the use of a set of swarm algorithms droop controllers, such as slime mould algorithm, sine cosine algorithm, and sparrow search algorithm. In the end, all of these methods are compared with a previous method called conventional droop control, which significantly reduces the voltage and frequency variations that arise during islanding or load changes connected to the microgrid to optimize the parameters of the PI controller. Also presents an ideal droop controller designed to ensure that DGs can operate in the proper operation of parallel-connected inverters in microgrids. It includes a controller based on a set of swarm algorithms droop controllers, such as SMA, SCA, and SSA. The controller reduces voltage and frequency variations that arise during islanding or load changes connected to the microgrid using PI controller.

## **1.9 Problem Statement**

The scope of this study deals with droop control application using a proportional-integral controller, which is designed to decentralize the control of active and reactive power management from the central controller, distribute it to the inverters, and maintain frequency values and voltage magnitude to restore it

to its nominal value. The PI control parameters of the inverters in a microgrid are obtained using three metaheuristic algorithms. The simulation results are compared with conventional techniques and the effectiveness of the metaheuristic optimization algorithms. The control strategy is analyzed in various disturbances when switching between islanded mode and grid connected and increased load in the microgrid.

### **1.10 Aim and Objective of the Thesis**

This thesis aims to use the set of swarm algorithms to develop an optimization of droop controller for microgrid and PI controller parameters; the objectives of the study are as follows to achieve this purpose:

1. The primary aim of the present work is to study and implement a novel droop control technique to enhance overall stability and efficiency in islanded microgrids. The droop control mechanism considered an auxiliary control loop, has been developed to ensure the better dynamic performance of droop-controlled distributed generators, providing frequency and voltage control in weakly connected systems.
2. To improve the conventional droop control and implement a microgrid system with two parallel connected inverters.
3. Conventional droop control model development using a set of algorithms for the optimal possible estimate of the PI controller t.
4. Improve the droop controller to guarantee that variations during islanding and load changes are as low as possible.
5. Active Power sharing for loads and Distribution of loads on RES.
6. Regulation of the voltage and frequency of RES and Improve efficiency and stability.

## 1.11 The Thesis Structure

The thesis consists of five chapters, which are as follows:

- ❖ Chapter One: This chapter presents an overview of the study, including the background of MG, the significance of the research, the problem statement, and the thesis objectives. In addition, studies on droop control in microgrids are presented, including using different methods. Finally, a summary of the structure of each chapter of this thesis.
- ❖ Chapter Two: This chapter introduces a microgrid model. A MATLAB-SIMULINK was developed to optimize the droop control parameter.
- ❖ Chapter Three: This chapter presents details of droop control and the technologies used, specifically the (SMA, SCA, and SSA).
- ❖ Chapter Four: This chapter presents the simulation results, discussing each in detail and examining how each method performs under various scenarios. The comparison aims to validate the model's accuracy.
- ❖ Chapter Five: In conclusion, the most essential findings are presented. Furthermore, some key recommendations are given to extend and enhance the existing study, including potential routes for future research.

# CHAPTER TWO: MICROGRID MODELING

---

---

## CHAPTER Two:

### **Microgrid Modeling**

#### **2.1 Power Electronic Converter**

Power electronics, the field of the study and development of semiconductor equipment for the effective conversion of electrical energy using advanced control techniques. Power electronics have become more significant in the world's most diverse regions of technology requiring electricity. When these technologies are used in the mobility, industrial, and energy sectors, they increase productivity and improve service quality[60]. The power converters can play various roles When integrated into a microgrid, including grid feeding, grid following, and grid creating. Power electronics technology remains in its early stages. Still, it is finding its way into various applications, including EVs, renewable energy generation (such as solar and wind power), small appliances like laptop chargers, and biomedical equipment. Soon, electrical energy will be consumed and handled by power electronics; that increases the role of power electronics in power conversion operations and indicates that power systems are transitioning from central distribution to distributed generation. Over 1000 GW of renewable energy have been installed today, including wind and PV systems managed by power electronics technology. Moreover, regions like electrification of transportation and energy conservation are increasing, creating a large market for power devices and packaging and power converter design. Factors like cost, functionality, weight, volume, and reliability are some of the factors driving this technology[61].

#### **2.2 Microgrid Modeling With The Proposed Control**

This section discusses the microgrid system structure as shown in Figure (2-1) and Figure (2-2), which consists of two micro sources (DGs) and load

components coupled to the low voltage distribution network via the line and switch. The DGs were presumed to be DC sources, as renewable energy sources often produce outputs and loads, which are inverted by the three-phase AC (SVPWM) inverter. LC filter is utilized to reduce high-frequency components and high-order harmonic a while keeping the pure sinusoidal voltage waveform through the load, three-phase VSI, inverter connected to DGs to converter the AC to DC, static switch (SS) is used to Switch between grid-connected mode and islanded mode. The reactive and active powers produced through the DGs are estimated using the calculated current and voltage values. The four micro sources use PQ control to maintain a steady output power level when grid-connected. DG1 and DG2 employ V/f control during grid-connected and islanding operations to keep the system's steady voltage. PI controllers are generally used in droop-controlled DG applications.

This controller is easy to design and operate and is considerably reliable. Droop control is employed in the DG units to enhance a microgrid's load-sharing and frequency stability and generate the reference frequency and voltage signal. Finally, the switching system SVPWM creates gate trigger pulses and delivers them to the VSI to regulate the frequency and voltage of the system. The simulation model in MATLAB/Simulink is utilized for optimization. Table (2-1) provides details of the parameters used in the microgrid system studied in this thesis.

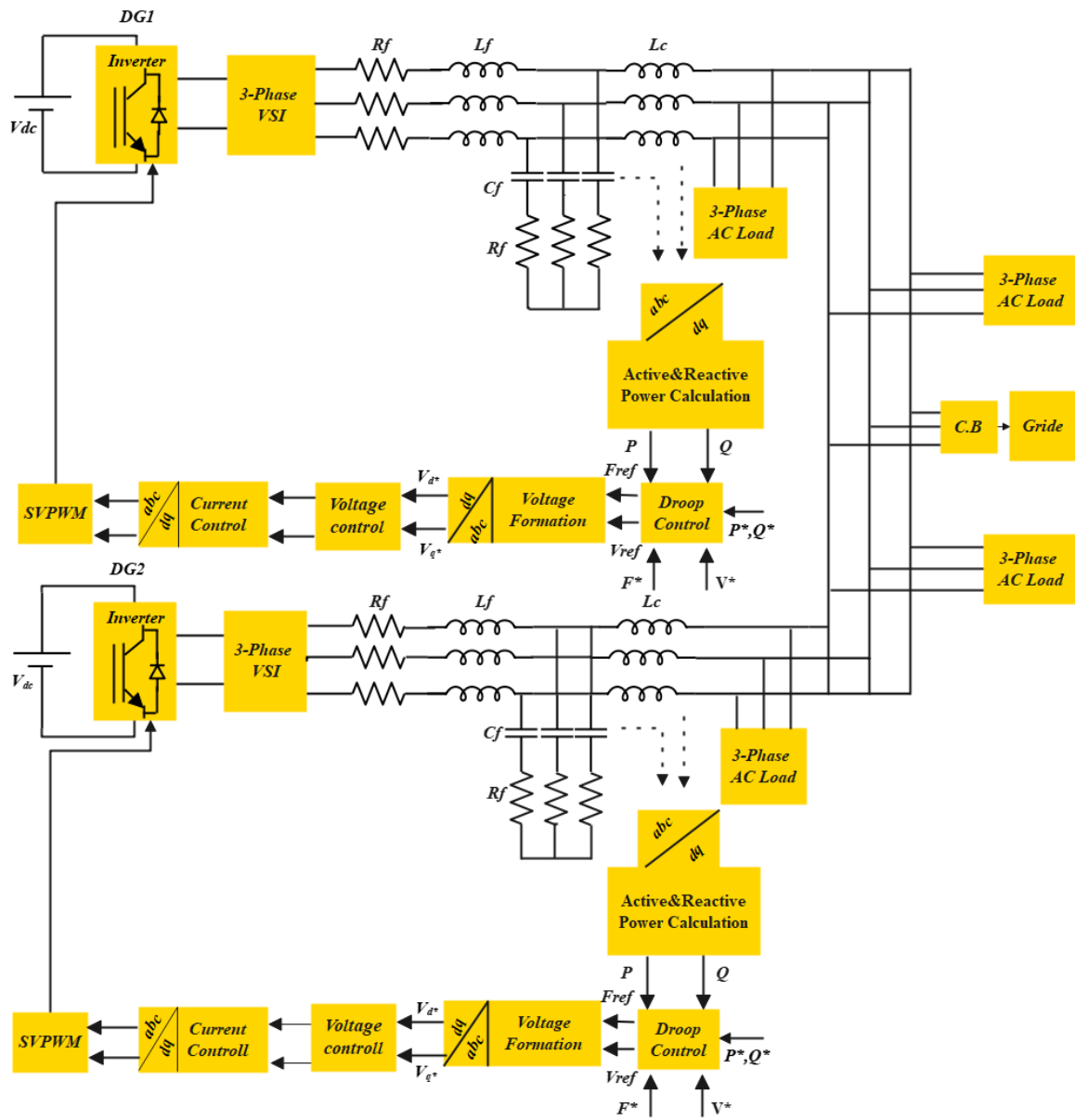


Figure 2-1 Structure of Microgrid

Figure (2-1) illustrates the studied network system, where two distributed generators and four loads were used;  $R_f$ ,  $C_f$ , and  $L_f$  refer to the resistance, capacitance, and inductance, respectively. The  $P$  and  $Q$  indicate the active and reactive powers for DG units,  $P^*$ , and  $Q^*$  reference the active and reactive powers for DG units. The nominal  $V^*$  and  $F^*$  are input to determine the reference  $V_{ref}$  and  $F_{ref}$  in the 'droop control' block. MG power is pumped into the main grid employing a three-phase circuit breaker.

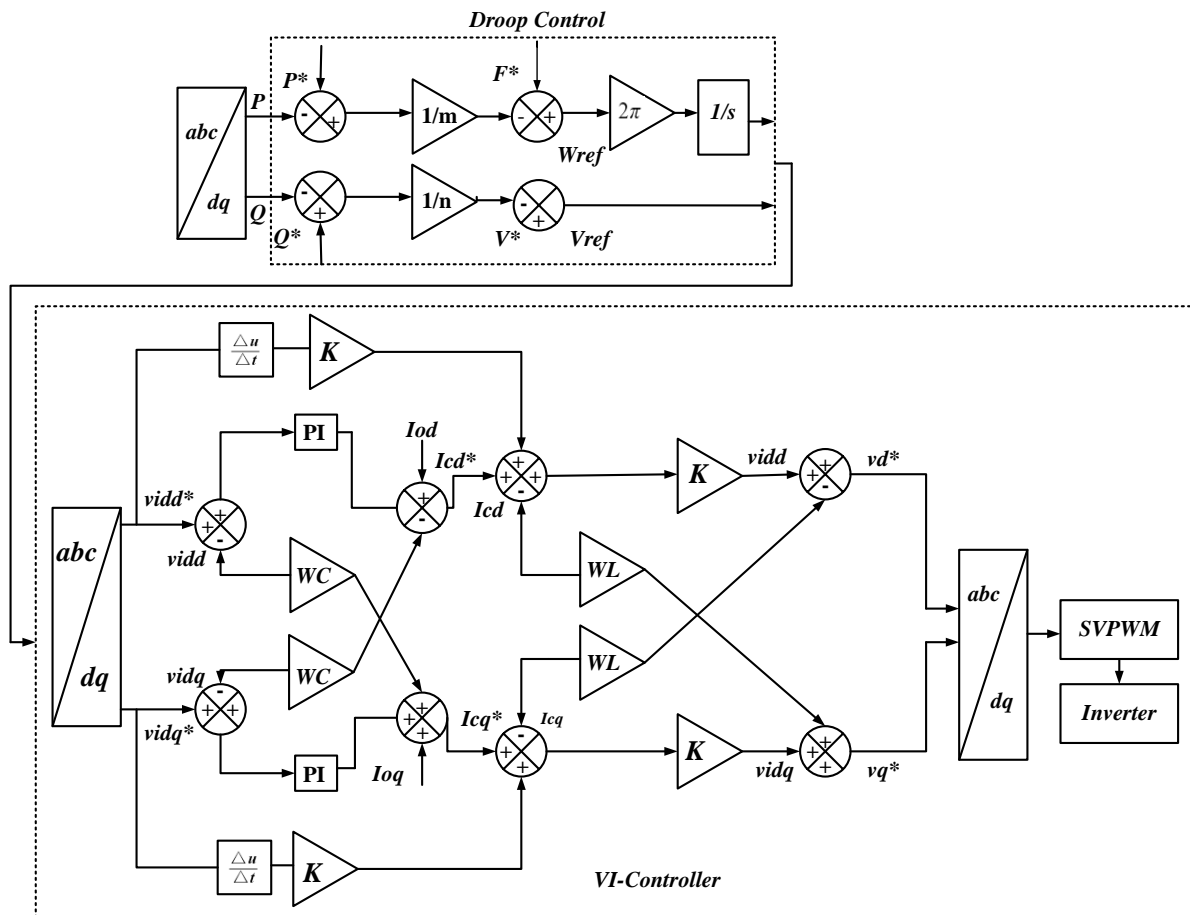


Figure 2-2 Structure internal of microgrid (Proposed controller)

In Figure (2-2),  $V^*$  and  $F^*$  represent grid-rated voltage and frequency magnitude, respectively.  $V_{\text{ref}}$  and  $W_{\text{ref}}$  are the reference voltage and frequency magnitude acquired from the droop control characteristic. The current and voltage signals of the DG and the grid are obtained and translated to the d-q frame of reference utilizing Park's transformation, applying Equations (2-14) and (2-15).

**Table 2-1 Details Parameters Microgrids[5].**

Parameters	Values
V	380v
R <sub>s</sub>	0.8929ohms
L <sub>s</sub>	16.58e-3H
Load1	Reactive load=20kw Active load= 40kw
Load2	Reactive load=10kw Active load= 20kw
Load3	Reactive load=30kw Active load= 60kw
Load4	Reactive and Active load is high
Droop Control coefficient	$1/m_1 = 5 \times 10^{-5}$ , $1/n_1 = 3 \times 10^{-4}$ , $1/m_2 = 0.15 \times 10^{-4}$ , $1/n_2 = 1 \times 10^{-4}$

### 2.3.1 Power control used to optimize droop control

A metaheuristic optimization algorithm can demonstrate auspicious results when addressing a specific optimization issue, yet the same algorithm can show poor performance on another optimization problem. According to the theory that there is no free lunch, the performance of all optimization search techniques, when amortized across the set of all potential functions, is equal. For instance, if an algorithm can effectively solve one problem, it does not follow that another algorithm will be effective. This theorem is the foundation for numerous nature-inspired optimization algorithms proposed occasionally [62]. So, this section explains the motivation for three optimization techniques (SMA, SCA, SSA). This study begins with interfacing a DG unit with a three-phase conventional grid. The controller phase receives voltage and frequency measurements from the terminals of the DG unit and the point standard coupling. In the initial case, the controller converts three-phase abc data to a synchronously spinning dq system and compares measured frequency voltage to reference values. Then, the PI controller parameter reduces the error among measured and reference values, resulting in current reference values ( $I_{cd}^*$  and  $I_{cq}^*$ ). In the end, the switching

system (SVPWM) creates gate trigger pulses and delivers them to the VSI to regulate the frequency and voltage of the system.

### 2.2.1.1 Voltage and frequency control

The voltage and frequency of a microgrid are determined by the generators or inverters supplying the active and reactive power, and they are controlled by curtailing power in droop control. The reference frequency and voltage produced using the droop control are fed to the voltages control, which generates the reference currents in the d-q frame. This controller aims to obtain the desired frequency and voltage values while eliminating the inaccuracy caused by DG insertion or load variations. The dynamics of this control may be described mathematically as Equations (2.1) and (2.2).

$$I_{cd}^* = -wC_f v_{idq} + (k_{pv} + \frac{k_{iv}}{s})(v_{idd}^* - v_{idd}) + i_{0d} \dots \dots \dots 2.1$$

$$I_{cq}^* = +wC_f v_{idd} + (k_{pv} + \frac{k_{iv}}{s})(v_{idq}^* - v_{idq}) + i_{0q} \dots \dots \dots 2.2$$

### 2.2.1.2 Current control

This controller is commonly utilized to reduce the error of the inductor impulse current and create the quantity of compensation needed to reduce the influence of short transients in the inverter's output current. The behavior of the current controller may be described by Equations (2.3) and (2.4).

$$v_d^* = I_{cd}^* - I_{cd} \left( k_{pv} + \frac{k_{iv}}{s} \right) - w \cdot L_f \cdot I_{cq} + v_{idd} \dots \dots \dots 2.3$$

$$v_q^* = I_{cq}^* - I_{cq} \left( k_{pf} + \frac{k_{if}}{s} \right) + w \cdot L_f \cdot I_{cd} + v_{iqq} \dots \dots \dots 2.4$$

### 2.2.2 Inverter

The inverter converts DC power into AC power with a specific output frequency and voltage. The term inverter commonly denotes a voltage source instead of a current source, which transforms energy from batteries or any other

constant DC voltage into an alternating current (AC) form by which magnitude and frequency may be controlled[11]. The primary purpose of the static power converter is to generate AC output waveforms from a DC power source. Inverters are classified into many types depending on the DC supply. An inverter is typically classified as a CSI when it has a larger inductor in series with a DC supply and a VSI when it has a larger capacitor through the DC bus. In a microgrid, inverters perform two principal operations: grid-following and grid-forming. CSIs enable grid-following operation, also known as PQ control and grid feeding. VSIs are commonly used in grid-forming operations to manage network voltage and frequency. Both the grid-following and grid-forming components use VSIs[63].

### 2.2.3 LC filter

LC filters as shown in Figure (2-3), are used when there is a local load between the inverter and the utility grid. The LC filter reduces output voltage ripples and minimizes high-frequency ripple currents in power electronics switches. The LC filter reduces high-frequency and high-order harmonics while maintaining a sinusoidal voltage waveform across the load. The transformer leakage inductance, grid impedance, or both act as coupling inductors[64]. The LC filter's cutoff frequency,  $f_c$ , is given by:

$$f_c = \frac{1}{2\pi\sqrt{LC}} \dots \dots \dots 2.6$$

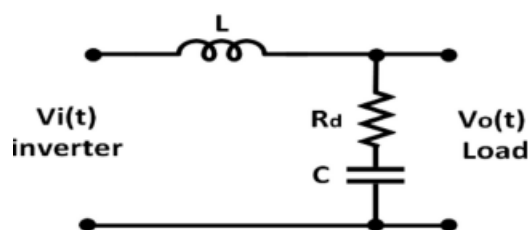


Figure 2-3 LC Filter Scheme[65]

### 2.2.4 dq Frame

Using the dq model makes controlling reactive and active power components easier because current and voltage components can represent them and accomplish decoupled control over reactive and active power[66]. Initially, the current and voltage signals of the grid and the DGs are measured and translated to the dq frame as a reference utilizing Park's transformation, applying Equations (2.7, 2.8). The converter's input voltage in the dq references frame is as follows[67]:

$$\begin{bmatrix} V_d \\ V_q \\ V_0 \end{bmatrix} = \frac{2}{3} \begin{bmatrix} \cos(\theta) & \cos\left(\theta - \frac{2\pi}{3}\right) & \cos\left(\theta + \frac{2\pi}{3}\right) \\ \sin(\theta) & \sin\left(\theta - \frac{2\pi}{3}\right) & \sin\left(\theta + \frac{2\pi}{3}\right) \\ \frac{1}{2} & \frac{1}{2} & \frac{1}{2} \end{bmatrix} \begin{bmatrix} V_a \\ V_b \\ V_c \end{bmatrix} \dots \dots \dots 2.7$$

The AC current that flows through the inductance and resistance is as follows:

$$\begin{bmatrix} I_d \\ I_q \\ I_0 \end{bmatrix} = \frac{2}{3} \begin{bmatrix} \cos(\theta) & \cos\left(\theta - \frac{2\pi}{3}\right) & \cos\left(\theta + \frac{2\pi}{3}\right) \\ \sin(\theta) & \sin\left(\theta - \frac{2\pi}{3}\right) & \sin\left(\theta + \frac{2\pi}{3}\right) \\ \frac{1}{2} & \frac{1}{2} & \frac{1}{2} \end{bmatrix} \begin{bmatrix} I_a \\ I_b \\ I_c \end{bmatrix} \dots \dots \dots 2.8$$

Where  $V_a, V_b, V_c$  : represent the per-phase voltage,  $I_a, I_b, I_c$  : represent the per-phase currents

To compute the reactive power (Q) and active power (P) that DGs supply to the loads in the dq reference frames is used in Equations (2.9, 2.10).

$$P = v_{0d}i_{0d} + v_{0q}i_{0q} \dots \dots \dots 2.9$$

$$Q = v_{0d}i_{0q} - v_{0q}i_{0d} \dots \dots \dots 2.10$$

Where: P: the active power before the filter, Q: the reactive power before the filter,  $v_{0d}$ : the output voltage on the d reference frame,  $v_{0q}$ : the output voltage

on the q reference frame,  $I_{od}$ : the output current on the d reference,  $I_{oq}$ : the output current on the q reference frame.

The instantaneous quantities for reactive and active power are determined for the power-sharing controllers after going through a low-pass filter in the following manner:

$$P = \frac{S}{S + \omega_c} (v_{od}i_{od} + v_{oq}i_{oq}) \dots \dots 2.11$$

$$Q = \frac{S}{S + \omega_c} (v_{od}i_{oq} - v_{oq}i_{od}) \dots \dots 2.12$$

Where P: refers to the active power, Q = refers to the reactive power

$\omega_c$ : The frequency of the filter cutoff, S: The operator of the Laplace transform.

### 2.3 Power Sharing

Power sharing is distributing loads among generating sources capable of producing electricity based on their rated capability for conventional sources and their available generated capacities for weather-dependent RESs. Reactive power, current sharing, harmonic current sharing, and load sharing represent other terms for power sharing. The accuracy of power-sharing enhances the system's voltage profile. This results in the production of higher-quality power. Low-capability DGs may be overwhelmed by inaccurate power sharing, necessitating separating them with protective devices. Power-sharing in the island mode is more important than the grid-connected mode. Accurate load distribution and sharing between DGs are essential during optimization [68].

### 2.4 Fitness Function

The PI controller's effectiveness depends on the selection of tuning parameters. In practical applications, it is difficult to derive an optimal PI parameter manually. Hence, several optimization algorithms have recently been employed to improve the performance of the various design methods in power

electronic converters and systems. Therefore, this present paper has optimized the tuning parameters of the controllers using three metaheuristic algorithms: SMA, SCA, and SSA. These metaheuristic optimization algorithms search for the optimal  $K_p$  and  $K_i$  parameters that optimize droop control. The optimization procedure of the PI control parameters in a metaheuristic optimization algorithms-based system begins by minimizing an error. Four types of errors were used in this study: ITAE, IAE, ITSE, and ISE, but the ITAE is a commonly employed error integration fitness function because of its easier application and superior results when compared to competitors such as ISE, IAE, and ITSE. Because of error squaring, the ITSE and ISE ITSE are extremely violent criteria that generate unworkable outcomes. Furthermore, compared to the ITAE, the IAE is an unsuitable choice since the ITAE incorporates the time multiplying error function and gives more realistic error indexing[69]. These errors are mathematically defined by the Equation below, and Table (4-2) illustrates the values obtained from the simulation of these errors. Furthermore, to analyze the system's ability and response to changes, the following system parameters are considered: (i) overshoot, (ii) rise time, and (iii) settling time. Tables (4-2) and (4-3) show the results obtained from the fitness function optimization process.

$$ITAE = \int_0^{\infty} t|e|dt \dots\dots\dots 2.13$$

$$ITSE = \int_0^{\infty} t \cdot e^2(t)dt \dots\dots\dots 2.14$$

$$IAE = \int_0^{\infty} |e(t)|dt \dots\dots\dots 2.15$$

$$ISE = \int_0^{\infty} e^2(t)dt \dots\dots\dots 2.16$$

**CHAPTER THREE:  
DROOP CONTROL BASED  
ON OPTIMIZATION  
TECHNIQUES**

## CHAPTER Three:

**Droop Control Based on Optimization Techniques****3.1 Concept of Droop Control**

The essential droop control is the initial stage of the inverter control approach. The droop controller regulates frequency and voltage according to the current loading conditions[70]. Droop control based on the conventional frequency and voltage droop controllers are employed in the AC grid-connected microgrid's active and reactive power flow control. The DGs' frequency and power droop control characteristics are developed with appropriate control gain selection rules for load sharing and stability enhancement, ensuring coordinated control across grid-connected conditions. Droop control is actively studied and widely used in parallel operation of DGs in a microgrid and frequency control in an interconnected AC power system. It is a decentralized power control scheme based on locally measured frequency or voltage values. It governs the relationship between active and reactive power with the system frequency and voltage, respectively, so that the DG units adjust their power output automatically in response to frequency or voltage deviation from the nominal value.

Hence, droop control naturally exhibits a decentralized mechanism, which becomes less complex than centralized control. Cascaded droop controls have been applied for inertia emulation of renewable energy sources and suppression of harmful sub-synchronous oscillations in microgrids[71]. Figure (3-1) shows the structure of droop control and information on the 'Voltage Formation' block. In Figure (3-1),  $f^*$  is grid-rated frequency,  $V^*$  is grid-rated voltage magnitude,  $f_{ref}$  is reference frequency, and  $V_{ref}$  is voltage magnitude. The voltage formation device generates three-phase  $u_{ref}$ , converted to  $u_{d-ref}$  and  $u_{q-ref}$  using Park's transformation.

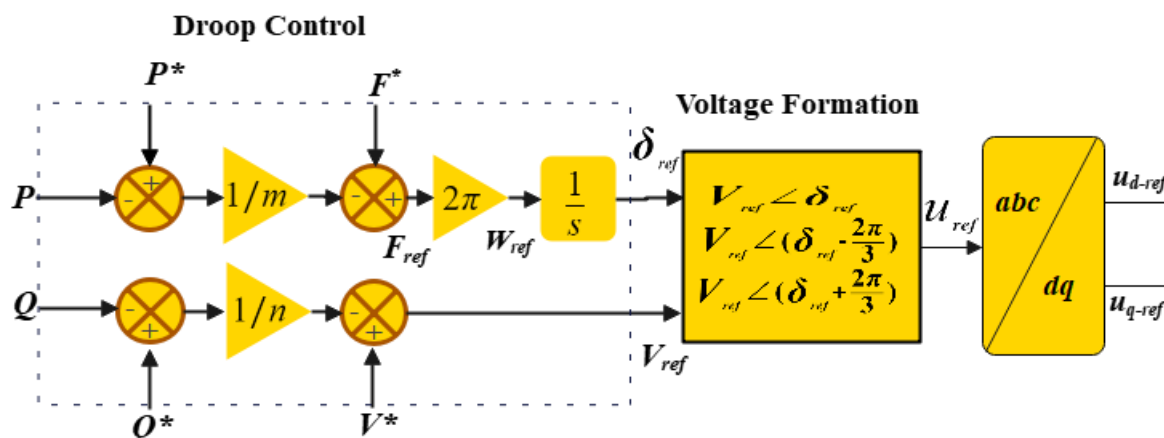


Figure 3-1 Details for Droop Control with Voltage Formation

### 3.1.1 Classification of droop control technique

The following classification of the droop control technique

#### ❖ Linear droop control

Linear droop control uses frequency, voltage, and power angle droop to generate an accurate reference. This section examines the categorizing of linear droop control techniques as follows[72]:

#### 1. Conventional Droop Control

This method depends on conventional droop control of synchronous generators. Every DG's real and reactive powers are calculated using its droop coefficient and nominal capacity. The droop coefficient is a virtual resistance on the DG inverters' grid side. The output resistance of DG inverters can be altered by modifying the droop coefficient. As a result, the output characteristics of every DG's inverter should be controlled by its local controller, which can also regulate microgrid frequency and voltage[72]. This enables an appropriate allocation of reactive power and load active demand to the many parallels connected to DGs in the microgrid. Figure (3-2), depicts the typical circuit model for a DG that is connected to the grid via its inverter:

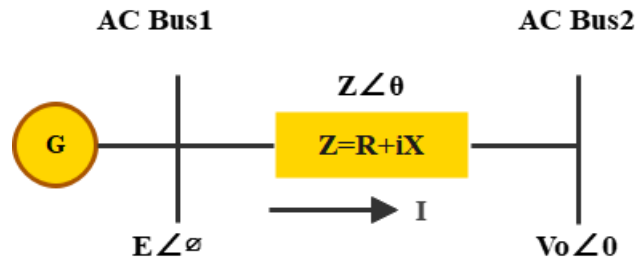


Figure 3-2 DG connected to the grid (AC Bus)

The injected active power and reactive power are calculated using the equations.

$$S = P + jQ \dots\dots\dots 3.1$$

$$P = \left( \frac{EV}{Z} \cos \varphi - \frac{V^2}{Z} \right) \cos \theta + \frac{EV}{Z} \sin \varphi \sin \theta \dots\dots 3.2$$

$$Q = \left( \frac{EV}{Z} \cos \varphi - \frac{V^2}{Z} \right) \sin \theta + \frac{EV}{Z} \sin \varphi \cos \theta \dots\dots 3.3$$

Where: E: is the inverter's output voltage amplitude, V: represents the voltage amplitude for the common AC bus, X: represents the inverter output reactance, L: is the inductance and Z: is the line impedance,  $\varphi$ : represents the phase angle differential between the PCC and Inverter output voltage,  $\theta$ : represents the line impedance phase angle.

In an inductive system, Z is operating as an imaginary reactance. The following formula can express the active and reactive power each inverter draws to a bus by simplifying the above equations.

$$P = \frac{EV}{X} \sin \varphi \dots\dots\dots 3.4$$

$$Q = \frac{EV \cos \varphi - V^2}{X} \dots\dots 3.5$$

So, the conventional droop characteristic in Figure (3-3), and can be expressed as follows in equations (3.6 and 3.7):

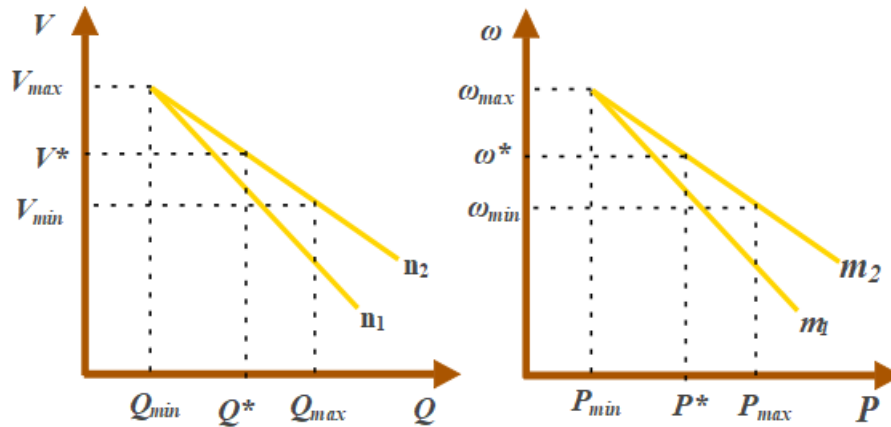


**Figure 3-3 Conventional droop characteristics**

$$f = f_n - m(P - P^*) \dots \dots \dots 3.6$$

$$v = v_n - n(Q - Q^*) \dots \dots \dots 3.7$$

Where:  $f$ : is the reference frequency,  $V$ : is the reference voltage,  $f_n$ : refers to the frequency characteristics' constant coefficients,  $V_n$ : refers to the voltage characteristics' constant,  $n$  and  $m$ : denote the droop coefficients voltage and frequency determined by Equations as follows:

$$m = \frac{f_i - f_{imin}}{P_i - P_{imax}} \dots \dots \dots 3.8$$

$$n = \frac{E_{imax} - E_{imin}}{Q_{imin} - Q_{imax}} \dots 3.9$$

Droop control can be defined using equations that illustrate the relationship between frequency and active power, as well as voltage and reactive power. This characteristic diagram represents the frequency and voltage response of a distributed generation unit. When frequency decreases, the permissible active power output of the distributed generation unit increases, leading to a rise in load. Frequency is regulated based on active power to ensure grid stability and balanced load distribution. Distributed generation units respond to frequency drops by increasing their active power output, thereby counteracting the frequency decline and stabilizing at a specific point, allowing power sharing among units. Similarly, as reactive power increases, voltage decreases, and vice versa.

The traditional droop method has several disadvantages, such as an inherent trade-off among regulation of voltage and load sharing, slow transient response, the line impedance mismatch across parallel-connected inverters that affects reactive and active power sharing, poor harmonic sharing of load across parallel-connected inverters in the instance of non-linear loads, load dependence on frequency and voltage, circulating current between DGs, inaccurate reactive power sharing, low power quality for unbalanced or non-linear loads, and ineffective performance with RES. See Figure (3-4)

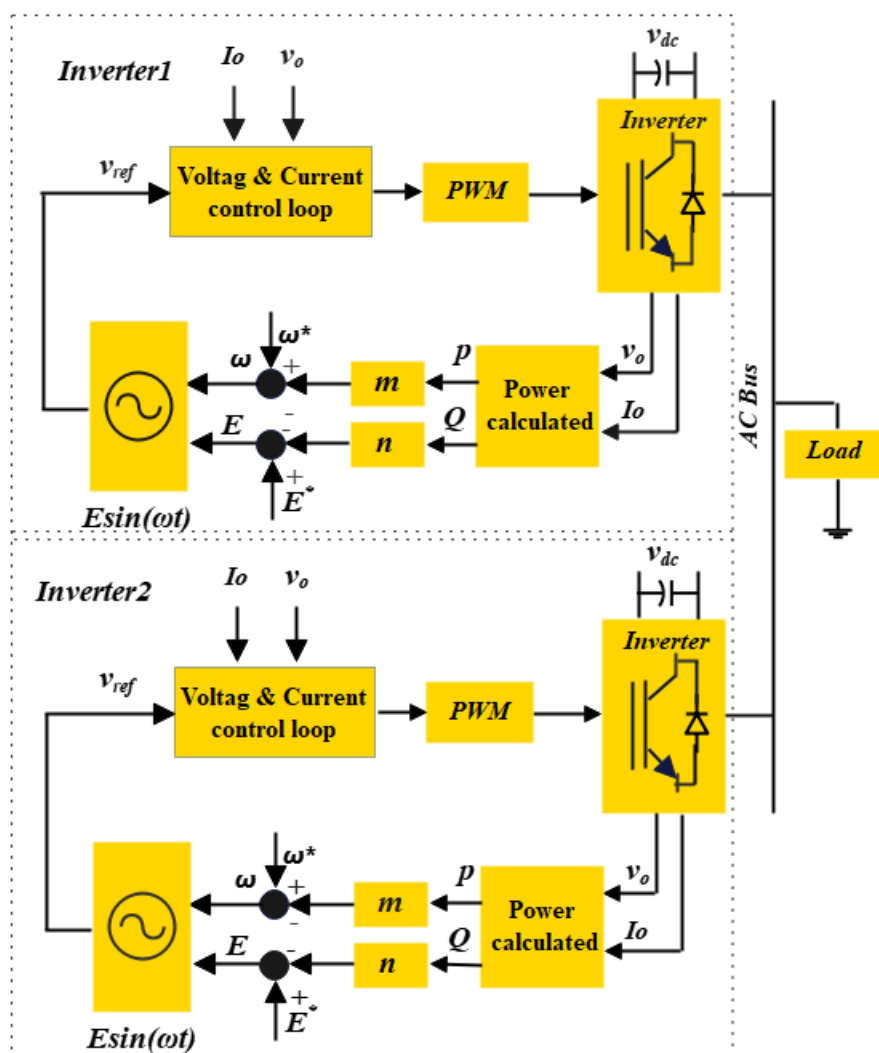


Figure 3-4 Conventional droop control[73].

## 2. Reverse Droop control (P-V and Q-F (VPD/FQB) method)

The conventional droop control is effective for high voltage system transmission because it has little line resistance to reactance ratio. However, it cannot be utilized in low-voltage and high-resistivity microgrids. In Equations (3-10 and 3-11),  $Z$  is considered the impedance of a perfect resistor[72]. The traditional frequency droop management method is effective in microgrids with primarily inductive line impedances but may not operate well in low-voltage microgrids with primarily resistive feeders. The inverter's active and reactive power still rises with  $E$ , but the reactive power rises with the power angle  $\phi$ , while the active power increases with voltage variation ( $E - V$ )[18].

$$P = \left( \frac{EV}{R} \cos \phi - \frac{V^2}{R} \right) \dots \dots \dots 3.10$$

$$Q = -\frac{EV}{R} \sin \phi \dots \dots \dots 3.11$$

Approximated as  $\sin \phi$ , the normal power system is around equivalent to zero ( $\cos \phi \approx 1, \sin \phi \approx \phi$ )

$$P \approx \frac{V}{R} (E - V) \dots \dots \dots 3.12$$

$$Q = -\frac{EV}{R} \phi \dots \dots \dots 3.13$$

Equations (3.12,3.13) demonstrate that the reactive power decreases as the angle between phases rises, whereas the active power is inversely proportional to the inverter bus voltage. Therefore, droop characteristics must be determined by the curves in Figure (3-5) and Equation (3-14,3-15)

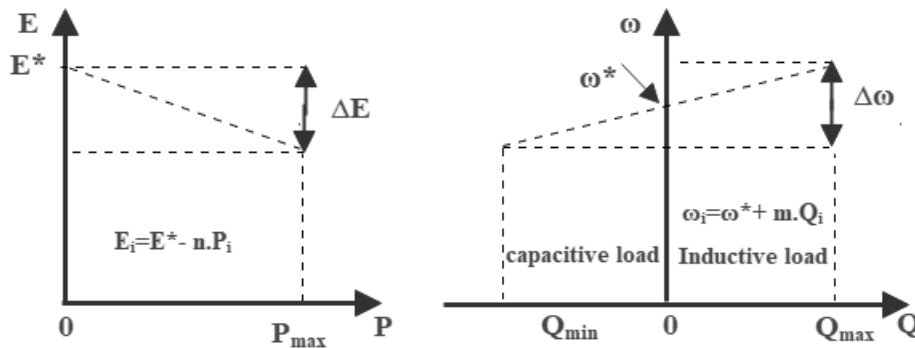


Figure 3-5 Reverse droop control curve[74].

$$E_i = E^* - n \cdot P_i \dots \dots \dots 3.14$$

$$\omega_i = \omega^* + m \cdot Q_i \dots \dots \dots 3.15$$

Where m: is the reactive power's (Q) boost coefficient, and n: is the active power's (p) drop coefficient.

Furthermore, P-V and Q-f droop control techniques frequently share equal active power under the resistive feeder impedance situation. This type of control provides enhanced performance for power transfer and controlling low-voltage AC microgrids with extremely resistant lines.

### 3. Virtual Impedance-Based Droop Control

Power sharing may be ineffective when employing CDC with complex line impedances. So, the authors suggested a droop controller that includes a loop made up of a virtual impedance. Its goal is to minimize the circulating current (both fundamental and harmonic) and power oscillation, and this method improves dynamic performance and adaptability to changing line impedances. It offers stable frequency management in steady-state situations and active power balance. A virtual impedance is proposed to decouple reactive and actual power to low x-to-r ratio lines. as shown in Figure (3-6)[75]. The virtual impedance is offered as a control method for power regulation and power-sharing in conjunction with droop control. Similarly, virtual impedances are used in converter control for harmonic voltage rectification, enhanced stability, and power-sharing applications[76]. Virtual impedances assist in regulating voltage within specific limitations, dampening the system, effectively sharing reactive

power, and decoupling active and reactive power. The reference voltage can be expressed by the equation as follows:

$$V_{ref} = V_0^* - Z_v I_0 \dots \dots \dots 3.16$$

Where  $V_0^*$ : represents the rated value of the voltage,  $Z_v$ : is the virtual impedance,  $I_0$  : represents the rated value of the current.

To obtain  $Z_v(s) = sL_v$  is to reduce the output voltage proportionally to the derivative of the output current. High harmonics originate from nonlinear loads. Instead of s cap L sub v, a high-pass filter can remove harmonic influences. So, it can express the reference voltage as follows:

$$V_{ref} = V_0^* - L_v I_0 \frac{s}{s + \omega_c} \dots \dots \dots 3.17$$

Where:  $\omega_c$  indicates the cutoff frequency of the high-pass filter.

The virtual impedance is adaptively adjusted to limit the inherent problems of line impedance mismatch. So, the adaptive virtual impedance can be calculated for each DGs:

$$\Delta Z_{vi} = k_i \frac{Q_i}{U_i} \dots \dots \dots 3.18$$

Where: -  $k_i$  : represents the coefficient of the adaptive virtual impedance  
 $Q_i$ ; represents the reactive power output,  $U_i$  : represents the output voltage amplitude.

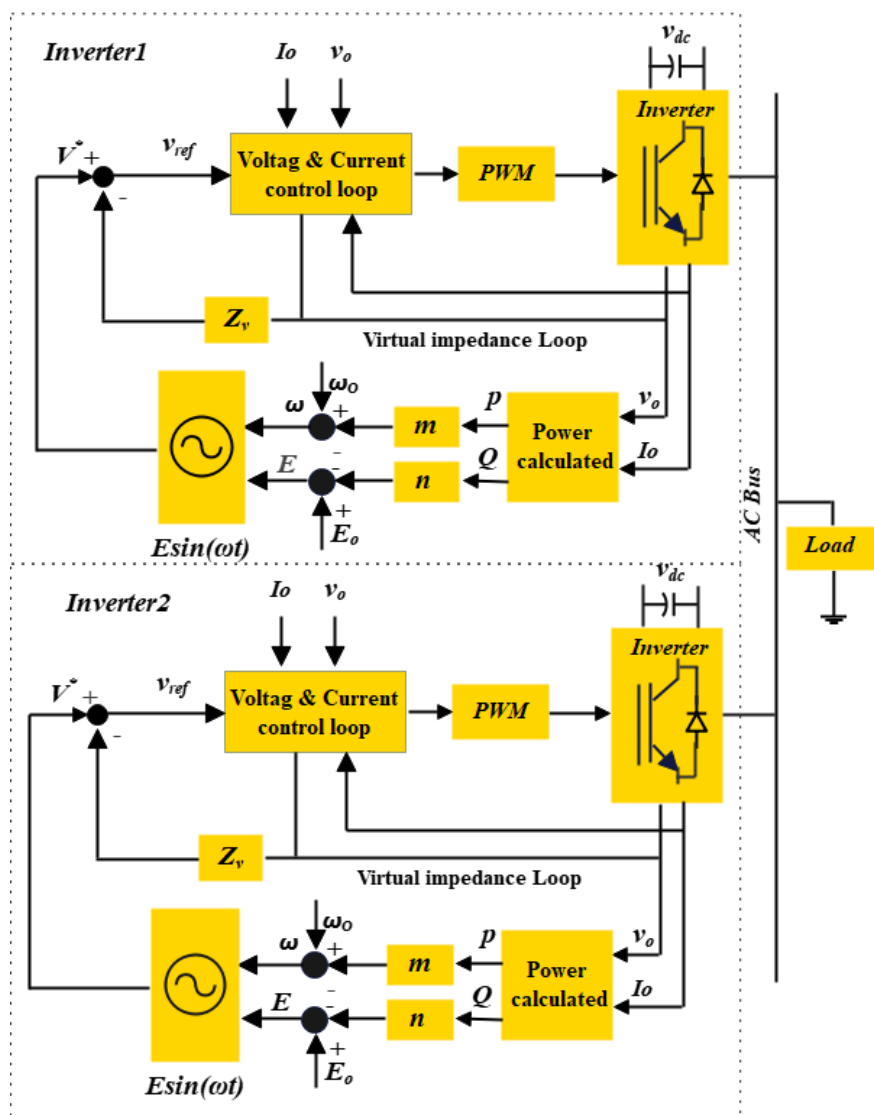


Figure 3-6 Virtual Droop Control[73].

#### 4. Adaptive Droop Control

The adaptive droop control approach has been presented to significantly keep the voltage amplitude with the correct reactive power-sharing and address the erroneous reactive and active power-sharing issue in islanded microgrids caused by line impedance mismatch while utilizing the CDC. The main objectives for the compensation droop control method are performance and line impedance compensation improvement via harmonics reduction. In this method, the maximum amount of reactive power  $Q_{\max}$  extracted from every unit is stored and compared to the reference value of reactive power  $Q_{\text{ref}}$ . The voltage amplitude

obeys the conventional Q/E droop equation if the maximal reactive power is smaller than the reference value[3].

$$E = E^* - nQ - n_{add}(Q - Q_{ref}) \dots \dots \dots 3.19$$

$$E = E^* - nQ - n_{add}(Q_{max} - Q_{ref}) \dots \dots \dots 3.20$$

The variation between the value reactive power of the reference and the output reactive power is used to set the desired voltage's magnitude. VSCs with a traditional voltage droop controller distribute reactive power among the microgrid's DGs. To correct a mismatch in the current sharing at the deviation in voltage and main level of control at the secondary level, an adaptive droop in d-q coordinates is used. To eliminate the current sharing mismatch, the droop resistances for the d and q subsystems are adjusted using the PI controller tuning. Equation(3.22) describes the relationship between DG and bus voltage[77].

$$V_i \angle \alpha_i = E_i \angle \delta_i - Z_i I_i \angle -\theta_i, i = 1, 2 \dots \dots \dots 3.21$$

$V_i$  can be represented in terms of reactive and active powers using equation (3.22)

$$V_i = E_0 - n_{qi} Q_i - \frac{r_i P_i}{E_i} - \frac{x_i Q_i}{E_i} \dots \dots \dots 3.22$$

The control factors determine the magnitude of the voltage on the  $i^{\text{th}}$  bus  $n_{qi}$  And  $E_0$ , VSC's reactive and active power, and connection impedance. To mitigate the effects of these factors, the VSC's voltage reference is adjusted to include a voltage drop in its connection impedance. So, Equation (3.23,3.24) modifies the typical E-Q droop[78].

$$E_i = E_0 + \left( \frac{r_i P_i + x_i Q_i}{E_0} \right) - n_{qi} Q_i \dots \dots \dots 3.23$$

$$D_i(P_i \cdot Q_i) = D_{Qi} + m_{Qi} Q_i^2 + m_{pi} P_i^2 \dots \dots \dots 3.24$$

Where:  $D_i$ ,  $m_{Qi}$ , and  $m_{pi}$  : represent the coefficients of the droop,  $r_i$ : is the feeding resistance,  $n_{qi}$  is the reactive droop coefficient,  $x_i$  : is the reactance.

The VSC voltage reference can be adaptively modified based on the reactive and active powers using the droop control of equation (3.25).

$$E_i = \left( E_0 + \frac{r_i P_i}{E_{0i}} \right) - \left( n_{qi} - \frac{X_i}{E_0} \right) Q_i \dots \dots 3.25$$

This controller eliminates the impact of the connection impedance among VSC and PCC[79].

### 5. Robust Droop Control

Robust droop control is presented to overcome traditional droop control's limitations and reduce the impact of nonlinear inductors on reactive power sharing, as shown in Figure (3-7); this control strategy adjusts the droop equation by subtracting the inverter's RMS output voltage from the voltage setting point. This approach compensates for the voltage loss caused by the droop and load effect.

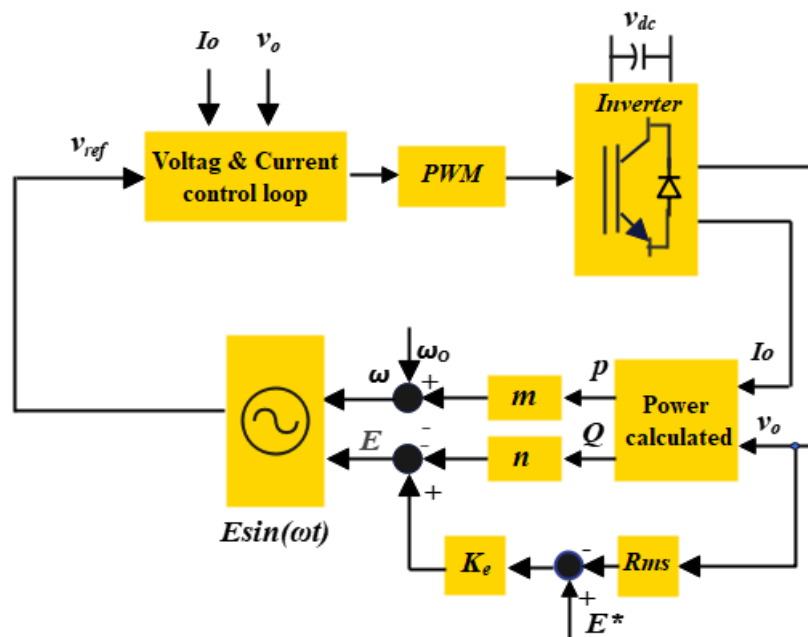


Figure 3-7 Robust Droop Control[73].

In addition, it keeps the load voltage inside the rated range despite poor reactive power sharing. The equations below express the robust droop control technique:

$$\Delta E = E - E^* = nP \dots \dots \dots 3.26$$

$$E = K_e(E^* - V_o) - nP \dots \dots \dots 3.27$$

$$\omega = \omega^* + mQ \dots \dots \dots 3.28$$

Where:  $V_o$  : represents the RMS value for the inverter's voltage output,  $K_e$ : indicates the amplifier, while m and n, are the coefficients of robust droop which are calculated using the following equations:

$$n = \frac{K_e}{P_{max}} \Delta E \dots \dots \dots 3.29$$

$$m = \frac{1}{Q_{max}} \Delta \omega \dots \dots \dots 3.30$$

Equation (3.26) can be put in steady-state form as follows:

$$nP = K_e(E^* - V_o) \dots \dots \dots 3.31$$

Equation (3.31) can be used to obtain the output voltage, as described below:

$$V_o = E^* - \frac{n}{K_e} P = E^* - \frac{nP}{K_e E^*} E^* \quad 3.32$$

Where:  $\frac{nP}{K_e E^*}$  represents the voltage drop ratio, which can be selected within the appropriate range by choosing a large  $K_e$ . The error of active power-sharing is oppositely proportional to  $n/k_e$ , but the voltage drop is proportional directly to  $n/k_e$ . This method can enhance voltage regulation while considerably reducing the influence of line impedance on power sharing.

## 6. Intelligent Droop Control

Generalized droop control (GDC) equations were derived using the CDC equations and the inverter's output active and reactive powers, as follows:

$$\Delta f = \frac{1}{K_f} \left( \frac{Z}{X} P' - P_0 \right) + \frac{K_R K_V}{K_f} \Delta V_s + \frac{K_R}{K_f} Q_0 \dots \dots \dots 3.33$$

$$\Delta V_s = \frac{1}{K_V} \left( \frac{Z}{X} Q' - Q_0 \right) - \frac{K_R K_f}{K_V} \Delta f - \frac{K_R}{K_V} P_0 \dots \dots \dots 3.34$$

$\Delta f$  and  $\Delta V_s$  are variations of the inverter's frequency and voltage, respectively.  $K_f = -\frac{1}{a}$ ,  $K_V = -\frac{1}{b}$ ,  $K_R = \frac{R}{X}$ ,  $P_0$ ,  $Q_0$  active and reactive powers,

respectively. According to equation (26),  $K_f$  impacts the weighting coefficients of  $Q_0$  and  $\Delta V_s$  In the second and third definitions.

### 7. Hybrid Droop Control

A Generalized Droop Control is created by comparing the virtual synchronous generator and Conventional Droop Control. When there are variations in the power reference, the GDC can reduce the active power settling time and suppress oscillations. Compared to droop control, GDC could offer inertia and damping characteristics. GDC can function as a CDC and a VSG for specific controller parameters. This type is called hybrid droop control. A triple droop approach is suggested. First, angle droop is employed to enhance the dynamic of active power management. Second, frequency droop enhances system stability and reduces frequency variations. Third, voltage droop is employed. This triple process is done by choosing the appropriate angle droop coefficients and frequency. The disadvantage of using the hybrid droop control method is the difficulty in doing a stability study of a microgrid system that incorporates hybrid droop control techniques[80].

### 8. Angle Droop Control

Modifying the phase angle for the DG voltage bus can control a microgrid's power flow. The Angle droop control is in two scenarios: no communication and communication across the web. Although the two approaches achieved great power-sharing with high resistivity networks, the system was at risk because of the high gain[81]. The active and reactive power injected into the grid by DG can be calculated as follows.

$$p = \frac{V \times V_t \sin(\delta - \delta_t)}{X_f} \dots \dots \dots 3.35$$

$$q = \frac{V^2 - V \times V_t \cos(\delta - \delta_t)}{X_f} \dots \dots 3.36$$

It can be observed that equation (3.37) shows that the actual power output of DG is directly proportional to the voltage phase angle, provided the value

voltage phase angle fluctuation is small enough; stated differently, the voltage phase angle and magnitude can be adjusted to regulate the active and reactive power of DG[81]. The averages of active and reactive powers are obtained by passing these instantaneous powers across a low-pass filter. The microgrid voltage at the bus can be observed.  $V_t \angle \delta_t$  is not directly controlled by the VSC (refer to Figure (3-8)). Therefore, it makes it evident that actual power may be controlled by adjusting  $\delta$ . In contrast, reactive power may be controlled by adjusting voltage magnitude, provided that the angle difference ( $\delta - \delta_t$ ) is low. Therefore, the power requirement can be divided among the DGs by lowering the voltage magnitude and angle as in conventional droop [82]. Conventional Q-V and P-f droop control indirectly alters the voltage phase angle by altering the frequency. However, the Q-V and P-  $\delta$  droop control approaches can directly regulate the magnitude and phase angle of the DG voltage output, which can be explained as:

$$\delta = \delta_{\text{rated}} - m \times (P_{\text{rated}} - P) \dots \dots 3.37$$

$$E = E_{\text{rated}} - n \times (Q_{\text{rated}} - Q) \dots \dots 3.38$$

Where  $\delta_{\text{rated}}$  : is the phase angle of DG,  $E_{\text{rated}}$  : is the nominal voltage and phase angle of DG. The coefficients n and m represent reactive and active power gains, respectively. Phase droop can significantly enhance DG's frequency stability and power flow regulation.

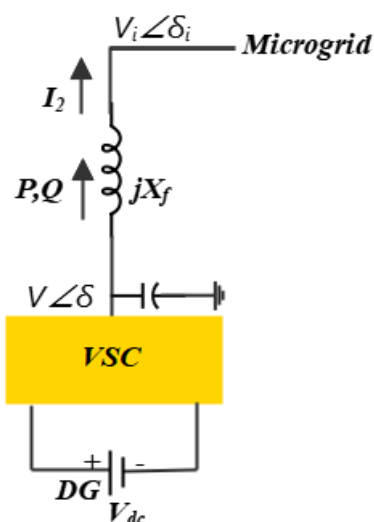


Figure 3-8 DG connected by VSC to a microgrid[83].

### 9. Virtual Frame Droop Control

This control method decouples reactive and active control in microgrids by defining a virtual reference frame for frequency and voltage. In pure inductive microgrids, the frequency (phase angle) of the DG inverter controls active power, while the inverter's output voltage controls reactive power. Active and reactive power can be expressed as follows[74]:

$$\begin{bmatrix} P^* \\ Q^* \end{bmatrix} = \begin{bmatrix} \sin \theta & -\cos \theta \\ \cos \theta & \sin \theta \end{bmatrix} \begin{bmatrix} P \\ Q \end{bmatrix} \dots \dots 3.39$$

The fundamental characteristics of droop equations use this translated active and reactive power. In the above reference structure, frequency and voltage are described similarly.

$$\begin{bmatrix} \omega^* \\ Q^* \end{bmatrix} = \begin{bmatrix} \sin \theta & \cos \theta \\ -\cos \theta & \sin \theta \end{bmatrix} \begin{bmatrix} \omega \\ E \end{bmatrix} \dots \dots 3.40$$

$E$  and  $\omega$  are calculated using the conventional droop equation. This strategy raises system stability by separating active and reactive power. However, it does not account for the negative effect of nonlinear loads on impedance.

### **10.V-I Droop Control**

The system decreases the problem of power-sharing into one of current sharing by employing a feed-forward mechanism, constant frequency, and droop signal injection. This approach improves stability and dynamic responsiveness and is suitable for inverters with a small current range and compact diameters[84].

#### **3.1.2 Advantages and disadvantages of droop control**

##### **❖ Advantages**

The main benefit of the droop control method is that it avoids key communication lines between parallel-connected inverters. The non-existence of communication links among parallel-connected inverters offers high reliability and flexibility[73]. There is no need for communication networks, adequate dependability, easy expansion, and low investment costs [72].

##### **❖ Disadvantages**

- 1- A significant drawback of droop control is the load-dependent frequency variance. Therefore, there is a phase discrepancy between the frequency of the utility's primary input voltage and the frequency of the inverter output voltage[42].
- 2- Variations in grid voltage and frequency: While in isolated mode, the microgrid's voltage and frequency are affected by changes in load. Increasing the gradient of the droop profile improves the microgrid's reaction to changes in load, but voltage and frequency control and microgrid stability suffer[72].
- 3- Harmonic load dispatch: While the conventional droop control is suitable for basic load distribution, it cannot manage harmonic load

dispatch in the face of non-linear loads [22]. Furthermore, it has poor power quality and delays dynamic response in the presence of harmonics.

- 4- Unknown and variation line impedances: The line impedances among parallel converters influence power flow. Differences in impedances between inverters and the point of standard connection produce a substantial circulating current between inverters, which lowers the precision of power dispatch[72].
- 5- DG output power fluctuations: Because renewable DGs' major energy sources are unpredictable, the conventional droop cannot provide a steady power supply to the microgrid[72].

### 3.2 Proportional-integral

The PI controller is the most commonly used approach for inverter control in microgrids. The most common and simplest method is associated with voltage and frequency droop control. The PI controller is frequently employed in a synchronous reference framework transformation by implementing its transfer function in the following manner:

$$C_{PI}(s) = K_p + \frac{K_i}{s} \dots \dots \dots 3.41$$

$K_p$ : proportional gain,  $K_i$ :integral gain

The PI controller's effectiveness can be improved using a cross-coupling term and feed-forward voltage. The feed-forward voltage can improve the controller's dynamics during voltage fluctuations. The main advantage of utilizing the PI in the dq frames is that it yields 0% steady-state error. As a result, it helps attain accurate reactive and real power flow in a network by directly managing the reactive and real current components. The PI in the dq reference

frames is an efficient strategy for managing electrical quantities; however, this strategy is not appropriate for distorting electrical amounts [63].

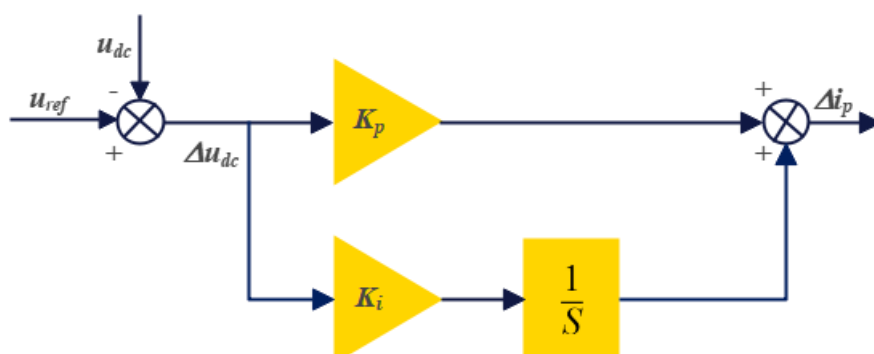


Figure 3-9 PI Control Structure Diagram

### 3.3 Concept of Optimization

Optimization determines the best values for a given problem's variables to minimize or maximize an objective function. Optimization challenges exist in a variety of domains of study. Several steps are required to address an optimization problem. First, the problem of the parameters must be determined. The Problems can be classed as continuous or discrete depending on their parameters. Second, the constraints applied to the parameters must be identified. Constraints divide optimization issues into two categories: constrained and unconstrained. An FF or OF is produced based on the parameters' nature, which must be maximized or minimized to obtain the optimal set of parameters. Third, investigate and consider the problem's objectives. In this scenario, optimization issues are divided into single-objective and multi-objective problems. Finally, according to the specified categories of parameters, restrictions, and number of targets, an appropriate optimizer must be selected and used to address the problem[85].

So, any mathematical optimization problem, either minimizing or maximizing a specific objective function, typically contains four major components: objective functions, decision variables, equality and non-equality constraints, and the optimization algorithm used[1]. A metaheuristic optimization algorithm could demonstrate auspicious results when addressing a specific type

of optimization issue, yet the same algorithm may demonstrate poor performance on other optimization problems [62]. Mathematical optimization mostly depends on the gradient-based construction of the associated function to get the optimum solution. Mathematical optimization has drawbacks, such as mathematical optimization methods being ridden from local optima traps. This means an algorithm that assumes the local solution to be the global solution. This fails to achieve the global optima. They are frequently useless for issues with expensive computational derivations that are unknown.

### **3.3.1 Classification of optimization algorithm**

The range of existing computing problems and the number of algorithms devised to tackle them is challenging to imagine. So, the algorithm can be classified into many types, as in Figure (3-10). Most real-world optimization problems face challenges, including non-linear constraints, high computational cost, dynamic/noisy objective functions, non-convex search landscape, and colossal solution space. These issues are the primary criteria for selecting an accurate or approximation algorithm to address complex problems[86]. Metaheuristic optimization algorithms have gained popularity in recent decades due to their reduced requirements computation capacity, simplicity, high performance, derivation-free mechanism, flexibility, and local optima avoidance compared to deterministic algorithms for optimization issues[87].

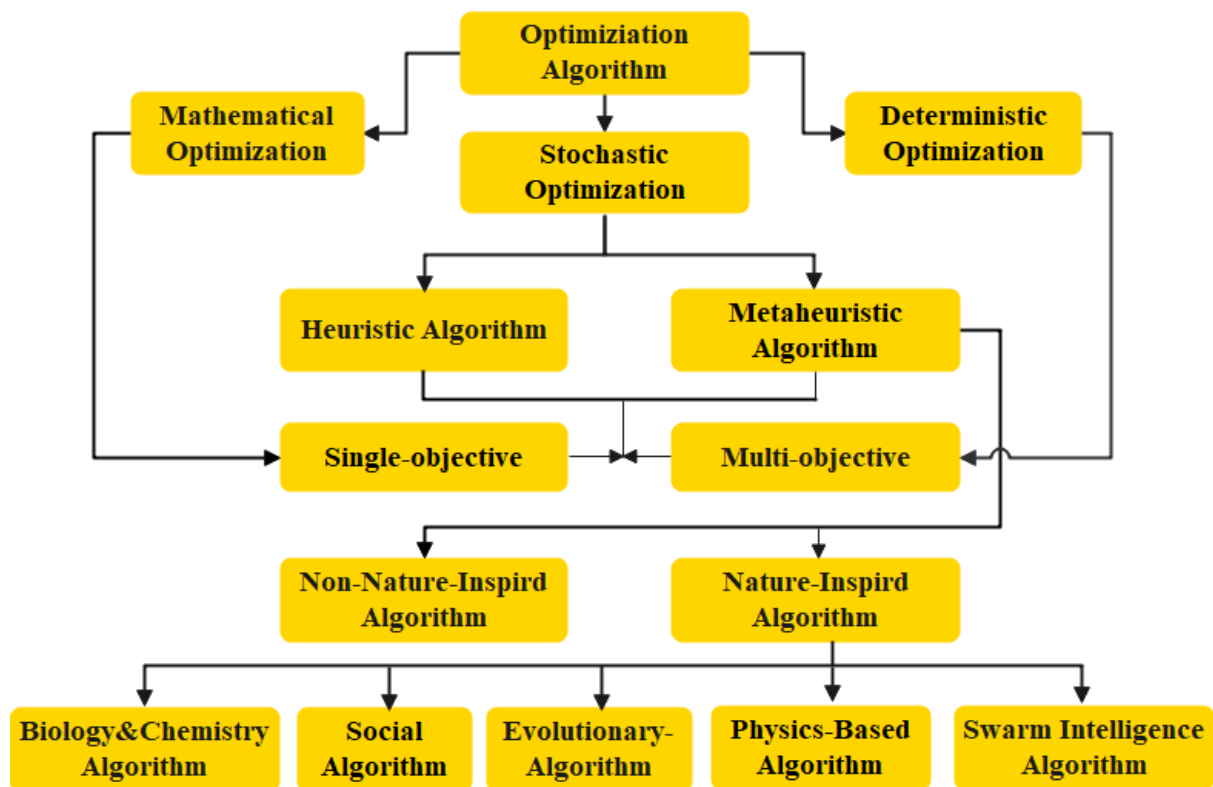


Figure 3-10 Optimization Algorithms Classification[86].

### 3.3.1.1 Metaheuristic optimization algorithms

Definition metaheuristic optimization algorithms, or simply metaheuristics, can be regarded as a set of higher-level procedures that provide an identical framework to guide algorithms that depend on heuristic rules toward the exploration and exploitation of the search space to improve potential solutions. These algorithms present different attributes to solve complex real-world optimization problems. Every iterative application of a metaheuristic optimization algorithm results in a solution. Being a higher-level procedure, the fundamental nature of metaheuristics is organized by abandoning the invariants in the details. The principal advantage of the generic nature of evolutionary algorithms is that they can quickly be adapted to solve the issue at hand with little adjustment. This has made it a desirable tool in diverse fields such as communication, control, scheduling, supply chain, and robotics. Metaheuristic algorithms play an important part in the optimization techniques arena. These

algorithms offer a robust, flexible design of a search component capable of finding and executing the complex underlying spatial movements of a swarm of particles, in addition to featuring manageable computational efficiency in terms of speed and robustness[87].

### **3.3.1.2 Swarm intelligent**

SI refers to the collective behavior of decentralized, self-regulating systems. Typically, SI systems are composed of a population of simple factors that interact individually with their environment and one another. Additionally, the SI can be characterized as a branch of artificial intelligence that is employed to mimic the collective behavior of natural social swarms, such as ant colonies, animal herding, fish schooling, bacterial growth, animal herding, and bird flocking[85]. to create swarm intelligent life systems having cooperative behavior using computers.

There are five fundamental principles of swarm intelligence [88].

- ❖ Proximity principle: The swarm must be capable of performing the basic space and time calculations.
- ❖ Quality principle: The swarm must have the ability to respond to environmental quality factors.
- ❖ Stability principle: The swarm should maintain the same behavior mode regardless of environmental changes.
- ❖ Diverse response: The swarm should not confine its resources to a narrow scope.
- ❖ Adaptability: The swarm should change its behavior mode when it is appropriate. Because it is difficult to cover all of the optimization methods utilized in MG applications

## 3.4 Optimization Techniques

### 3.4.1 Slime Mould Algorithm

The SMA is a swarm intelligence algorithm that depends on the food-capture principle of the physarum polycephalum (a kind of slime mould) and the oscillatory pattern accrued of slime moulds in nature proposed by (Li et al. 2020)[87]. Slime mould can oscillate and contract while it obtains food throughout the gauge feeding process. At the same time, a network of varying-thickness veins is created among different sources of food, the network's thicknesses corresponding to the source's food quality. SMA is inspired by a biological oscillator that employs adaptively weights to mimic both negative and positive feedback processes produced by the slime's wave propagated to find an optimum food connect path with favorable exploration and exploitation inclinations. Additionally, finding a food source may involve exploring unfamiliar locations.

The physarum polycephalum uses a fan-like pattern to food search, link to a vein network, and create the best possible path. Furthermore, the venous network can contract in response to the rhythmic feedback produced by individual slime bacterium to tracer the covered region and area. SMA is a swarm intelligence method in which every potential solution refers to a slime-mold individual. A negative and positive feedback system links individuals to create a venous network for intra-group collaboration and rivalry.

#### 3.4.1.1 Mathematical model of SMA

The mathematical formulation steps are as follows [87]: The SMA includes three basic elements: approaching, wrapping, and acquiring or oscillating food

- ***Approach food***

Slime mould can toward food based on the odor in the air. The slime bacteria will identify which direction the food according to its focus, causing

the biological oscillator to generate larger waves. The contraction behavior near the food may be expressed in the following way:

$$\overrightarrow{X(t+1)} = \begin{cases} \overrightarrow{X_B(t)} + vb \cdot (\overrightarrow{W} \cdot \overrightarrow{X_a(t)} - \overrightarrow{X_b(t)}), & r < p \\ vc \cdot \overrightarrow{X(t)}, & r \geq p \end{cases} \dots\dots 3.42$$

Where:  $\overrightarrow{X(t)}$  : indicates Slime bacteria's position vector at iteration time t.  $\overrightarrow{X_B(t)}$ : indicates the individual's position vector which has the highest focus  $vb=$  represents a parameter with a range between  $[-a, a]$ ,  $\overrightarrow{W}$ : indicates the weight of a slime mould,  $\overrightarrow{X_a(t)}$  &  $\overrightarrow{X_b(t)}$ : It describes two individuals randomly selected based on the slime mould,  $vc$ : represents the parameter that minimizes a linear from 1 to 0. The random integer r falls between 0 and 1, an and p can be defined by using the equation as follows:

$$a = \text{arctanh}\left(-\left(\frac{t}{MAX\_t}\right) + 1\right) \dots\dots\dots 3.43$$

$$p = \tanh|S(i) - DF| \dots\dots\dots 3.44$$

Where: t: denotes the current iteration number, MAX\_t: denotes the maximum iteration number, S(i): represents the fitness value of  $\overrightarrow{X(t)}$ , DF: This shows the fitness value of the optimum solution obtained in the current iteration. arctanh(.): denotes the inverse hyperbolic function, and tanh(.): denotes the tangent function hyperbolic.

$\overrightarrow{W}$  the slime mould's weight, which is defined as follows:

$$\overrightarrow{W(\text{Smell-Index}(i))} = \begin{cases} 1 + r \cdot \log\left(\frac{bf - S(i)}{bf - wf} + 1\right) & , \text{condition} \\ 1 - r \cdot \log\left(\frac{bf - S(i)}{bf - wf} + 1\right) & , \text{other} \end{cases} \dots\dots\dots 3.45$$

$$\text{Smell-Index} = \text{sort}(S) \dots\dots\dots 3.46$$

Where: r= denotes the random number in  $[0, 1]$ , bf: indicates the optimum fitness obtained during the current iterative process, wf: denotes the worst fitness function created by the present iterative process, Smell-Index = indicates a sorted

series of fitness functions (ascending from the lowest value problem),  $S(i)$ : indicates an individual's fitness function and ranks them in the first half of the population.  $S$  is divided into two parts based on the grading of fitness function: the superior (top) and inferior (bottom) of individuals.

- **Wrapping food**

This component mathematically represents the contraction method of venous tissue forming slime mold when seeking. Mathematically simulated positive and negative feedback among food-focused participants and the explored slime mold's viscosity, as seen in Equation (3.42). Moreover, the settings mimic the slime mould's technique of discovering food by detecting air odors. It is recognized to be given extra weight when the focus of the food is high. In contrast, if there is insufficient focus on food in the region, its weight reduces, prompting it to explore other areas in search of food, according to the previous mechanism.

$$\vec{X}^* = \begin{cases} \text{rand} \cdot (Ub - Lb) + Lb & , \text{rand} < z \\ \vec{X}_B(t) + \vec{vb} \cdot (w \cdot \vec{X}_a(t) - \vec{X}_b(t)) & , r < p \dots \dots \dots 3.47 \\ \vec{vc} \cdot \vec{X}(t) & , r \geq p \end{cases}$$

Where:  $r$  and  $\text{rand}$  are randomly chosen values in the range  $[0, 1]$ ,  $Z$ = denotes the variable that allows values between  $[0,0.1]$ ,  $U_b$ : indicates the upper of the seek range, and  $L_b$ : indicates the lower search range.

- **Oscillation parameters**

Slime mold depends on a biological oscillator's propagation wave to change cytoplasmic movement in veins, resulting in higher food concentration. and are used  $\vec{vb}$  and  $\vec{vc}$  to imitate the slime mould's vein width fluctuations.  $W$  updates the food rate by identifying the food's quality and mimicking the slime's oscillation frequency, permitting the slime to select the best food source. Slime mould can move quickly towards food when they obtain high-quality food but

may take longer if the food focus is limited to individual locations.  $\vec{vb}$  and  $\vec{vc}$  oscillate randomly in the interval  $[-a, a]$ . Where  $\vec{vb}$  is distributed among  $[-a, a]$  and  $\vec{vc}$  between  $[-1, 1]$ . Moreover,  $\vec{vb}$  mimics whether slime molds will be chosen to seek out or approach new food sources if a novel one is discovered. Slime moulds separate organic material from other sources in search of superior food, even when a better food source is found. This process effectively improved the local optimal problem by giving slime molds more opportunities to acquire higher-quality food. Each of these components is adaptive and modified by utilizing iterative methods. Figure (3-11) shows the step optimization of the Slime Mould Algorithm.

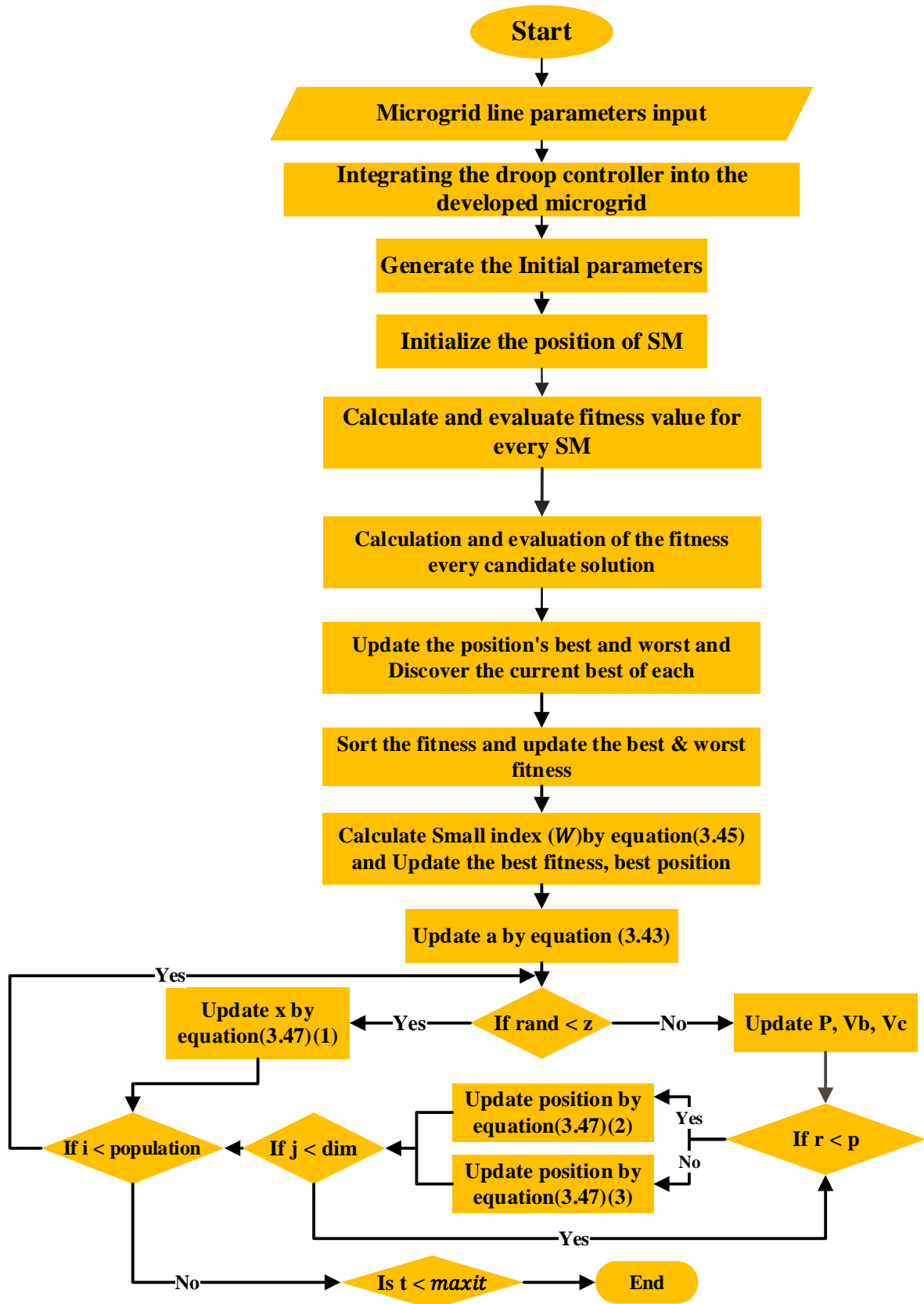


Figure 3-11 Flowchart Slime Mould Algorithm

### 3.4.2 Sine Cosine Algorithm

The Sine-Cosine algorithm is a nature-based metaheuristic optimization method based on the mathematical ideas of sine and cosine functions proposed by Mirjalili 2016 [89]. It is intended to tackle complex optimization issues and confined and unconstrained problems effectively. The SCA is founded on the concept that sine and cosine functions may be used to simulate the oscillatory behavior of particles seeking an ideal solution in a search space. The algorithm mimics the exploration and exploitation process by altering the frequency and amplitude of the sine and cosine operations, resulting in efficient convergence to an optimum solution. The SCA uses two search algorithms: a population search technique and a local search technique. These two techniques are responsible for local exploitation and global exploration[90]. SCA can help with a wide range of practical engineering issues. According to a mathematical framework, it is principally derived using the sine and cosine principles. The SCA generates many initial randomly candidate solutions and needs them to vary outwards or toward the optimal solution utilizing a mathematical model according to sine and cosine functions. The SCA algorithm has three stages: startup, exploration, and development[91].

#### 3.4.2.1 Advantages and disadvantages of SCA

❖ **Advantages:**

- 1-The SCA algorithm effectively addresses real issues with confined and unknown search spaces.
- 2- SCA can explore various areas of the search space, avoiding the local optimal and aiming closer to the global optimal.
- 3- SCA moves different initial random solutions toward the possible potential region of convergence. Furthermore, SCA uses variables with random and

adaptive patterns to quickly move problematic solutions into a suitable zone, and SCA is simple, adaptive, and hassle-free[90].

❖ **Disadvantages:**

The SCA has clear drawbacks, like a slow convergence rate and a tendency to slip into the local optimal.

### 3.4.2.2 Mathematical model of SCA

Here's a detailed explanation of the SCA[92]:

- 1- Population Initialization: A group of candidate solutions, sometimes known as particles, is produced at random from the problem's search space. Every solution is expressed as a vector of choice variables.
- 2- Amplitude and Frequency: The SCA defines the sine and cosine functions using the value of "r1" and the parameter "r2." The amplitude linearly reduces over iterations, and "r2" is a random value in the interval [0, 1]. These parameters control the particle's movement through the search space.
- 3- Exploration and Exploitation: The algorithm balances exploration and exploitation by adjusting the sine and cosine operations. Exploration represents a global search in which particles travel randomly in the search space to discover new and exciting regions. Exploitation is a type of local search in which particles adjust their positions according to the best solution discovered thus far to fine-tune the search.
- 4- Position Update: The positions of particles are updated utilizing the sine and cosine operations, and the optimal solution is determined. Equation (3.52) analyzes the modified positions and identifies the new best solution.
- 5- Stopping Criteria: The algorithm iterates the preceding steps until a specified stopping requirement is satisfied. This can include accomplishing a target level of solution accuracy, completing the maximum number of iterations, or meeting any other user-defined criterion.

The possible solutions in SCA are established as a matrix

$$X = \begin{pmatrix} x_{(1,1)} & x_{(1,2)} & \cdots & x_{(1,d)} \\ x_{(2,1)} & x_{(2,2)} & \cdots & x_{(2,d)} \\ \vdots & \vdots & \vdots & \vdots \\ x_{(n,1)} & x_{(n,2)} & \cdots & x_{(n,d)} \end{pmatrix} \dots \dots \dots 3.48$$

The following entries express the row vector:

$$X_n = [x_{n,1}, x_{n,2}, \dots, x_{n,d}] \dots \dots \dots 3.49$$

Like other optimization techniques, the initialization phase includes creating this matrix, including size (cap N times d). Furthermore, the position update formulations are calculated using trigonometric functions and encoding steps[90]. The following equations for updating positions are proposed in both phases:

$$X_i^{t+1} = X_i^t + r_1 \times \sin(r_2) \times |r_3 P_i^t - X_i^t| \dots \dots \dots 3.50$$

$$X_i^{t+1} = X_i^t + r_1 \times \cos(r_2) \times |r_3 P_i^t - X_i^t| \dots \dots \dots 3.51$$

Where:  $X_i^t$ : represents the current solution's position at the  $t_{th}$  iteration in the  $i_{th}$  dimension  $r_1$ ,  $r_2$ , and  $r_3$ : are random numbers  $r_2 \in [0, 2\pi]$ ,  $r_3 \in [-2, 2]$ , and  $P_i^t$ : represents the destination point's location in the  $i_{th}$  dimension. These two equations are integrated and used as follows:

$$X_i^{t+1} = \begin{cases} X_i^t + r_1 \times \sin(r_2) \times |r_3 P_i^t - X_i^t|, & r_4 < 0.5 \\ X_i^t + r_1 \times \cos(r_2) \times |r_3 P_i^t - X_i^t|, & r_4 \geq 0.5 \end{cases} \dots \dots \dots 3.52$$

Where:  $r_4$  =represents a random number in the range [0,1].

The parameter  $r_1$  specifies the next position's region (or movement direction), which may be within or outside the area between the solution and destination. The parameter  $r_2$  determines how far the movement must be towards or away from the goal. The parameter  $r_3$  assigns the weight of a random to the destination, indicating whether it should be emphasized ( $r_3 > 1$ ) or minimized ( $r_3 < 1$ ) in

determining the distance. Lastly, the parameter  $r_4$  in Equation (3.52) alternates among the sine and cosine components[92]. The impact of Sine and Cosine on Equations (3.50 and 3.51) is depicted in Figure (3-12).

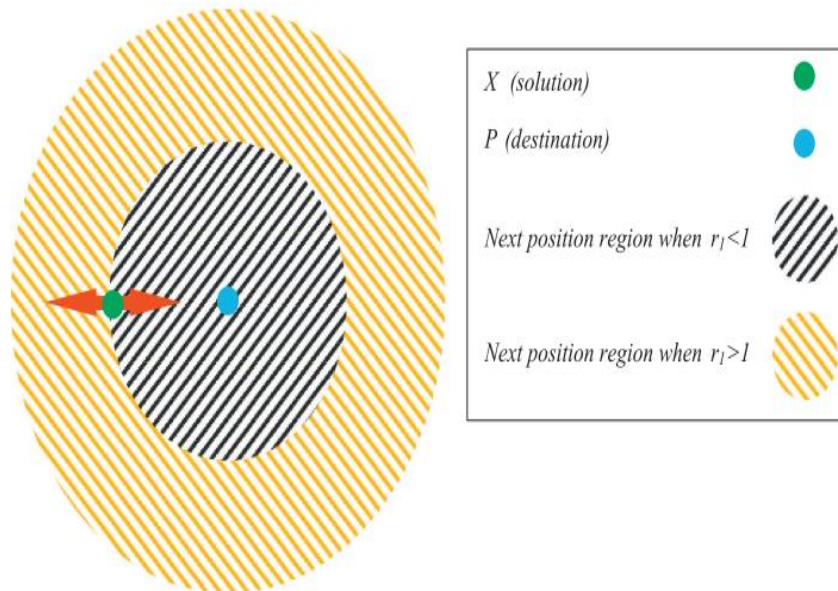


**Figure 3-12 The Effect Function of The Sine Cosine[89]**

This diagram depicts how the suggested equations determine the in-search space between two solutions. The cyclic structure of sine and cosine functions enables a solution to be moved around another. Utilizing the defined space between two solutions can be ensured by doing this. The solutions should be able to search beyond the boundaries between their respective targets to explore the search space. This can be accomplished by altering the range of sine and cosine functions.

The random position, whether side or outside, is obtained by specifying a random value for  $r_2$  between  $[0, 2\pi]$  in Equation (3.52). This process ensures that the search space is explored and exploited. An algorithm must be capable of equilibrium between exploration and exploitation to obtain possible areas of the search space and finally converge to the global optimal. To achieve equilibrium between exploration and exploitation, the following equation is used to alter the sine and cosine values in Eqs adaptively (3.50) to (3.52)[89].

$$r_1 = a - t \frac{a}{T} \dots \dots \dots 3.53$$

Where: a: is a constant, t: is the current iteration

T: represents the maximum number of iterations.

The SCA algorithm begins the optimization process by generating a set of random answers. The algorithm then keeps the best solutions found thus far, assigns them as the target point, and updates additional solutions about them. Meanwhile, the sine and cosine function ranges are modified to emphasize search space exploitation as the iteration counter rises. The SCA algorithm stops the optimization process if the iteration counter exceeds the maximum number of iterations. Other termination conditions, such as the maximum number of function evaluations or the correctness of the determined global optimal, can also be considered.

The SCA algorithm can theoretically find the global optimal of optimization problems for the following reasons[93]:

- 1- SCA improves and generates random solutions to a given problem. Hence, it has an inherent advantage over individual-based algorithms in high exploration and local optimum avoidance.
- 2- Promising areas of the search space are exploited if sine and cosine return values between [-1,1].
- 3- Explore different areas of the search space if the sine and cosine operators recover a value larger than 1 or lower than -1.
- 4- During optimization, the global optimum's best approximation is always kept in a variable as a destination point and is never lost.
- 5- The SCA algorithm smoothly transitions from exploration to exploitation by utilizing an adaptive ranging in the sine and cosine operators.

- 6- The suggested algorithm treats optimization issues as black boxes, so it is easily adaptable to problems in various domains, provided the problem is properly formulated.
- 7- Because the solutions always updated their locations around the best solution acquired thus far, there is a preference for the best areas of the search spaces through optimization.

Figure (3-13) shows the step optimization of the SCA.

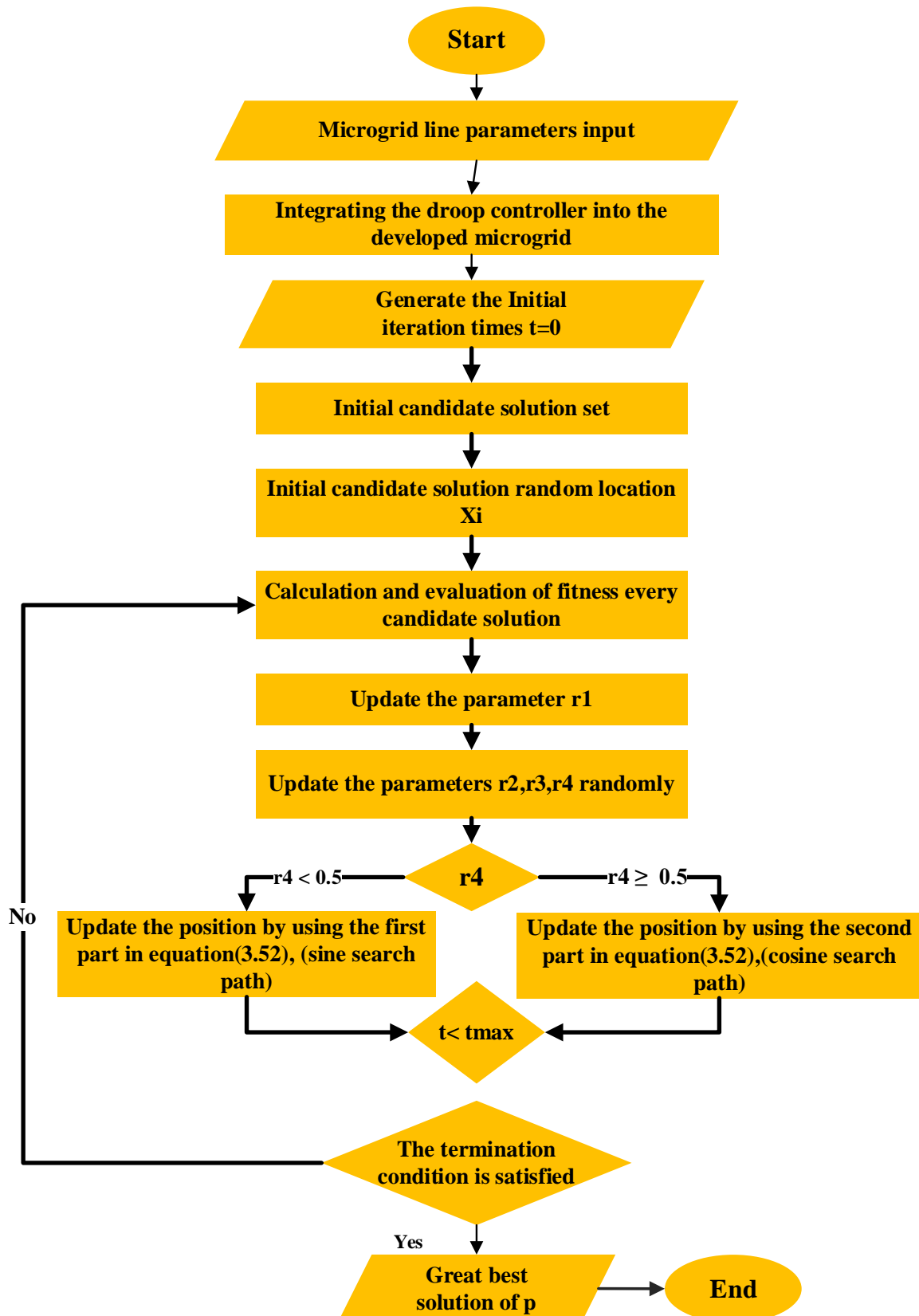


Figure 3-13 Flowchart Sine Cosine Algorithm

### 3.4.3 Sparrow Search Algorithm

SSA is a swarm intelligence algorithm of optimization proposed by (Xue and Shen 2020)[94] inspired by the communal wisdom, anti-predation, and foraging behaviors of sparrows. SSA is classified into three stages: producer(discoverer), Scroungers (follower), and Scouters (investigators or alerts)[95].

- ❖ Discoverers: Discoverers typically perform a function with high environmental fitness; therefore, they are in charge of extensively seeking food, exchanging information about foraging directions with others, and directing the population's flow in the foraging orientation. Discoverers are considered dominant in sparrow populations because they have a superior location in search space and typically offer information about the position of food to the population[96].
- ❖ Followers (Scroungers): The follower closely monitors the finder and will promptly follow if they locate food. Scroungers join a group of discoverers with the highest fitness value to explore foraging information[96].
- ❖ Investigator (Alerters): Alerters are primarily responsible for scouting, observing the action surrounding the food and early warning missions, and recognizing and communicating danger to the rest of the population.

The SSA algorithm features fewer parameters, faster performance, and a larger search capacity.

#### 3.4.3.1 Mathematical model SSA

To simplify the mathematical approach, the following hypotheses are derived for sparrow behavior[94].

- 1- Producers usually have significant energy reserves and offer foraging regions or directions for all intruders. It is responsible for identifying

areas with abundant food resources. Individual fitness values determine the degree of energy reserves.

- 2- When sparrows detect a predator, they chirp as an alarm signal. Producers must direct every scrounger to a safe region when the alert value exceeds the safety threshold.
- 3- If a sparrow discovers a better food source, it can become a producer, but the ratio of producers to scroungers doesn't change throughout the population.
- 4- The sparrows with the highest energy would operate as producers. Multiple famished scroungers are more inclined to fly to different locations for food to gain energy.
- 5- The scroungers pursue the producer who can give the best food in their quest for food. Meanwhile, certain scroungers may constantly monitor producers and compete for food, raising their predation rate.
- 6- When faced with danger, sparrows at the group's perimeter move rapidly to a safer region, whereas those in the center walk randomly to stay close to others.

The basic phases of SSA can be described as follows[97]:

**Step 1:** Generate and initialize the solution. The population size, producer ratio (PD), maximum number of replicates, and sparrow ratio are all calculated at this phase. The initial Sparrow position can be expressed in the following matrix:

$$X = \begin{bmatrix} x_{1,1} & x_{1,2} & \cdots & \cdots & x_{1,d} \\ x_{2,1} & x_{2,2} & \cdots & \cdots & x_{2,d} \\ \vdots & \vdots & \vdots & \vdots & \vdots \\ x_{n,1} & x_{n,2} & \cdots & \cdots & x_{n,d} \end{bmatrix} \dots\dots\dots 3.54$$

Where: n represents the number of sparrows, d: represents the dimensions of the parameters to be optimized.

**Step 2:** In the SSA, producers with better fitness values search or provide directions to food sources, while scroungers obtain the food source that producers discovered. The fitness value for each sparrow can be written as the following vector:

$$F_X = \begin{bmatrix} f([x_{1,1} & x_{1,2} & \cdots & \cdots & x_{1,d}]) \\ f([x_{2,1} & x_{2,2} & \cdots & \cdots & x_{2,d}]) \\ \vdots & \vdots & \vdots & \vdots & \vdots \\ f([x_{n,1} & x_{n,2} & \cdots & \cdots & x_{n,d}]) \end{bmatrix} \dots \dots \dots 3.55$$

$F_X$  = indicates the individual's fitness value. Based on Rules (1) and (2), update the location of the discoverer can expressed in the following manner:

$$X_{i,j}^{t+1} = \begin{cases} X_{i,j}^t \cdot \exp\left(\frac{-i}{\alpha \cdot \text{iter}_{max}}\right) & \text{if } R_2 < ST \\ X_{i,j}^t + Q \cdot L & \text{if } R_2 \geq ST \end{cases} \dots \dots \dots 3.56$$

$$\text{With } X = [X_1, X_2 \cdots X_i \cdots X_n]^T, X_i = [X_{i,1}, X_{i,2} \cdots X_{i,d}] \dots \dots \dots 3.57$$

Where:  $X_{i,j}^t$  indicates the sparrow's position and that of the  $i$ th sparrow in the  $j$ th dimension,  $t$  denotes the current iteration number,  $\alpha$ : is a random number  $\in (0,1]$ ,  $\text{iter}_{max}$  represents the maximum number of iterations,  $Q$ : is a random number that follows a normal distribution,  $L$ : represents a  $1 \times d$  matrix with all elements equal to 1,  $R_2$ : is the warning threshold  $\in [0,1]$ ,  $ST$  is the safety threshold  $\in [0.5,1]$ . When  $R_2 < ST$ , the sparrow does not find the predator and the engaged sparrow carries out various searching behaviors. If  $R_2 \geq ST$  indicates that a few sparrows have found the predator, the discoverer must direct the colony to a safe location to forage. The variance in the finder's position's range of values is shown by Equation (3.58).

$$y = \exp\left(\frac{-x}{a \cdot T_{max}}\right) \dots \dots \dots 3.58$$

Where:  $y$  indicates the range of value fluctuation for the finder's position, and  $x$  indicates the iteration time. As  $x$  grows larger,  $y$  gradually narrows from

(0,1) to around (0,0.3). When  $x$  is less, the likelihood that  $y$  takes on a value near 1 is greater, and as it rises, the distribution of  $y$  value becomes more uniform. If  $R2 < ST$ , the band of value fluctuation for every dimension of the sparrow becomes narrower. This search technique makes the SSA exceptionally competent in local search, but it also causes a tendency to fall back on local optimum solutions in the last rounds.

**Step 3:** Because sparrows have a smart anti-predation behavior that helps them avoid predators, so after the population's position has been updated a few sparrows are chosen as scouts (exploration) who are in charge of identifying and alerting others. Typically, they comprise 10–20% of the entire population. Scroungers may discover the best food sources by following producers, and certain scroungers are continually monitoring producers for new food sources. The following is an explanation of the scrounger's position update formula:

$$X_{i,j}^{t+1} = \begin{cases} Q \cdot \exp\left(\frac{X_{\text{worst}}^t - X_{i,j}^t}{i^2}\right) & \text{if } i > n/2 \\ X_P^{t+1} + |X_{i,j}^t - X_P^{t+1}| \cdot A^+ \cdot L & \text{if } i \leq n/2 \end{cases} \dots\dots\dots 3.59$$

Where:  $X_{\text{worst}}^t$ : shows the worst location of the  $t$ -generation sparrow populations,  $X_P^{t+1}$ : represents the optimal position held by the producer,  $A^+$  represents a  $1 \times d$  matrix with every element selected at random 1 or -1,  $A^+ = A^T(AA^T) - 1$ . When  $i > n/2$  The sparrow could not find food and had to relocate. When  $i \leq n/2$  the sparrow traveled to the current optimum location to obtain more food. According to rule (6), the mathematical model can be expressed as follows.

$$X_{i,j}^{t+1} = \begin{cases} X_{\text{best}}^t + \beta \cdot |X_{i,j}^t - X_{\text{best}}^t| & \text{if } f_i > f_g \\ X_{i,j}^t + K \cdot \left(\frac{|X_{i,j}^t - X_{\text{worst}}^t|}{(f_i - f_w) + \varepsilon}\right) & \text{if } f_i = f_g \end{cases} \dots\dots\dots 3.60$$

Where:  $X_{\text{best}}^t$  represents the optimum position of the sparrow population,  $K$  is a random number  $\in [-1,1]$ ,  $\beta$  represent a random number that follows the conventional normal distribution,  $f_i$ : is the current sparrow individual's fitness value,  $f_g$ : is the best fitness value for the present area,  $f_w$ : is the worst fitness value for the present area,  $\varepsilon$  is a lower number that prevents the denominator from becoming zero,  $f_i > f_g$ : shows that this sparrow isn't optimally situated in the present foraging region. When in danger, it moves near the optimum location, when  $f_i = f_g$  indicates that sparrows in the center of the population are aware of the risks and need to stay near other sparrows to limit their danger of being caught.

**Step 4:** Each individual's location is compared to the final repeat. An update is performed if the new position is superior to the prior one and the position is kept the best. Some sparrows' survival rates may improve following the final two steps.

**Step 5:** If the number of repeats is less than the maximum, proceed to step 2. Otherwise, the process ends, and the best answer is obtained.

**Summary:** The discoverer finds the food and spreads the information about its location to the entire sparrow population. In contrast, the follower follows the producers in forages to find and get the food. Every sparrow will observe the conduct of the other individuals in the group. When the sparrows have a significant intake in the group, their attackers compete with them for food, increasing their predation rate. If danger approaches, the monitor will immediately sound an alarm. Once the alarm signal hits a certain threshold, they stop foraging, and the entire population will follow the finder, and the colony will transfer to a new location.

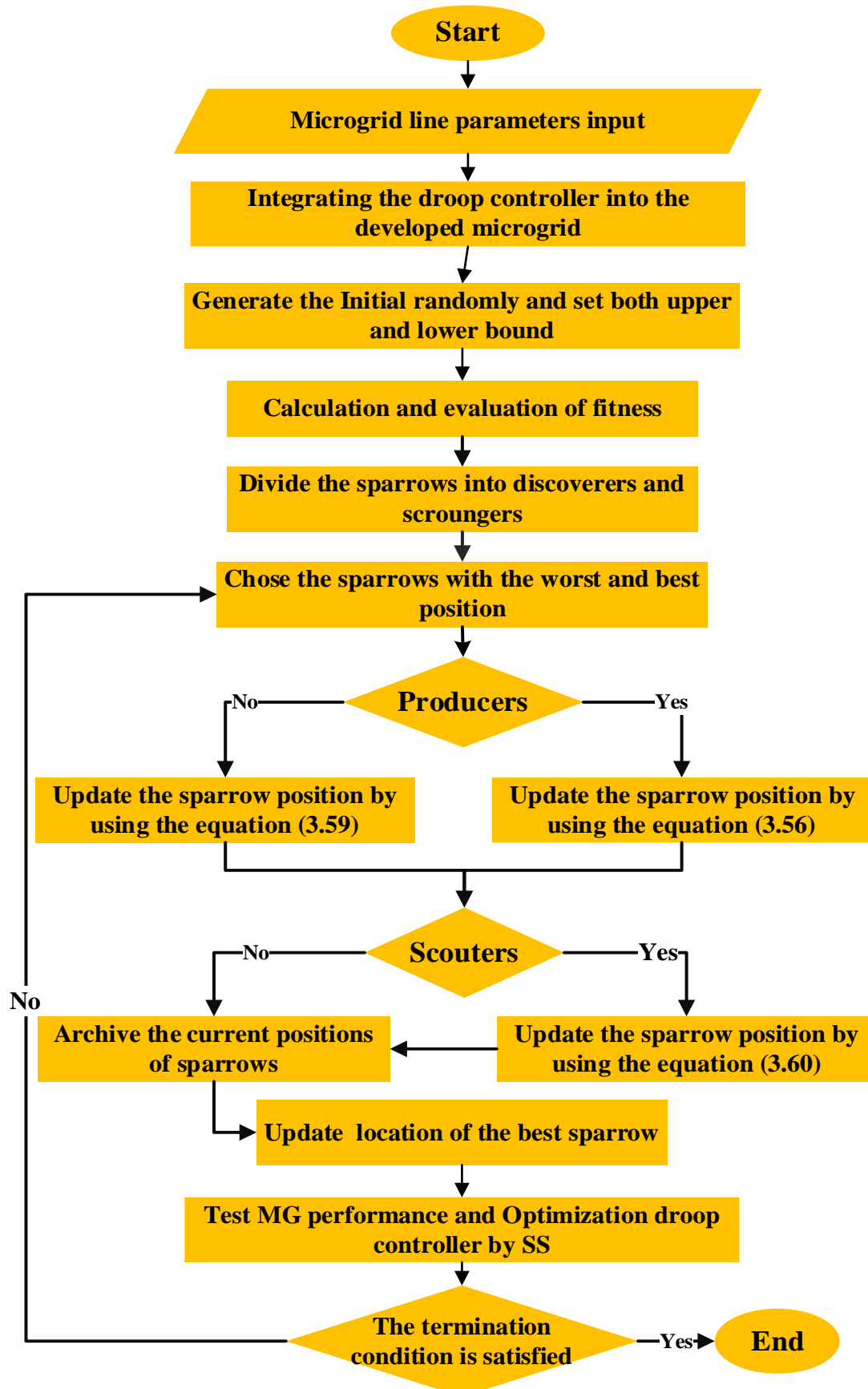


Figure 3-14 Flowchart Sparrow Search Algorithm

### Summary

**Table 3-1 Comparison between SMA, SCA, and SSA.**

Factor	SMA	SCA	SSA
Biological Inspiration	Simulates the behavior of slime mould in searching for food and adapting to the environment	Inspired by sine and cosine functions to simulate exploration and exploitation	Inspired by the behavior of sparrows in foraging and avoiding predators
Algorithm Type	Nature-inspired metaheuristic optimization	Mathematical function-based metaheuristic optimization	Swarm intelligence-based metaheuristic optimization
Search Mechanism	Balances exploration and exploitation by mimicking the expansion of slime mould toward food sources	Uses sine and cosine functions to control movement between potential solutions	Uses two types of sparrows: explorers (scouts) and producers/scroungers for food search
Exploration Strategy	Moves based on simulated pheromone intensity	Uses sinusoidal functions to control search movement	Birds explore search space through collective flight behavior
Exploitation Strategy	Effectively utilizes previously visited paths to improve solution accuracy	Balances exploration and exploitation through sine-cosine function control	Shifts from exploration to exploitation based on resource distribution and predator presence
Balance Between Exploration and Exploitation	Strong balance between exploration and exploitation	Moderate	Moderate
Adaptability to Environment	High	Low	High
Ability to Avoid Local Optima	Good ability to avoid local optima (High)	Good for initial random search (Moderate)	Reduces the probability of getting trapped in local optima (High in early iterations )
Ease of Implementation	Medium	Easy	Medium
Convergence Rate	Moderate to fast convergence rate	Moderate to slow convergence rate in some cases	Fast convergence rate compared to other algorithms
	May be slow initially when broader exploration is needed	It may require an improved transition between exploration and exploitation	Requires careful parameter tuning for optimal performance
Advantages	Performs well in nonlinear optimization problems	Relies only on mathematical functions, reducing computational complexity	Dynamic and adapts to changing environments

# CHAPTER FOUR: RESULTS AND DISCUSSION

## CHAPTER Four:

**Results & Discussion****4.1 Case Studies and Proposed Test System**

In this chapter, the performance to achieve the optimal droop controller based on a PI controller obtained utilizing metaheuristic optimization algorithms: SMA, SCA, and SSA, compared to the conventional droop control, in minimizing the deviations in frequency and voltage of a microgrid is discussed. This study's relevant data is presented in four case studies: island mode, transition of the operation mode, load change mode, and equal load. The microgrid was modeled and simulated in MATLAB/Simulink, and the output of the metaheuristic optimization algorithms controller is compared with the PI controller without optimization, as stated in Chapter 2, using the parameters shown in Table (2-1). Table (4-1) illustrates the parameters PI obtained from optimization.

**Table 4-1 PI control parameters.**

Methods	Control Parameters			
	$k_{pv}$	$k_{iv}$	$k_{pf}$	$k_{if}$
Conventional -PI	10	100	10	100
SSA -PI	9.754	141.8863	9.754	141.8863
SCA-PI	10.1556	71.4183	10.1556	71.4183
SMA-PI	13.5812	92.6527	92.6527	13.5812

**4.1.1 Results of change in microgrid operation mode****4.1.1.1 Analysis of voltage and frequency regulation**

A Microgrid System can operate in two primary modes: grid-connected and islanded. The MGS generally changes its operation mode due to scheduled maintenance or unexpected faults in the main power grid. However, in both situations, the MGs must maintain a steady and reliable supply by regulating the frequency and voltage of the consumers.

Figures (4-1 and 4-2) show the simulation results obtained from the proposed controller for regulating frequency and voltage during the microgrids' operation mode transition. However, as shown in Figure (4-1), all controllers start at a frequency below 49.8 HZ, which shows a transient response when adjusted to reach the desired frequency around 50 HZ.

A significant frequency deviation is observed across all control methods at the initial period ( $t = 0\text{s}$  to  $0.5\text{s}$ ). This deviation likely represents a disturbance or the system's attempt to stabilize. It is noted that the SMA-PI method achieves the fastest stabilization and the least overshoot, effectively suppressing oscillations and converging to 50HZ compared to the other methods. The PI-traditional controller shows an overshoot above 50.05HZ before quickly stabilizing near 50HZ. The SSA-PI method exhibits slower stabilization with more significant oscillations. In contrast, the SCA-PI method demonstrates better transient performance than the SSA-PI method, with smaller overshoot and faster stabilization toward 50HZ.

At the period ( $0.5\text{s}$  to  $2\text{s}$ ), all control methods begin stabilizing the frequency around the nominal value of 50 HZ, with some slight differences. Although stabilizing near 50, the PI-traditional controller exhibits noticeable oscillations, indicating less effective damping. In contrast, the SSA-PI method continues to show oscillations. The SCA-PI method demonstrates smaller oscillations than the SSA-PI method, indicating improved stability. The SMA method, however, keeps the frequency very close to 50HZ with minimal oscillations, reflecting excellent stability and rapid convergence.

All control methods converge near 50HZ over period ( $2\text{s}$  to  $5\text{s}$ ). The SMA-PI method demonstrates the best performance, with minimal oscillations compared to the other methods.

Also, observe the figure's frequency deviation values for each control method. The SMA-PI shows a frequency deviation of 0.05HZ from the nominal

frequency, while the SCA-PI method exhibits a deviation of 0.1HZ, and the SSA-PI shows a deviation of 0.15HZ; in contrast, the PI without optimization method results in a deviation of 0.25 HZ, all these values fall well within the acceptable deviation range ( $\pm 0.5$  Hz) while dealing with microgrids. Comparing these values, we notice that the PI-traditional controller demonstrates the highest frequency deviation, making it the least efficient in maintaining frequency stability. On the other hand, the SSA-PI method shows a noticeable improvement compared to the PI-traditional controller, resulting in less severe oscillations, although they remain relatively prominent. However, The SCA-PI method performs better than the SSA-PI and the PI-traditional controller, providing faster stability and significantly reducing oscillations, thereby enhancing control performance. The SMA-PI method demonstrates the best performance among all the systems, as it combines exploratory and exploitative performance, delivering an extremely stable and rapid response with the lowest level of oscillation.

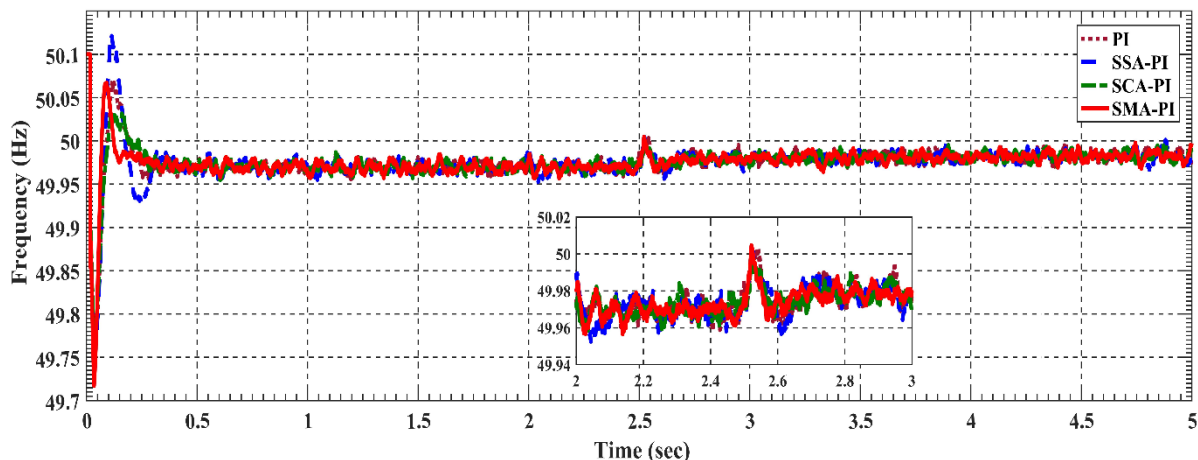
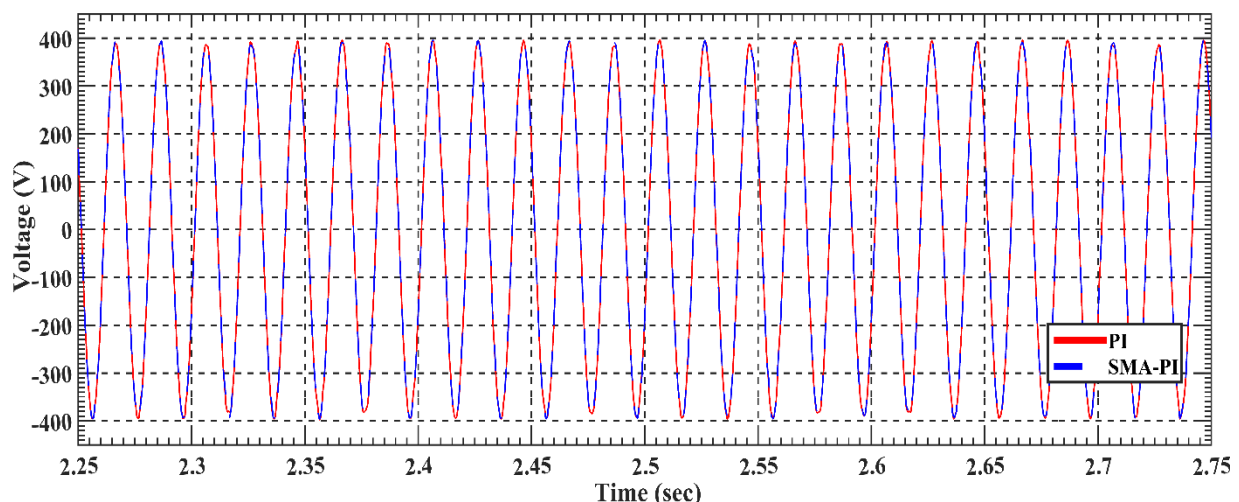


**Figure 4-1 System Frequency Response During Change MG Operation Mode.**

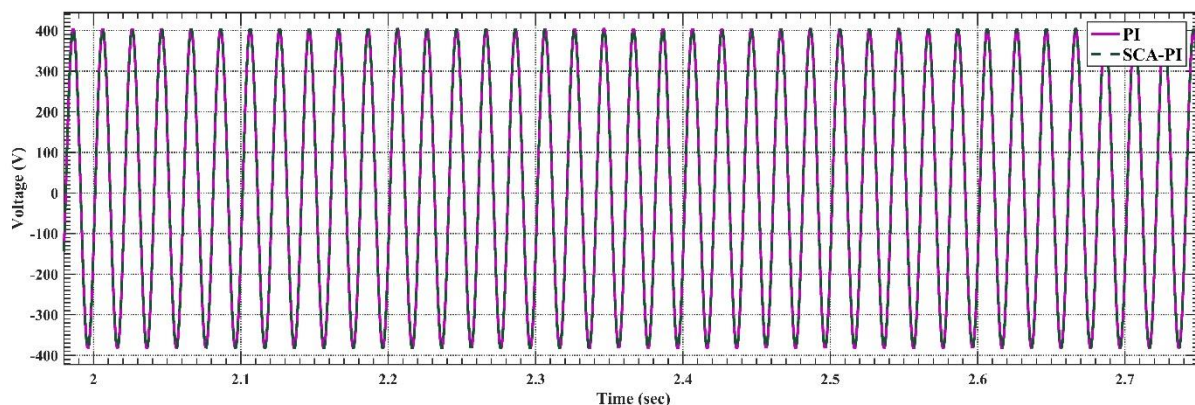
Figure (4-2 a) shows that the voltage waveforms for both techniques are sinusoidal, oscillating between (-400 and +400). However, there are slight differences in smoothness and amplitude. The voltage waveform of the SMA-PI appears smoother compared to that of the PI-Conventional Controller, indicating reduced oscillations caused by switching the microgrid between its modes.

Additionally, it minimizes ripple disturbances. This results in a purer signal, improving voltage quality and stability.

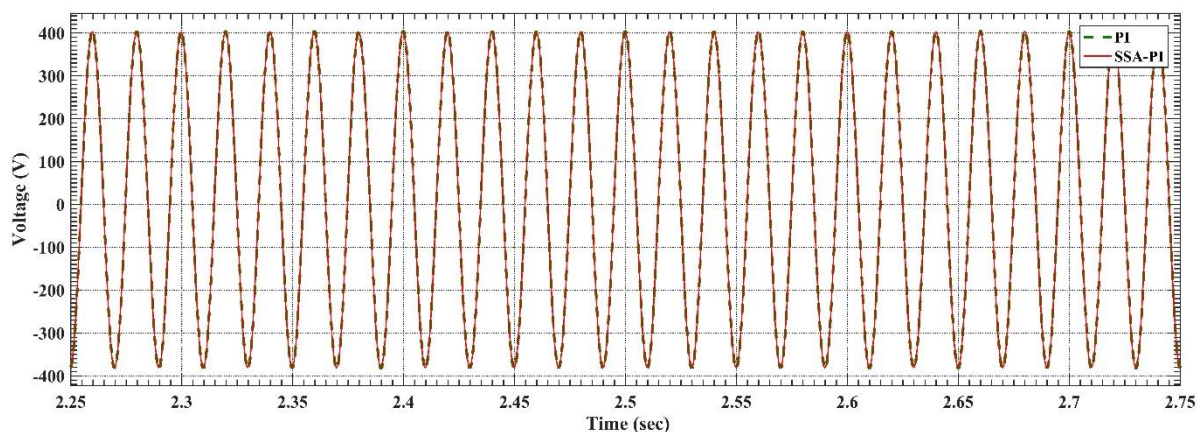
In contrast, the PI-Conventional Controller shows sharp transitions in voltage during the switching of the microgrid modes, albeit slightly. This reflects its reactive nature without additional filtering, leading to higher oscillations. While this indicates a faster response, it compromises voltage quality. We also observe from Figure (4-2 b,c) that the SCA-PI, SSA-PI, and PI-conventional controllers maintain voltage stability over time. All methods show identical waveform shapes, which indicates similar system performance and improvements being minor or not visible. We notice no significant changes in the waveform, suggesting the switching process was carried out smoothly.



(a)



(b)



(c)

**Figure 4-2 System Voltage Response During Change MG Operation Mode.**

#### 4.1.1.2 Analysis of active power and reactive power

From Figure (4-3a, b), active power increases rapidly at the initial time ( $t = 0$ ), indicating an overshoot. The magnitude of the overshoot and its stabilization vary depending on the control method used. The SMA-PI method exhibits the lowest overshoot compared to the other methods, while the SSA-PI shows the highest overshoot. The PI- traditional control method and the SCA-PI demonstrate moderate levels of overshoot. As for the reactive power at this time, it also shows an overshoot. However, the SMA-PI method stabilizes faster than other methods, reaching a steady state faster with minimal oscillations. This indicates lower fluctuations in reactive power after the initial transient period, reflecting better stability and performance. On the other hand, the PI-conventional controller exhibits slower response times and higher oscillations.

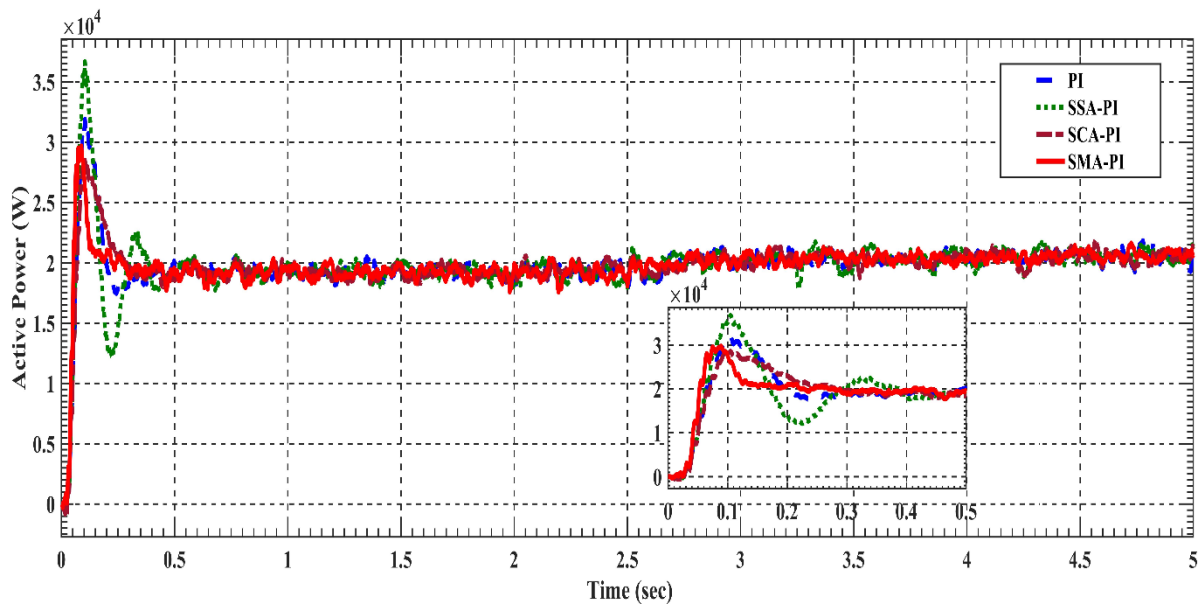
At the period ( $t=0.5s$ ), the active power stabilizes across all control methods, transitioning to a more stable performance. The SMA-PI method demonstrates the most stable performance, with minimal oscillations after stabilization, achieving a steady state more quickly and smoothly than the other methods. The SSA-PI method shows greater oscillations and slower damping compared to the different approaches, and although it achieves a faster rise time compared to the

SMA-PI, it suffers from a higher overshoot. The PI-traditional controller exhibits moderate performance but still shows some oscillations. The SCA-PI method, on the other hand, achieves a balanced performance between overshoot and stability. At this time, the reactive power exhibits continuous oscillation and does not stabilize with the PI- conventional controller, although it attempts to move toward stability. In the SSA-PI method, reactive power shows oscillation, but it is less severe than with the PI-conventional controller, appearing closer to stabilization. The SCA-PI method demonstrates greater stability than the SSA-PI method and the PI-conventional controller, though it still experiences some fluctuations. The reactive power in the SMA-PI method appears at values closer to the stable state than the other methods.

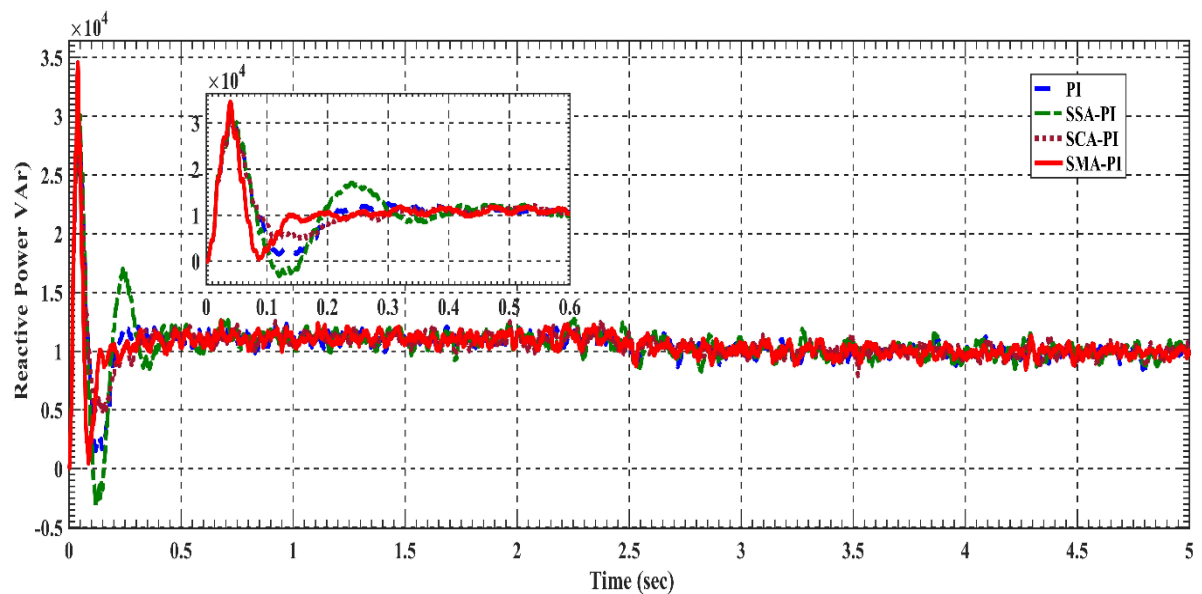
After period ( $t=0.5$  s) seconds, the power achieves noticeable stability, with minor oscillations. However, there is no significant change in the power value across all control methods. This indicates that the system operates without any significant deviations or fluctuations. After this time, the reactive power does not exhibit full stability and continues to oscillate slightly around the steady-state value in the case of the PI-conventional controller. The SSA-PI method shows moderate stability in reactive power. In the SCA-PI method, the system is almost stable now, achieving a nearly constant state for reactive power. In the SMA-PI method, oscillations are negligible at this time, and the reactive power remains at its steady value.

As for load sharing and power sharing, the PI-conventional controller is the least efficient method in terms of load sharing and power sharing. It simplistically distributes the load without considering dynamic improvements, leading to uneven load distribution and failing to achieve balanced allocation or appropriate dynamic response. In the SSA-PI method, load distribution occurs more quickly; however, high oscillations may result in unstable loads on some sources. The SCA-PI method demonstrates a more balanced distribution of power sharing. The

SMA-PI method is considered the best for power sharing, as it achieves higher efficiency, better stability, and minimal oscillations in load distribution.



(a)



(b)

**Figure 4-3 (a) Analysis Active Power (b) Analysis Reactive Power During Change MG Operation Mode.**

**Table 4-2 Optimization of objective functions in different modes.**

Mode	Methods	Rise time (sec)	Overshoot%	settling time (sec)
Transition	Conventional -PI	0.4110	0.2352	0.497561
	SSA-PI	0.4801	0.3151	0.497929
	SCA -PI	0.4059	0.2325	0.497453
	SMA-PI	0.3958	0.2247	0.497060
Islanded	Conventional -PI	0.4972	0.2624	0.497618
	SSA-PI	0.4976	0.3536	0.497429
	SCA -PI	0.4915	0.2602	0.497544
	SMA-PI	0.4243	0.2324	0.497025
Load change (equal load)	Conventional -PI	0.4936	0.2025	0.498165
	SSA-PI	0.4948	0.2938	0.498041
	SCA -PI	0.4877	0.2030	0.498231
	SMA-PI	0.4864	0.2005	0.497659
Load change (increase load)	Conventional -PI	0.4977	0.2805	0.497349
	SSA-PI	0.4931	0.3364	0.497242
	SCA -PI	0.4830	0.2693	0.497391
	SMA-PI	0.4554	0.2600	0.496812

## 4.1.2 Results of islanded microgrid operation mode

### 4.1.2.1 Analysis of voltage and frequency regulation

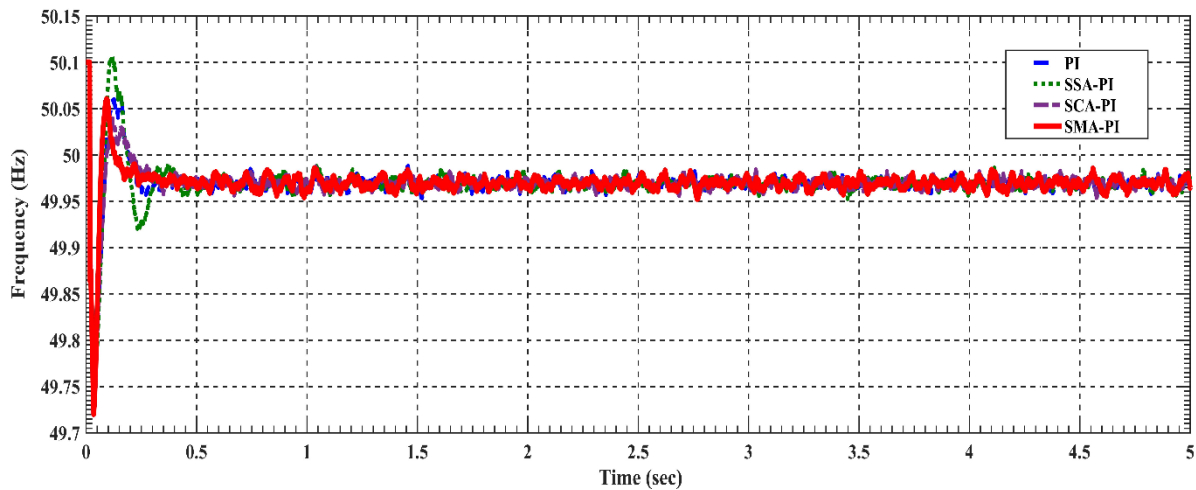
During islanded operation, a microgrid's frequency and voltage may fluctuate rapidly due to a power imbalance between supply and demand. The microgrid's DG units lack the necessary fast response characteristics to stabilize the frequency adequately. The microgrid's dynamic behavior in the islanded mode was analyzed.

Figure (4-4) shows the microgrid frequency. During the test period, at the initial period ( $t=0s$  to  $0.5s$ ), the system exhibits a significant initial deviation from the nominal frequency of 50 Hz due to a transient disturbance, causing a frequency drop. All applied control techniques demonstrate varying capabilities in damping oscillations and returning to the steady-state frequency. The SSA-PI method shows large initial oscillations, indicating weaker control during disturbances. It exhibits the highest overshoot, slowest damping, and clear instability, reflecting poor performance when handling sudden loads in this scenario. The SCA-PI method performs relatively well, showing fewer

oscillations than the SSA-PI method but slightly more than the SMA method. The PI-conventional controller performs better than the SSA-PI method but worse than the SCA-PI and SMA-PI methods, reflecting the moderate efficiency of traditional tuning techniques. The SMA-PI method provides the smoothest and fastest stabilization, reducing oscillations quickly and approaching the nominal frequency of 50 Hz more efficiently. It outperforms the other techniques in minimizing transient deviations and maintaining steady system performance. It demonstrates a faster response with minimal overshoot and quicker damping of oscillations.

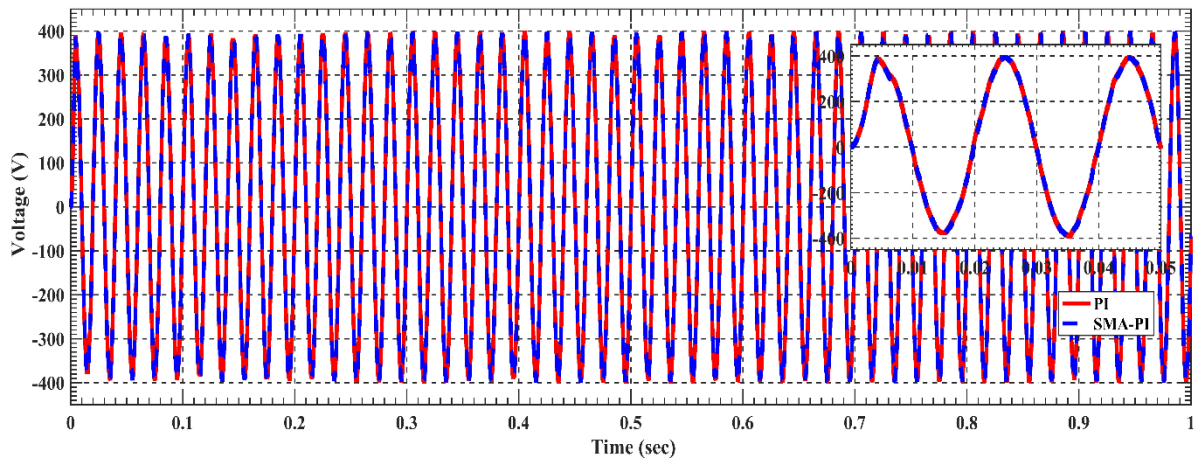
At 1.5s, all control techniques achieve stability. However, the SMA-PI method exhibits superior suppression of high-frequency oscillations and smaller steady-state error, achieving a stable frequency near the nominal value faster than other methods due to its shorter settling time. This highlights better tuning of controller parameters. The SSA-PI and SCA-PI methods take longer to stabilize, indicating they are less effective in mitigating system dynamics in this scenario. The PI-conventional controller achieves moderate stabilization time, which remains acceptable but suggests that traditional tuning methods may not fully address complex system dynamics.

After 1.5s, the SSA-PI method continues to exhibit higher-frequency oscillations even after the transient period, indicating suboptimal tuning for steady-state conditions. It suffers from the largest fluctuations even in the steady state, reflecting poor performance in frequency regulation. The SCA-PI method and PI-conventional controller both exhibit noticeable but improvable oscillations and perform better than the SSA-PI method under steady-state conditions. The SMA-PI method demonstrates the smoothest response with minimal oscillations, achieving the best stability with very small fluctuations around the nominal frequency of 50 Hz.

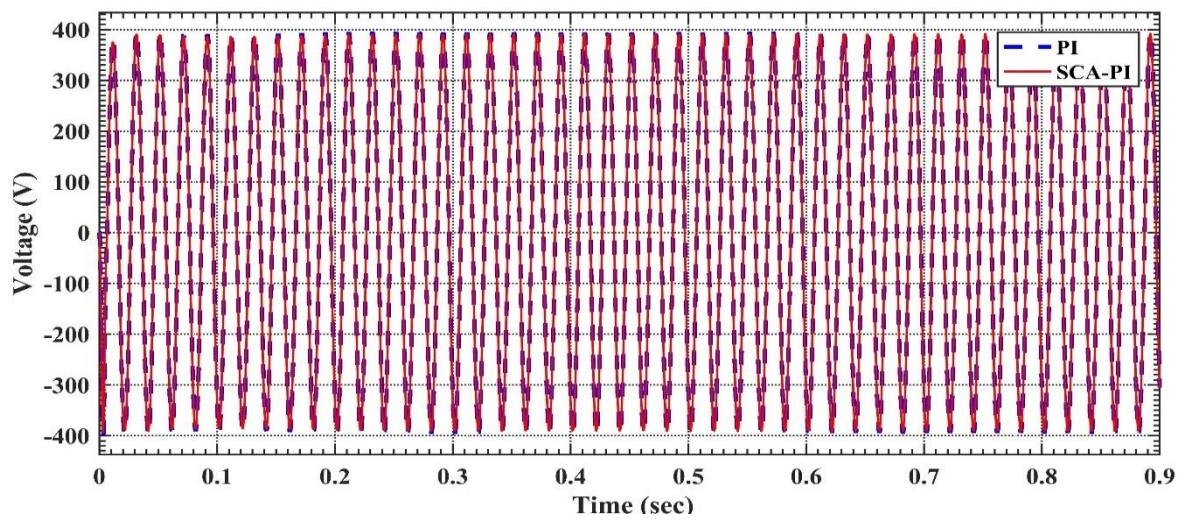


**Figure 4-4 System Frequency Response During Islanded MG Operation Mode.**

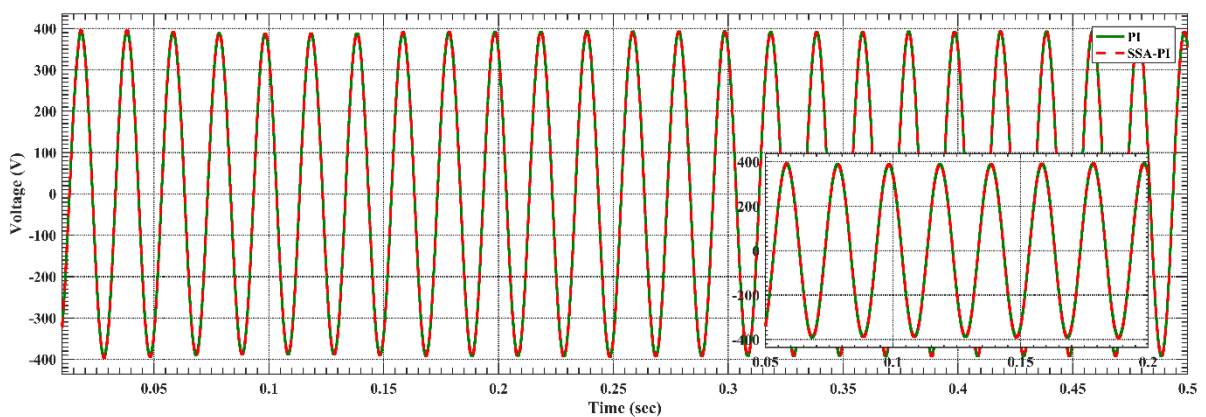
The islanded mode of a microgrid requires precise control because any changes in load or power generation significantly affect voltage stability. From Figure (4-5), it can be observed that with the PI-conventional controller method, the voltage appears noticeably oscillatory, with some deviations at the peaks and troughs. This method may not be sufficient to reduce disturbance or handle rapid changes in load or energy imbalance in the islanded mode of the microgrid. In contrast, the SMA-PI method demonstrates a more stable and smoother response, with a clear oscillation reduction. This smoothness indicates a better capability to mitigate the impact of dynamic changes, maintaining voltage stability under system fluctuations. Figure (4-5b) shows that the SCA-PI in the islanded mode slightly improves compared to the PI- conventional controller, as the voltage appears smoother in certain areas, indicating better voltage stability. Figure (4-5c) shows that the two systems are identical, achieving good voltage stability.



(a)



(b)



(c)

**Figure 4-5 System Voltage Response During Islanded MG Operation Mode.**

### 4.1.2.2 Analysis of active power and reactive power

Figure (4-6a, b) shows the waveform active and reactive power. At the period ( $t= 0s$  to  $0.5s$ ), the system experiences a sharp increase in active power due to load changes and grid conditions. The PI-conventional controller exhibits significant oscillations before stabilizing, while the other techniques greatly reduce these oscillations. The SMA-PI method demonstrates faster and more efficient stabilization in reducing oscillations, making it ideal for microgrid applications in islanded mode. At this time, the reactive power increases for all methods. It is observed that the SSA-PI method shows high initial oscillations and appears less stable compared to other methods, with a significant overshoot before starting to decrease. In contrast, the SMA-PI method stabilizes faster, with reduced oscillations and steady behavior near zero. The PI-conventional controller shows slightly higher oscillations than the SMA-PI method but remains more stable than the SSA-PI approach. The SCA-PI method demonstrates performance similar to the PI- conventional controller but with slight overall stability and efficiency improvements. The sources may experience a sudden surge, leading to high oscillations. The PI-conventional controller exhibits slower adaptation, resulting in power mismatches and inefficient load sharing. In contrast, the optimized SMA-PI strategy ensures smoother load transitions, reduces stress on the sources, and prevents overloading, enabling more reliable system performance.

At the period ( $t= 0.5s$  to  $1s$ ) second, most control techniques converge toward the required steady-state power value. The SSA-PI method shows noticeable instability with significant oscillations compared to other techniques. Reactive power at this time, with the PI-conventional controller, reactive power reaches a relatively stable state, though some oscillations persist around the steady-state value. In the SSA-PI method, oscillations in reactive power continue, albeit with a slow reduction in amplitude, keeping the technique far from

---

achieving stability compared to other methods. The SCA-PI method reduces oscillations to a minimal level, bringing reactive power closer to steady-state conditions.

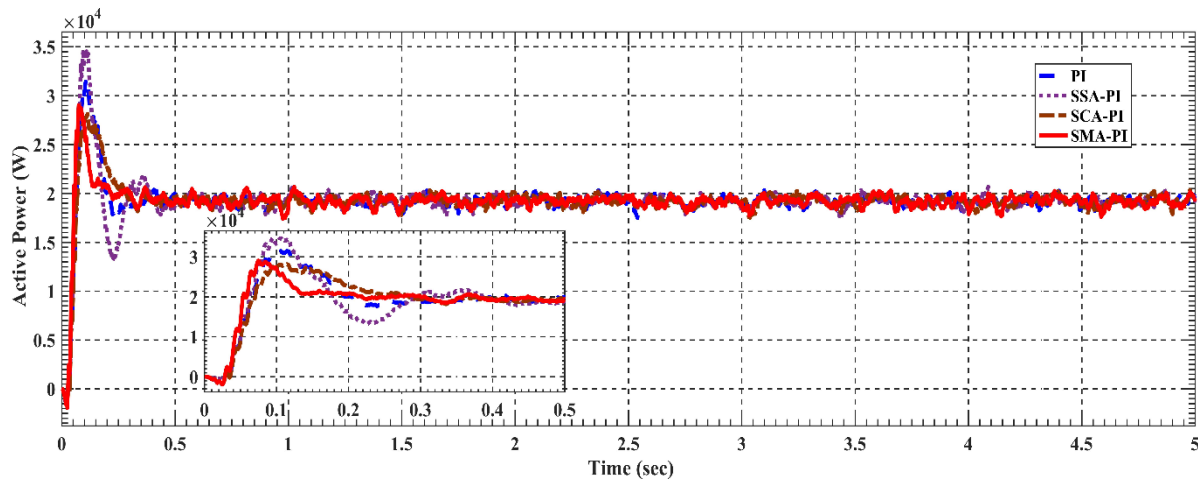
Meanwhile, the SMA-PI method achieves complete stabilization of reactive power, reaching the steady-state condition much faster than all other strategies. After 1s, active and reactive power achieve relative stability across all strategies. The system stabilizes, but the oscillation level varies depending on the control strategies. The SSA-PI and SCA-PI still show some instability, which may result in uneven load sharing or increased stress on certain sources. This highlights the need for more robust control strategies to ensure a balanced and reliable operation during this period.

Overall, the PI-conventional controller proves less effective than the optimized strategies, showing long-term oscillations. Both the SCA-PI and SSA-PI methods deliver acceptable performance but experience larger oscillations than the SMA-PI method.

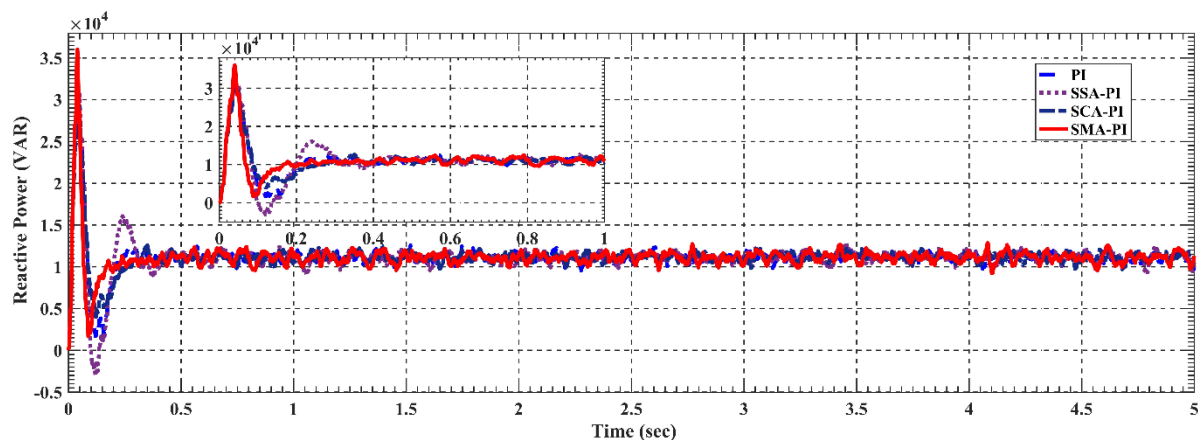
In the islanded mode of a microgrid, distributed generators must operate together to meet the load demand. Control strategies directly affect how these sources share the load, as poor control can lead to uneven load distribution, causing some units to become overloaded. Effective strategies ensure proportional load sharing, where each source contributes based on capacity, improving system efficiency and reliability. From the observed dynamics of active power sharing, it is clear that deviations from nominal values are managed differently depending on the control strategy applied. The SMA-PI method achieves efficient load distribution and faster stabilization, reducing the strain on individual sources.

Regarding source interaction, control strategies influence how sources respond to varying load conditions. The PI-conventional controller often

struggles to adapt quickly to sudden changes, resulting in prolonged overshoots. In contrast, the SMA-PI method handles load variations more effectively by dynamically adjusting control parameters, ensuring all sources remain synchronized and balanced under different loading scenarios.



(a)



(b)

**Figure 4-6 (a) Analysis Active Power (b) Analysis Reactive Power During Islanded MG Operation Mode.**

### 4.2.3 Results of load change (equal load)

#### 4.2.3.1 Analysis of voltage and frequency regulation

This system used four loads with different values, as shown in the table. When these loads were equalized to the value of the first load, the results were depicted in Figure (4-7). Figure (4-7) shows that the initial frequency

significantly drops below the nominal value of 50 Hz due to load disturbances and changes in their values, disrupting the microgrid. Subsequently, the system recovers and stabilizes over time.

Upon analyzing the control strategies, observed that the PI-conventional controller showed a slight drop in frequency between ( $t=0s-0.2s$ ) before gradually improving. The SSA-PI method shows a sharp drop with strong oscillations. SCA-PI shows a mild frequency drop, less severe than the SSA-PI method. The SMA-PI method demonstrates the best response among all strategies, with faster recovery and better stabilization. During the transitional period ( $t= 0.1s - 0.5s$ ), the system's behavior with Using the PI-conventional controller, the system experiences moderate oscillations but gradually approaches the nominal value of 50 Hz. With the SSA-PI method, the system shows significant oscillations during the transition ( $t=0.1s - 0.5s$ ), with a noticeable delay in damping disturbances. The SCA-PI method results in relatively fewer oscillations than the SSA-PI method during the transition ( $t= 0.1s- 0.5s$ ). However, the system still shows some fluctuations before nearing stability. The SMA-PI method demonstrates superior performance, with the least oscillations compared to other methods and a very fast return to the nominal value, achieving stability during the transitional period ( $t= 0.1- 0.3s$ ).

After each transitional period, the system begins to stabilize, with the degree of stability and the level of oscillations varying depending on the control strategy used.

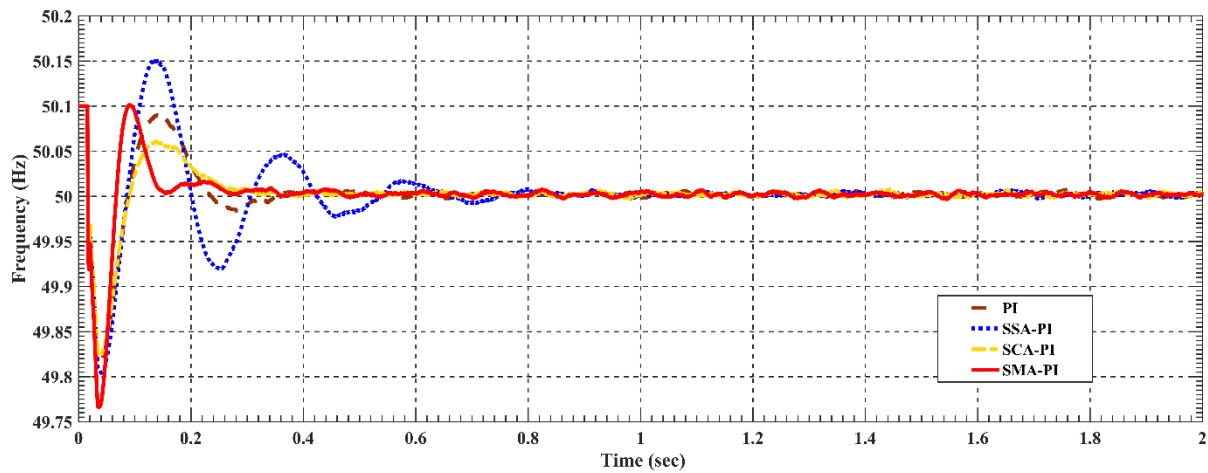
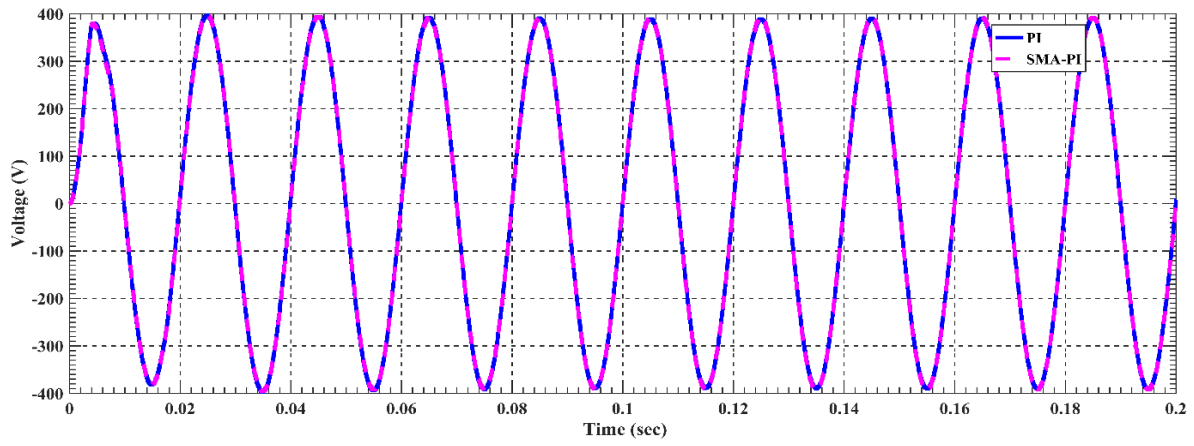
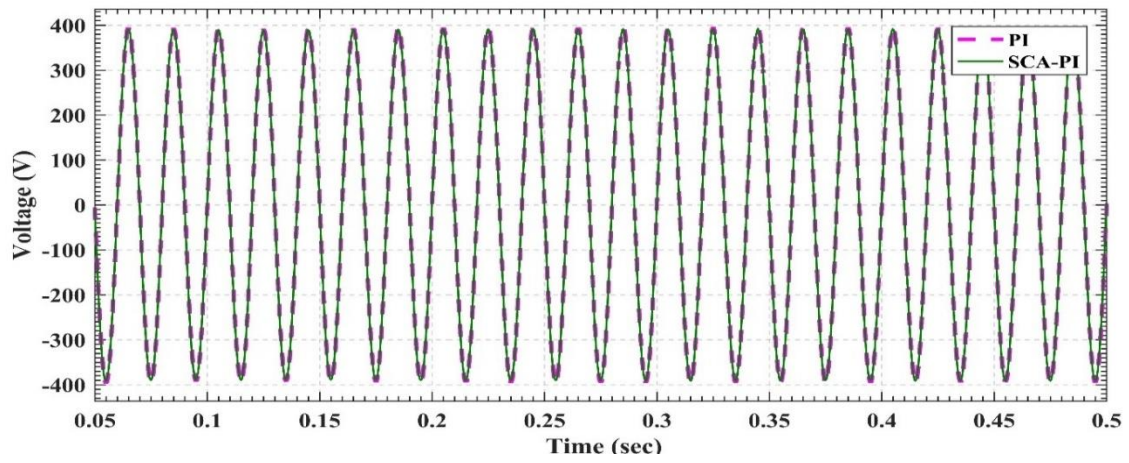


**Figure 4-7 System Frequency Response during equal loads.**

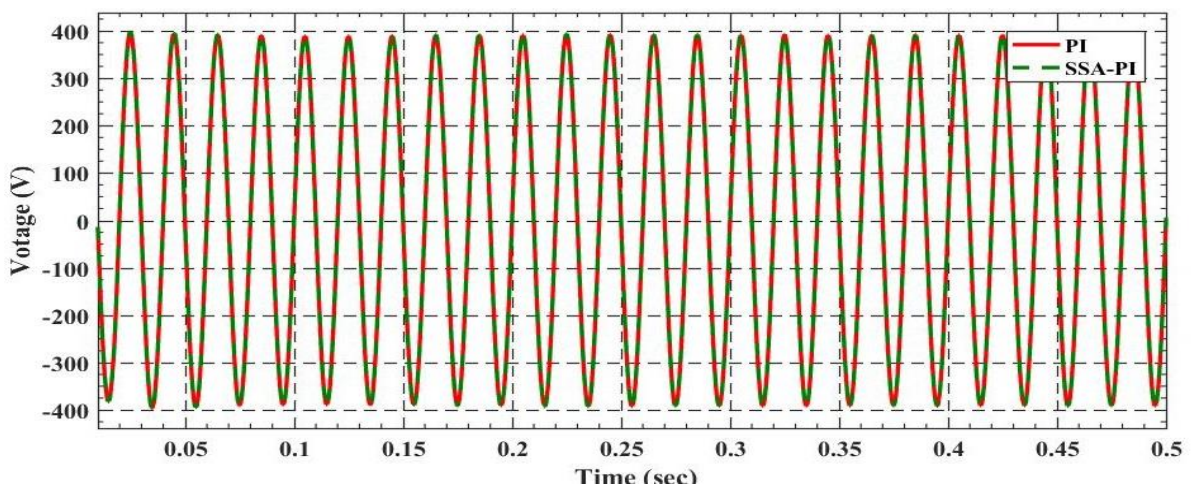
In this scenario and from Figure (4-8a, b,c), each power source operates steadily when all loads are equal, reducing voltage variations and ensuring balanced energy distribution. The figure shows that the sinusoidal waveform is regular, without distortions or abnormal peaks, indicating high power quality in the grid. This is a positive indicator of system performance, demonstrating that the voltage in the grid remains stable and balanced at all time points. This stability signifies that the microgrid is functioning effectively with load balance and sufficient energy supply for each system part. When comparing all the methods, it is evident that the voltage waveform is identical, which indicates that the improved system using the SMA-PI, SCA-PI, and SSA-PI techniques does not fundamentally alter the resulting waveform. However, it may enhance dynamic characteristics such as stability or response. In conclusion, the load balancing scenario demonstrated by the simulation represents an ideal state for voltage, showcasing optimal grid performance.



(a)



(b)



(c)

Figure 4-8 System Voltage Response During Equal Loads.

### 4.2.3.2 Analysis of active power and reactive power

From Figure (4-9), observe the dynamic performance of different methods and their impact on active power during the time interval ( $t= 0s - 0.2s$ ). The PI-conventional controller shows a slow response with a gradual increase in active power. It exhibits slightly low oscillations but takes longer to reach the peak active power value. The SSA-PI rapidly increases active power, resulting in a high overshoot exceeding  $3.5 \times 10^4$ . This method exhibits the highest oscillations, making the system less stable in the initial phase. The SCA-PI responds faster than the conventional controller and exhibits lower oscillations than the SSA-PI. However, its oscillations remain higher compared to the SMA-PI method. The SMA-PI method demonstrates excellent performance, balancing response speed and reduced oscillations. It outperforms the other methods by achieving a moderate rise without a significant overshoot of the peak power value. Similarly, during this period, the reactive power experiences significant fluctuations initially, and the nature of these fluctuations varies depending on the control strategy employed. In the PI-conventional controller method, the reactive power suffers from a sharp increase followed by high oscillations, causing the system to take longer to respond and remain far from stability. The reactive power exhibits severe oscillations in the SSA-PI method, forming a high-amplitude wave. In contrast, the SCA-PI method shows a gradual reduction in oscillations faster than the SSA-PI method, with the reactive power approaching stability, though it still experiences moderate oscillations. As for the SMA-PI method, the system demonstrates the best initial response, with the oscillations in reactive power decreasing rapidly and nearing stability. This results in the system achieving better stability compared to the other methods.

At the period ( $t= 0.2s - 0.6s$ ), the active power shows slight oscillations with a slow trend toward stabilization. The performance of different methods during this period is as follows: Using the PI-conventional controller, the active

---

power shows persistent oscillations and a gradual inclination toward stability, highlighting the controller's limited effectiveness in quickly damping oscillations. In the SSA-PI method, active power oscillations persist significantly during this period, indicating considerable difficulty moving toward stability. With the SCA-PI, the active power shows moderate oscillations that gradually decrease. This suggests the system is heading toward stability with better performance than the SSA-PI method. In the SMA-PI method, the active power demonstrates stable behavior.

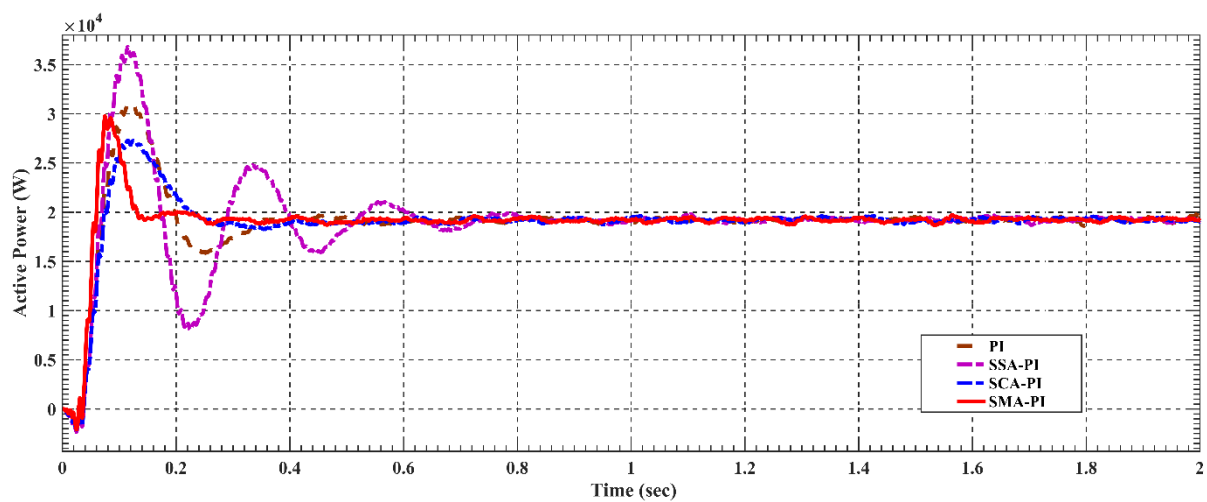
After 0.6s, minimal oscillations were observed compared to the other methods. In the case of the PI-conventional controller, it is also observed that the reactive power continues to suffer from persistent oscillations, leading to a slow system response in reaching a stable state. In the SSA-PI method, oscillations persist with noticeable delays in reducing the amplitude of reactive power. Regarding the SCA-PI method, the reactive power significantly reduces oscillations, resulting in greater system stability. However, it still lags slightly compared to the performance of the SMA-PI method, which achieves near-complete stability in reactive power during this period. At the time interval ( $t=0.8s - 1.2s$ ), the active power starts to approach the steady-state value in the PI-conventional controller. However, it takes longer than other methods, as slight oscillations are still observed. In the SSA-PI method, the oscillation of active power gradually decreases but remains noticeable, indicating that the system does not stabilize effectively compared to other methods. In the SCA-PI method, the system shows significant improvement in stability, with more consistent performance and low oscillations in active power. In the SMA-PI method, the system demonstrates almost ideal performance during this period, as the active power stabilizes and reaches the steady-state value faster than other methods without noticeable oscillations. During this period, it is observed that in the PI-conventional controller method, the oscillations in reactive power gradually

decrease but at a slow rate, leaving the system far from achieving complete stability. In the SSA-PI method, the oscillations in reactive power persist but gradually diminish, showing a slight improvement in the system's performance. However, it does not match the performance of the SMA-PI method. In the SCA-PI method, the oscillations become less severe and approach stability, resulting in good system performance; however, it remains less efficient than the SMA-PI method. In the SMA-PI method, the reactive power reaches a nearly stable state, with oscillations barely noticeable compared to the other methods.

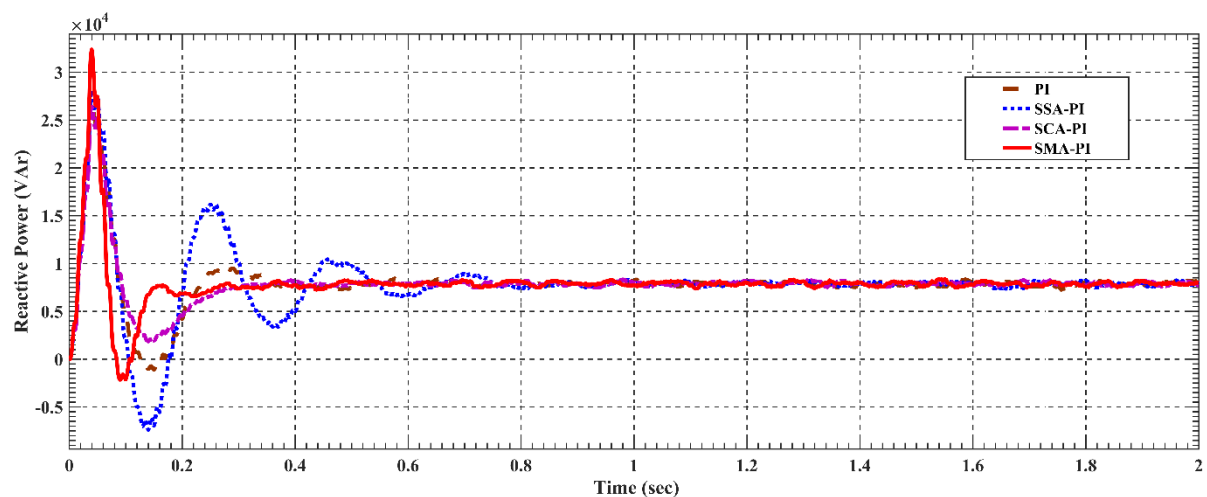
After a period ( $t=1.2s$ ), in the PI- conventional controller method, the active power reaches the steady-state stage but takes a relatively longer time to achieve. This highlights the limitations of traditional control in achieving rapid stabilization compared to other methods. In the SSA-PI method, the system stabilizes gradually; however, the active power still shows slight fluctuations. In contrast, when comparing the system's performance in this method with the SCA-PI and SMA-PI methods, it is evident that this method performs poorly. The system is nearly stable in the SCA-PI method, with a good dynamic response and active power. This method's performance can be considered excellent compared to the PI- conventional controller and SSA-PI methods. Still, it is slightly inferior to the SMA-PI method, as the latter stabilizes earlier within this period. At this time, the conventional controller method utilizing PI shows that reactive power starts to stabilize. Yet, it continues to exhibit minor fluctuations, suggesting that the system is not as efficient when compared to alternative methods. In the SSA-PI method, the reactive power approaches a stable state but still lags, showing less severe oscillations than in previous periods. In the SCA-PI method, the system achieves a nearly stable state. In the SMA-PI method, the reactive power maintains a near-complete state of stability.

Regarding power sharing and load sharing in this scenario, when the distributed loads are equal in value, the burden is shared fairly among the sources.

This reduces stress on any individual source, leading to more efficient resource utilization and minimizing electrical losses caused by unbalanced operations. This also makes it easier for controllers to balance the sources, reducing oscillations and accelerating active and reactive power stabilization. However, if the loads are distributed unevenly, some sources may become overloaded, increasing the probability of failures in the microgrid. This imbalance could also lead to oscillations in the microgrid's voltage and frequency due to the difficulty of matching supply with demand.



(a)



(b)

**Figure 4-9 (a) Analysis Active Power (b) Analysis Reactive Power During equal loads**

## 4.2.4 Results of load change (increase load)

### 4.2.4.1 Analysis of voltage and frequency regulation

In this scenario, two additional loads are introduced to the studied microgrid to test the performance of the developed control techniques during sudden load changes. The first load, with a value of 30KW, is added at a simulation time of 1s, and the second load, with a value of 40KW, is introduced at a simulation time of 2s. This results in a sudden increase in the system's total load.

Figure (4-10) shows that, during the time interval ( $t=0s - 0.1s$ ), there is an initial disturbance in the frequency. In the PI-conventional controller method, the frequency shows fluctuations and a noticeable drop at the start of the disturbance, followed by a sudden rise due to the load increase. In the SSA-PI method, the frequency decreases more significantly than in the PI-conventional controller method, followed by a sharp and rapid growth, resulting in larger oscillations than the other methods. In the SCA-PI method, the frequency drops less than in the SSA-PI method but more than in the PI-conventional controller method, showing an initial attempt at stabilization with relatively lower oscillations. The SMA-PI method has a noticeable initial drop in frequency, but it recovers quickly with the least oscillations compared to the other methods.

At the period ( $t= 0.1s - 0.5s$ ), in the PI-conventional controller method, the frequency oscillates around the nominal frequency of 50 Hz. This method shows medium-range oscillations in frequency and takes longer to achieve stability, with gradual improvement over time. In the SSA-PI method, the frequency shows large oscillations preventing stabilization during this period. Although the response is rapid, the overshoot is excessive and poorly controlled, leaving the frequency unstable for a longer duration compared to other methods. The overshoot gradually decreases in the SCA-PI method, and the frequency

oscillations are less severe than in the SSA-PI method, reflecting better control, though not optimal. The system continues its gradual attempt to reach stability. The SMA-PI method demonstrates the best response during this period. The frequency shows reduced oscillations and achieves stability faster than the other methods.

At the period ( $t=1s$ ), the introduction of the first load causes a noticeable drop in frequency due to the increased power demand in the system. As a result, the system oscillates due to the dynamic impact of the load, which was suddenly introduced to the network. The control methods used for the studied microgrid system differ in their responses to the resulting oscillations. Some methods, such as the SMA- PI algorithm, demonstrate faster performance in damping the oscillations and restoring stability.

At the period ( $t= 1s-2s$ ), at this point, after the oscillation caused by the first load, the frequency gradually returns to its nominal value of 50HZ with variations in response speed and stability depending on the control strategy. At 2s, introducing the second load leads to another frequency oscillation. It is observed that some control techniques used in the studied microgrid system, such as the SSA-PI algorithm, cause more significant frequency oscillations compared to others. In contrast, the SMA-PI algorithm appears more stable and faster in restoring the frequency to its nominal value of 50HZ. The frequency settles slowly in the PI-conventional controller method, but oscillation remains noticeable until the end of the period. In the SSA-PI method, the oscillation continues, but it is less compared to the beginning, taking longer to reach a stable state. The frequency reaches relatively good stability with minor fluctuations in the SCA-PI method. In the SMA-PI method, the frequency is almost constant at 50HZ by the end of this period.

After the time of 2.5 s, almost all control methods begin to achieve frequency stabilization. However, the SMA-PI algorithm remains the best in

terms of faster convergence to the nominal frequency and minimizing oscillations.

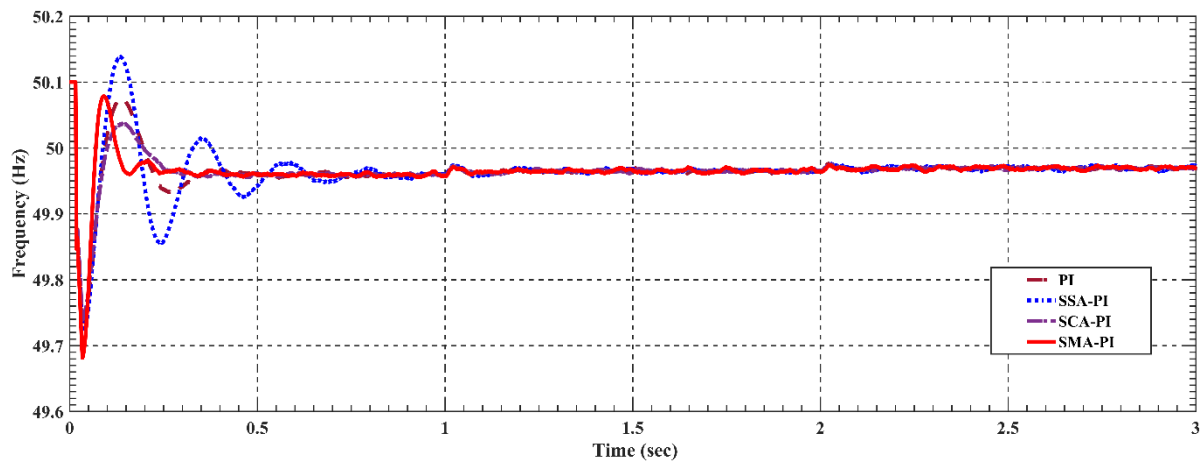
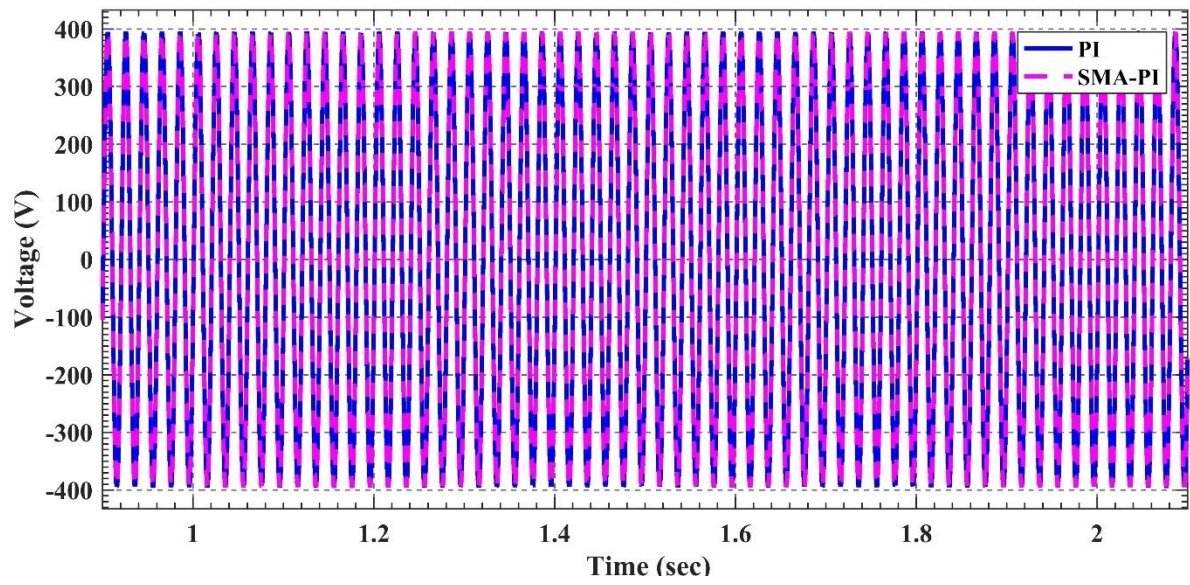
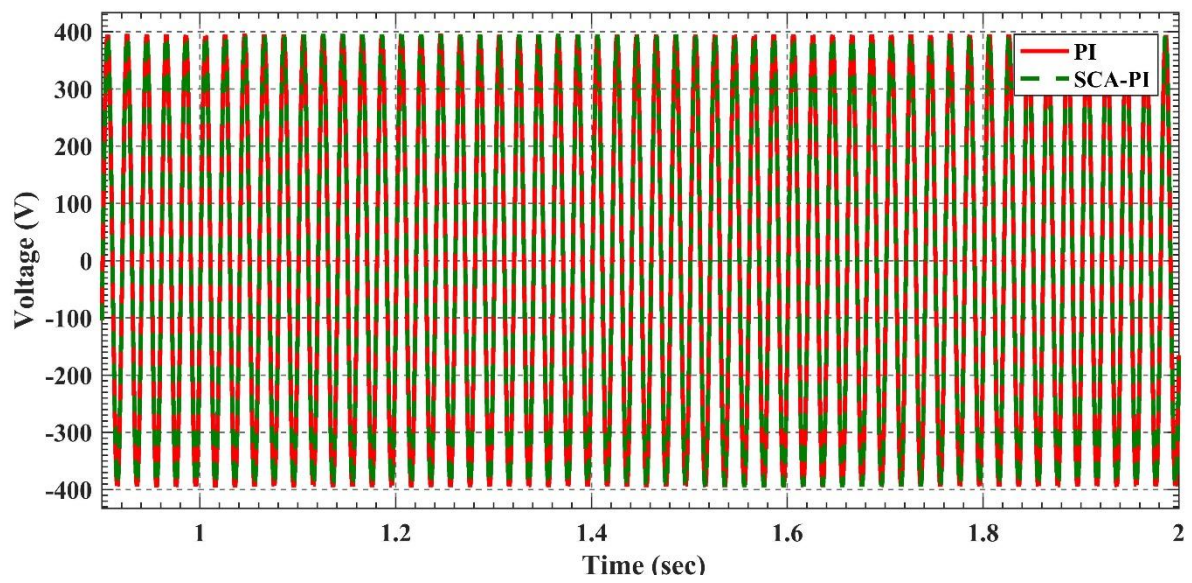


**Figure 4-10 System Frequency Response During Increased Loads.**

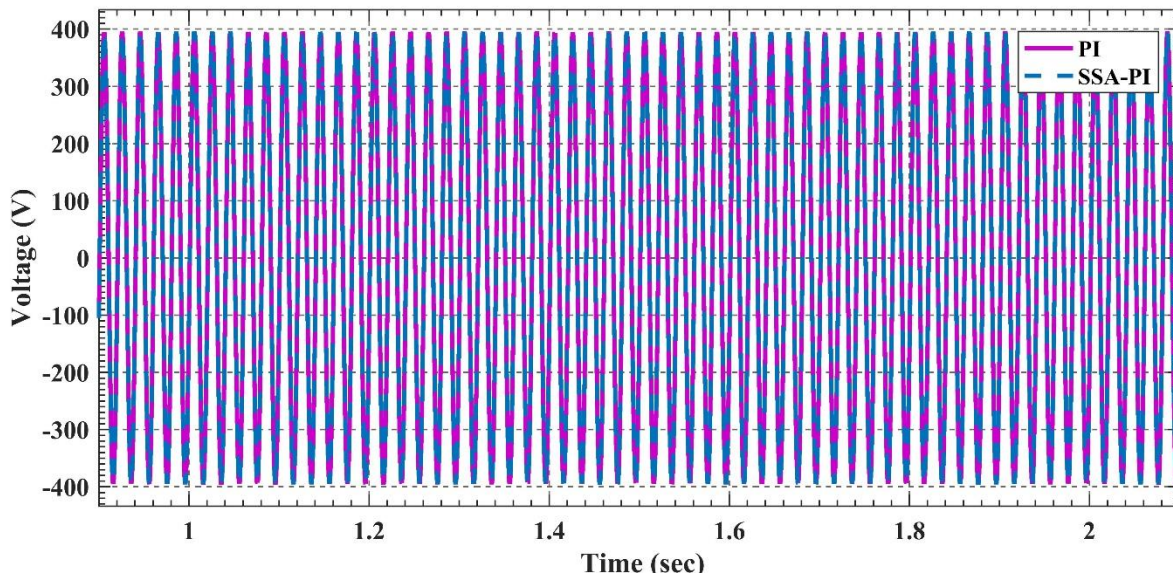
In this scenario and from Figure (4-11a,b,c), voltage waveforms can also be observed, and there is no significant difference between all methods, as the signals for systems are very similar, following the same waveform with minimal variation. When the first load is added at 1s, a slight disturbance in voltage may occur due to the sudden load increase. However, the voltage is not significantly affected, indicating that methods successfully maintain grid stability. When the second load is introduced at 2s, an additional voltage change is expected due to the sudden increase in loads. However, the voltage remains unaffected by this increase, demonstrating that the control system effectively balances the disturbance caused by load increments.



(a)



(b)



(c)

**Figure 4-11 System Voltage Response During Increase Loads.**

#### 4.2.4.2 Analysis of active power and reactive power

At the start of the system operation and before introducing the loads, the active power begins from zero and gradually increases with relative system stability, unaffected by new loads. When a load is introduced at time 1, it causes a rapid and noticeable increase in active power to meet the new energy demand. Oscillations appear at this stage due to the system's reaction to the newly introduced load. The system's performance varies depending on the control technique used in the studied microgrid system.

When analyzing control methods over specific time intervals, starting ( $t=0s$  -  $0.2s$ ), the PI-conventional controller method shows an initial response in active power but with a high overshoot, which is undesirable as it may lead to system instability. The system's response contains minor oscillations but is not ideal. In contrast, the SSA-PI method shows significant initial oscillations in active power, with a noticeable increase in overshoot compared to the PI-conventional controller. The system takes longer to stabilize the oscillations during this phase.

The SCA-PI method demonstrates performance similar to that of the SSA-PI method, with a high overshoot but relatively less oscillation and disturbance. However, its control speed is slightly slower than the SSA-PI method's.

On the other hand, the SMA-PI method significantly reduces the initial surge in active power and shows more stable behavior, even during the startup phase. It demonstrates strong control capabilities without imposing excessive load on the system. When analyzing the reactive power between 0s and 0.2s before the loads are introduced, the system in all techniques exhibits a fast initial response accompanied by high fluctuations as the control techniques attempt to manage them. The PI- Conventional Controller shows significant fluctuations. The SSA-PI demonstrates a faster response than other methods but suffers from a high peak in reactive power. The SCA-PI shows system behavior similar to the SSA-PI, with both techniques achieving a relatively fast and stable response compared to the PI-Conventional Controller. The SMA-PI shows relatively lower fluctuations but is less stable during this period.

In the time interval ( $t= 0.2s - 1s$ ), the PI- conventional controller system gradually reduces oscillations. However, achieving stability is relatively slow, with the active power value fluctuating around the reference value for longer. With the SSA-PI method, oscillations in active power remain present during this period but begin to decrease. However, the system's response is relatively unstable compared to other methods. Improvement occurs slowly for the SCA-PI method but shows fewer oscillations than the SSA-PI method.

In contrast, the SMA-PI method demonstrates the least amount of oscillation in active power and reaches a nearly stable value, indicating greater efficiency in managing the system. At time 1, when the load is introduced, all control techniques exhibit a sudden increase in active power, with each method showing a different response. The SMA-PI algorithm, in particular, is distinguished by its faster response compared to the other methods. Between 0.2s and 1s, the system shows an improvement in reactive power fluctuations compared to the PI-

Conventional Controller, approaching stability. The SMA-PI achieves the best balance among the methods during this period, with more stable reactive power and reduced oscillations. When the first load is introduced, all control techniques show an immediate response to this change, resulting in noticeable instability and clear oscillations in the reactive power with the PI-Conventional Controller. However, the SMA-PI and the SCA-PI show a more stable response, with better damping of reactive power oscillations. Among them, the SMA-PI demonstrates superior stability and faster responsiveness.

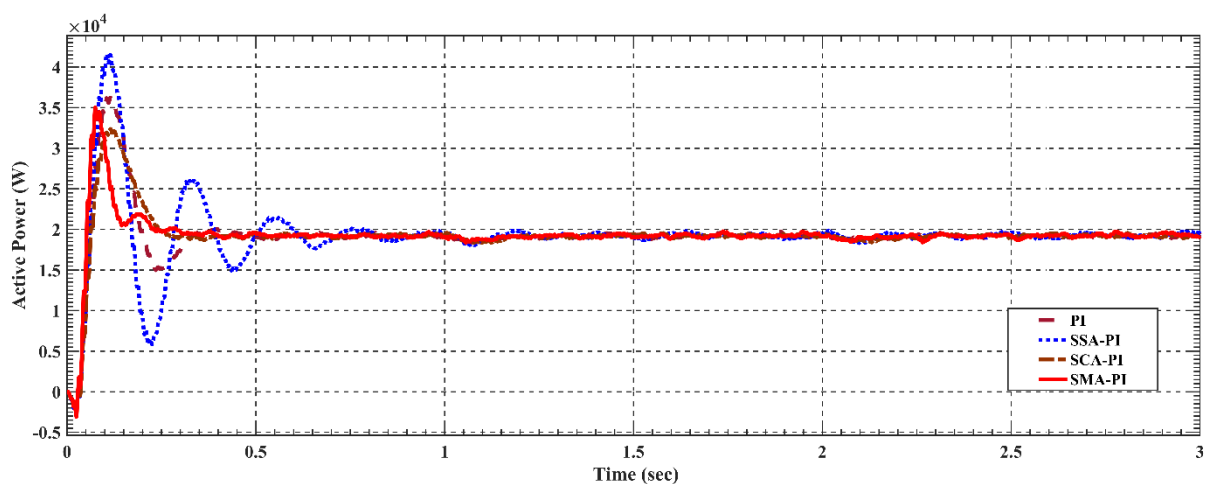
From the period ( $t=1s - 2s$ ), after the initial impact of the load at point 1s, the system begins to restore the stability of active power. It is observed that the system experiences oscillations for a relatively longer period before reaching a state of relative stability. Using the SSA-PI method, the active power continues to oscillate with larger values compared to other techniques. In contrast, with the SCA-PI method, the system's performance improves compared to the SSA-PI; however, the damping speed is slower than that of the SMA-PI method. The SMA-PI method demonstrates rapid restoration of active power with minimal oscillations, making it the most efficient among the methods.

At the priode ( $t= 2s$ ) , the second load is introduced, increasing active power and causing oscillations similar to those observed when the first load was introduced. The control techniques respond differently: With the PI-Conventional Controller, the active power exhibits slow oscillations with delayed damping. The SSA-PI method shows clear instability with large oscillations. The SCA-PI method results in relatively fewer oscillations than the SSA-PI but remains slower than the SMA-PI method. The SMA-PI method demonstrates a quick response and effective damping of oscillations. At time 2s, with the introduction of the second load, a change occurs in the reactive power, leading to an immediate response accompanied by fluctuations. The PI-Conventional Controller struggles to manage the system, showing difficulty in control and prolonged oscillations before beginning to stabilize. The SSA-PI shows some residual oscillations in

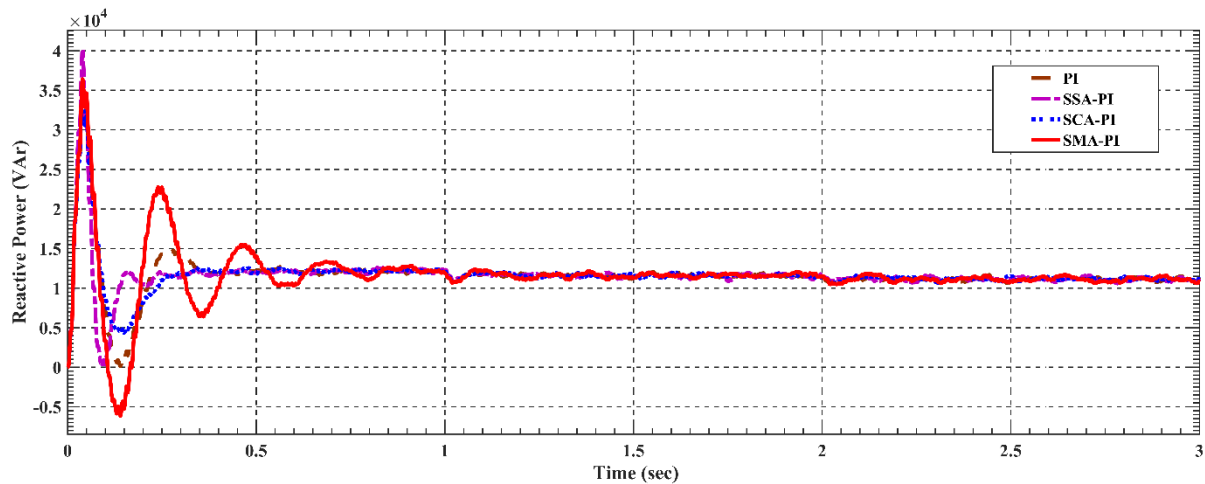
reactive power but eventually stabilizes. The SMA-PI and the SCA-PI demonstrate better stability with minimal oscillations during this period, making them the most effective in maintaining system stability.

After 2.5s, all control techniques stabilize the active and reactive power, with variations in the speed and degree of stability among the methods. The SMA-PI demonstrates higher efficiency and faster stability achievement. The SCA-PI performs moderately, while the SSA-PI and the PI-Conventional Controller take longer to stabilize and exhibit more significant oscillations.

In this scenario, regarding load sharing and power distribution, the grid shares power according to the specified power ratio (30kw, 40kw) of the total load at the time of load addition. As a result, the power supplied by the network to other loads in the studied network system is reduced. It is worth noting that the power consumed by the load always equals the sum of the power supplied by the main grid and the power provided by the microgrid. Analyzing the impact of these control techniques on load sharing and power distribution reveals that the SMA-PI demonstrates a balanced dynamic response, leading to effective load and power distribution compared to other methods.



(a)



(b)

**Figure 4-12 (a) Analysis Active Power (b) Analysis Reactive Power During Increase loads**

**Table 4.3 Optimization of objective functions in different modes for error percentage**

Mode	Methods	ITAE	ITSE	IAE	ISE
Transition	Conventional -PI	0.1312	0.3012	0.06597	2.481
	SSA-PI	0.1374	0.3389	0.07227	2.515
	SCA -PI	0.1286	0.2675	0.06305	2.478
	SMA-PI	0.1259	0.2627	0.06257	2.457
Islanded	Conventional -PI	0.1228	0.2647	0.06282	2.045
	SSA-PI	0.1281	0.288	0.06862	2.07
	SCA -PI	0.1253	0.2517	0.06067	2.03
	SMA-PI	0.1208	0.2571	0.06086	2.027
Load change (equal load)	Conventional -PI	0.1259	0.2775	0.063	2.01
	SSA-PI	0.1305	0.3081	0.06773	2.033
	SCA -PI	0.1273	0.2787	0.06207	2.008
	SMA-PI	0.1286	0.2782	0.06221	2.033
Load change (increase load)	Conventional -PI	0.1276	0.2925	0.06391	2.052
	SSA-PI	0.1271	0.2873	0.06879	2.079
	SCA -PI	0.1234	0.2731	0.06166	2.052
	SMA-PI	0.1208	0.2334	0.0598	2.031

This table shows the error values obtained from the techniques used under the studied conditions. SMA has a slightly lower integral time absolute error (ITAE) and consistently outperforms other methods in all cases. However, the SCA Method is better by 0.1273% in scenarios of equal load loads. The IAE, ISE, and ITAE show varying performance levels across the different methods.

## Summary

**Table 4-4 Evaluation of Control Methods for Frequency and Voltage Stability in Microgrids**

Factor	Conventional PI	SSA-PI	SCA-PI	SMA-PI (Best)
Frequency Stability	Moderate - noticeable oscillations	Weak - high oscillations	Good - less oscillation than SSA	Excellent - least oscillations and fastest stabilization
Frequency Overshoot	High	High	Moderate	Very low
Settling Time	Long	Long	Moderate	Fastest stabilization
Voltage Stability	Moderate - some oscillations	Weak - clear fluctuations	Good - reduced oscillations	Excellent - more stable voltage
Active Power Regulation	Unbalanced - weak distribution	Unstable - high overshoot	Relatively stable - some fluctuations	Excellent - smooth response and fast stabilization
Reactive Power Regulation	Continuous oscillations	High fluctuations	Less oscillations	Least oscillations - best stability
Adaptability to Load Changes	Slow and weak response	Weak response with oscillations	Good response	Fastest response and least oscillations
Load Sharing Efficiency	Weak - unbalanced distribution	Unstable - uneven loading	Good - some improvements	Excellent - balanced power distribution

**CHAPTER FIVE:  
CONCLUSION AND  
RECOMMENDATIONS**

## CHAPTER Five:

### **Conclusion & Recommendations**

#### **5.1. Conclusion**

Droop control is an effective method that can be used to control the power and voltage of parallel electric power circuits. This study developed a droop control system structure based on Proportional Control (PI), a metaheuristic optimization technique based on proportional integral controller optimization techniques designed to improve a conventional droop control system for a microgrid. The algorithms can effectively generate droop performance and provide droop characteristic robustness analysis. The limitations of the conventional droop control have been explained. Three different technologies, Slime Mould Algorithm (SMA), Sine Cosine Algorithm (SCA), and Sparrow Search Algorithm (SSA), are used to tune the PI droop control gain. The droop control system of each power inverter in the microgrid was connected by using this algorithm. A microgrid simulation test system is included to validate the relative merits of the selected controllers. In this thesis, five chapters were presented. The first chapter provided an overview of microgrids, including their types, operating modes, control methods, and ways to enhance their performance and stability. It also discussed the importance and objectives of this study and reviewed relevant literature review. The second chapter explained the model and its design process, while the third chapter detailed droop control and the methods used in the study. In the fourth chapter, the results obtained from simulating different operating conditions were presented, including mode-switching simulations. Finally, the fifth chapter included the conclusion, recommendations, and references.

The studied droop controller performs frequency regulation following bus voltage regulation in the topology of the droop control strategy. Relevant data are presented in four case studies: island mode, transition of the operation mode,

load change (increase load), and load change (equal load). When the grid-connected mode is switched to the inverter control, the control performance is important for both mode switching and avoiding voltage and frequency overshoot. Droop parameter setting can adjust the percentage of load sharing between DGs and minimize steady-state errors. In this case, we observe from the results that the SMA-PI method outperforms the other methods in terms of the objective functions studied. For example, the overshoot reached 0.2247%, compared to 0.2325% for the SCA-PI method, 0.3151% for the SSA-PI method, and 0.2352% for the PI-conventional Controller method. Similarly, the system's settling time is improved drastically with the variable droop gain technique while keeping the frequency deviation nearly the same, and the rise time was 0.3958%, indicating that it is the best method in terms of stability and speed of response to changes. The error value was (0.1259,0.2627,0.06257,2.457) %, reflecting its superiority over the SCA-PI, the PI-Conventional Controller, and the SSA-PI methods. We observe this superiority of the SMA-PI method in all cases regarding the overshoot ratio. However, in the case where the load is equal, the positional function for the integral time absolute error (ITAE) and integral absolute error (IAE) using the SCA-PI method is better than the other methods, reaching 0.12735% and 0.06207%, respectively. As for load sharing and power sharing, In the islanded mode of a microgrid, distributed generators must operate together to meet the load demand. Control strategies directly affect how these sources share the load, as poor control can lead to uneven load distribution, causing some units to become overloaded. Effective strategies ensure proportional load sharing, where each source contributes based on capacity, improving system efficiency and reliability. When the distributed loads are equal in value, the burden is shared fairly among the sources in a scenario with equal load. This reduces stress on any individual source. In the scenario of increased load, regarding load sharing and power distribution, the grid shares power dependent on the specified power ratio (30kw, 40kw) of the

total load at the time of load addition. As a result, the power delivered by the network to other loads in the studied network system is reduced.

The limitations of this study include the following: The metaheuristic approach used to optimize the droop control parameters requires more computational effort and is time-consuming. It can also require more data and training and may be less reliable if implemented without proper modification.

## **5.2. Recommendations**

This study suggests control of microgrid systems and parameters optimizing with metaheuristic optimization algorithms. However, future research directions would be as follows:

- 1- The interface circuit should be developed with higher reliability. It will enhance efficiency and maintain better continuity of service for microgrid systems.
- 2- In future works, the developed Droop Control Algorithm parameters should be optimized using different optimization techniques based on PID control parameters instead of PI control parameters.
- 3- Comparison can be performed for the Droop Control Algorithm against metaheuristic algorithms with varying points of starting or delta values to determine the influence of these terms on system performance.
- 4- Different applications can be handled using the designed Microgrid Simulator System, and the setup for the developed project can be implemented commercially and should be used for commercial research projects.
- 5- Additionally, the real microgrid system can be enhanced by adding energy storage units and renewable energies, and the proposed algorithm can be validated under real conditions.

- 6- In future work, different methods will be used to check the accuracy of the methods, and more focus will be given to the optimization of the coefficient droop control.

---

---

## REFERENCE

- [1] M. Z. Kreishan and A. F. Zobaa, "Optimal allocation and operation of droop-controlled islanded microgrids: A review," *Energies*, vol.14, no.15,2021,doi: 10.3390/en14154653.
- [2] S. D. Al-Majidi, H. D. S. Altai, M. H. Lazim, M. K. Al-Nussairi, M. F. Abbod, and H. S. Al-Raweshidy, "Bacterial Foraging Algorithm for a Neural Network Learning Improvement in an Automatic Generation Controller," *Energies*, vol. 16, no. 6. 2023. doi: 10.3390/en16062802.
- [3] S. G. Ndeh, B. J. Ebot, A. F. Akawung, N. D. Khan, and T. Emmanuel, "Decentralized Droop Control Strategies for Parallel-Connected Distributed Generators in an AC Islanded Microgrid: A Review," *2023 7th Int. Conf. Green Energy Appl. ICGEA 2023*, pp. 83–90, 2023, doi: 10.1109/ICGEA57077.2023.10126012.
- [4] H. Han, Y. Liu, Y. Sun, M. Su, and J. M. Guerrero, "An improved droop control strategy for reactive power sharing in islanded microgrid," *IEEE Trans. Power Electron.*, vol. 30, no. 6, pp. 3133–3141, 2015, doi: 10.1109/TPEL.2014.2332181.
- [5] I. Colak, R. Bayindir, M. Al-Nussairi, and E. Hossain, "Voltage and frequency stability analysis of AC microgrid," *INTELEC, Int. Telecommun. Energy Conf.*, vol. 2016-Septe, 2016, doi: 10.1109/INTLEC.2015.7572471.
- [6] A. J. Mohammed, S. D. Al-Majidi, M. K. Al-Nussairi, M. F. Abbod, H. S. Al-Raweshidy, "Design of a Load Frequency Controller based on Artificial Neural Network for Single-Area Power System." *IEEE,2022 57th International Universities Power Engineering Conference (UPEC), Istanbul, Turkey, 2022.* doi: 10.1109/UPEC55022.2022.9917853.
- [7] F. Agha Kassab, R. Rodriguez, B. Celik, F. Locment, and M. Sechilariu, "A Comprehensive Review of Sizing and Energy Management Strategies for Optimal Planning of Microgrids with PV and Other Renewable Integration," *Appl. Sci.*, vol. 14, no. 22, 2024, doi: 10.3390/app142210479.
- [8] E. Planas, A. Gil-De-Muro, J. Andreu, I. Kortabarria, and I. Martínez De Alegría, "General aspects, hierarchical controls and droop methods in microgrids: A review," *Renew. Sustain. Energy Rev.*, vol.17, pp.147–159,2013,doi: 10.1016/j.rser.2012.09.032.
- [9] W. Issa, S. Sharkh, and M. Abusara, "A review of recent control techniques of drooped inverter-based AC microgrids," *Energy Sci. Eng.*, vol. 12, no. 4, pp. 1792–1814, 2024, doi: 10.1002/ese3.1670.
- [10] E. Hernández-Mayoral *et al.*, "A Comprehensive Review on Power-Quality Issues, Optimization Techniques, and Control Strategies of Microgrid Based on Renewable Energy Sources," *Sustain.*, vol. 15, no. 12, 2023, doi: 10.3390/su15129847.
- [11] K. B. Syariah and G. Ilmu, *Power Electronics Drives, and Advanced Application*, 1<sup>st</sup> Edition, 27March 2020, Boca Raton, no. september 2016, p.790, doi:https://doi.org/10.1201/9781315161662.
- [12] S. M. Hosseinimoghadam, Seyed Mohammad Sadegh; Roghanian, Hamzeh; Dashtdar, Masoud; Razavi, "Size Optimization of Distributed Generation Resources in Microgrid

- 
- 
- Based on Scenario tree.” 8th IEEE International Conference on Smart Grid, Paris, FRANCE, pp. 67–72, 2020.
- [13] S. Sarwar, D. Kirli, M. M. C. Merlin, and A. E. Kiprakis, “Major Challenges towards Energy Management and Power Sharing in a Hybrid AC/DC Microgrid: A Review,” *Energies*, vol. 15, no. 23, 2022, doi: 10.3390/en15238851.
- [14] M. A. Hossain, H. R. Pota, M. J. Hossain, and F. Blaabjerg, “Evolution of microgrids with converter-interfaced generations: Challenges and opportunities,” *Int. J. Electr. Power Energy Syst.*, vol. 109, no. January, pp. 160–186, 2019, doi: 10.1016/j.ijepes.2019.01.038.
- [15] I. Y. Chung, W. Liu, D. A. Cartes, and K. Schoder, “Control parameter optimization for a microgrid system using particle swarm optimization,” *2008 IEEE Int. Conf. Sustain. Energy Technol. ICSET 2008*, pp. 837–842, 2008, doi: 10.1109/ICSET.2008.4747124.
- [16] M. Shirkhani *et al.*, “A review on microgrid decentralized energy/voltage control structures and methods,” *Energy Reports*, vol. 10, pp. 368–380, 2023, doi: 10.1016/j.egyr.2023.06.022.
- [17] R. Rajan, F. M. Fernandez, and Y. Yang, “Primary frequency control techniques for large-scale PV-integrated power systems: A review,” *Renew. Sustain. Energy Rev.*, vol. 144, no. March, p. 110998, 2021, doi: 10.1016/j.rser.2021.110998.
- [18] H. Han, X. Hou, J. Yang, J. Wu, M. Su, and J. M. Guerrero, “Review of power sharing control strategies for islanding operation of AC microgrids,” *IEEE Trans. Smart Grid*, vol. 7, no. 1, pp. 200–215, 2016, doi: 10.1109/TSG.2015.2434849.
- [19] P. Unruh, M. Nuschke, P. Strauß, and F. Welck, “Overview on grid-forming inverter control methods,” *Energies*, vol. 13, no. 10, 2020, doi: 10.3390/en13102589.
- [20] S. Ferahtia, A. Djerioui, H. Rezk, A. Chouder, A. Houari, M. Machmoum, “Adaptive Droop based Control Strategy for DC Microgrid Including Multiple Batteries Energy Storage Systems,” *Energy Storage*, vol. 48, p. 103983, 2022.
- [21] K. Twaisan and N. Bar, “Integrated Distributed Energy Resources (DER) and Microgrids: Modeling and Optimization of DERs,” *Electron.*, vol. 11, no. 18, 2022, doi: 10.3390/electronics11182816.
- [22] J. Schiffer, R. Ortega, A. Astolfi, J. Raisch, and T. Sezi, “Conditions for stability of droop-controlled inverter-based microgrids,” *Automatica*, vol. 50, no. 10, pp. 2457–2469, 2014, doi: 10.1016/j.automatica.2014.08.009.
- [23] S. Arunima and B. Subudhi, “Distributed Control for Accurate Voltage/Frequency Regulation and Power Sharing in a Microgrid,” *5th Int. Conf. Energy, Power, Environ. Towar. Flex. Green Energy Technol. ICEPE 2023*, pp. 0–5, 2023, doi: 10.1109/ICEPE57949.2023.10201542.
- [24] W. Yuan, Y. Wang, D. Liu, and F. Deng, “Adaptive droop control strategy of autonomous microgrid for efficiency improvement,” *PEDG 2019 - 2019 IEEE 10th Int. Symp. Power Electron. Distrib. Gener. Syst.*, pp. 972–977, 2019, doi: 10.1109/PEDG.2019.8807589.

- 
- [25] S. Sinha, S. Ghosh, and P. Bajpai, "Power sharing through interlinking converters in adaptive droop controlled multiple microgrid system," *Int. J. Electr. Power Energy Syst.*, vol. 128, no. March 2020, p. 106649, 2021, doi: 10.1016/j.ijepes.2020.106649.
- [26] M. H. Marzebali, M. Mazidi, and M. Mohiti, "An adaptive droop-based control strategy for fuel cell-battery hybrid energy storage system to support primary frequency in stand-alone microgrids," *J. Energy Storage*, vol. 27, no. September 2019, p. 101127, 2020, doi: 10.1016/j.est.2019.101127.
- [27] M. Ghazzali, M. Haloua, and F. Giri, "Modeling and Adaptive Control and Power Sharing in Islanded AC Microgrids," *Int. J. Control. Autom. Syst.*, vol. 18, no. 5, pp. 1229–1241, 2020, doi: 10.1007/s12555-019-0222-2.
- [28] G. B. Alexandre and G. S. Belém, "Adaptive Droop control for voltage and frequency regulation in isolated microgrids," *Rev. Principia - Divulg. Científica e Tecnológica do IFPB*, vol. 1, no. 53, p. 150, 2021, doi: 10.18265/1517-0306a2020v1n53p150-165.
- [29] S. Abdalfatah, E. E. El-kholy, and H. Awad, "Power-Sharing in Microgrids by Adaptive Virtual Impedance and Fuzzy Logic," *Eng. Res. J.*, vol. 179, no. 0, pp. 68–74, 2023, doi: 10.21608/erj.2023.315739.
- [30] Z. Peng, J. Wang, Y. Wen, D. Bi, Y. Dai, and Y. Ning, "Virtual synchronous generator control strategy incorporating improved governor control and coupling compensation for AC microgrid," *IET Power Electron.*, vol. 12, no. 6, pp. 1455–1461, 2019, doi: 10.1049/iet-pel.2018.6167.
- [31] A. M. Abouassy, D. E. A. Mansour, and T. F. Megahed, "Accurate Power Sharing in Islanded AC Microgrid Using A Virtual Complex Impedance," *Renew. Energy Power Qual. J.*, vol. 21, no. May, pp. 91–96, 2023, doi: 10.24084/repqj21.230.
- [32] M. D. Pham and H. H. Lee, "Effective Coordinated Virtual Impedance Control for Accurate Power Sharing in Islanded Microgrid," *IEEE Trans. Ind. Electron.*, vol. 68, no. 3, pp. 2279–2288, 2021, doi: 10.1109/TIE.2020.2972441.
- [33] F. Gothner, R. E. Torres-Olguin, J. Roldan-Perez, A. Rygg, and O. M. Midtgard, "Apparent Impedance-Based Adaptive Controller for Improved Stability of a Droop-Controlled Microgrid," *IEEE Trans. Power Electron.*, vol. 36, no. 8, pp. 9465–9476, 2021, doi: 10.1109/TPEL.2021.3050615.
- [34] A. Arabpour and H. Hojabri, "An improved centralized/decentralized accurate reactive power sharing method in AC microgrids," *Int. J. Electr. Power Energy Syst.*, vol. 148, no. November 2022, p. 108908, 2023, doi: 10.1016/j.ijepes.2022.108908.
- [35] H. Lai, K. Xiong, Z. Zhang, and Z. Chen, "Droop control strategy for microgrid inverters: A deep reinforcement learning enhanced approach," *Energy Reports*, vol. 9, pp. 567–575, 2023, doi: 10.1016/j.egyr.2023.04.263.
- [36] S. Kanwal, M. Q. Rauf, B. Khan, and G. Mokryani, "Artificial neural network assisted robust droop control of autonomous microgrid," *IET Renew. Power Gener.*, 2023, doi: 10.1049/rpg2.12739.
- [37] X. Ding, R. Yao, X. Zhai, C. Li, and H. Dong, "An adaptive compensation droop control strategy for reactive power sharing in islanded microgrid," *Electr. Eng.*, vol. 102, no. 1,

- 
- 
- pp. 267–278, 2020, doi: 10.1007/s00202-019-00870-1.
- [38] M. Alzayed, M. Lemaire, S. Zarrabian, H. Chaoui, and D. Massicotte, “Droop-Controlled Bidirectional Inverter-Based Microgrid Using Cascade-Forward Neural Networks,” *IEEE Open J. Circuits Syst.*, vol. 3, no. July, pp. 298–308, 2022, doi: 10.1109/ojcas.2022.3206120.
- [39] F. Habibi, Q. Shafiee, and H. Bevrani, “Online generalized droop-based demand response for frequency control in islanded microgrids,” *Electr. Eng.*, vol. 101, no. 2, pp. 409–420, 2019, doi: 10.1007/s00202-019-00791-z.
- [40] S. A. Shezan *et al.*, “Optimization and control of solar-wind islanded hybrid microgrid by using heuristic and deterministic optimization algorithms and fuzzy logic controller,” *Energy Reports*, vol. 10, no. October, pp. 3272–3288, 2023, doi: 10.1016/j.egy.2023.10.016.
- [41] M. S. O. Yeganeh, A. Oshnoei, N. Mijatovic, T. Dragicevic, and F. Blaabjerg, “Intelligent Secondary Control of Islanded AC Microgrids: A Brain Emotional Learning-Based Approach,” *IEEE Trans. Ind. Electron.*, vol. 70, no. 7, pp. 6711–6723, 2023, doi: 10.1109/TIE.2022.3203677.
- [42] M. Srikanth and Y. Venkata Pavan Kumar, “A State Machine-Based Droop Control Method Aided with Droop Coefficients Tuning through In-Feasible Range Detection for Improved Transient Performance of Microgrids,” *Symmetry (Basel)*, vol. 15, no. 1, 2023, doi: 10.3390/sym15010001.
- [43] T. A. Jumani, M. W. Mustafa, M. M. Rasid, N. H. Mirjat, Z. H. Leghari, and M. Salman Saeed, “Optimal voltage and frequency control of an islanded microgrid using grasshopper optimization algorithm,” *Energies*, vol. 11, no. 11, 2018, doi: 10.3390/en11113191.
- [44] M. Sedighizadeh, M. Esmaili, and A. Eisapour-Moarref, “Voltage and frequency regulation in autonomous microgrids using Hybrid Big Bang-Big Crunch algorithm,” *Appl. Soft Comput. J.*, vol. 52, pp. 176–189, 2017, doi: 10.1016/j.asoc.2016.12.031.
- [45] J. Naik, P. K. Dash, and R. Bisoi, “Optimized droop controller based energy management for stand-alone micro-grid using hybrid monarch butterfly and sine-cosine algorithm,” *Sustain. Energy Technol. Assessments*, vol. 46, no. May, p. 101310, 2021, doi: 10.1016/j.seta.2021.101310.
- [46] A. Maulik and D. Das, “Optimal Operation of Droop-Controlled Islanded Microgrids,” *IEEE Trans. Sustain. Energy*, vol. 9, no. 3, pp. 1337–1348, 2018, doi: 10.1109/TSTE.2017.2783356.
- [47] M. A. Ebrahim, R. M. A. Fattah, E. M. Mohamed Saied, S. Mohamed Abdel Maksoud, and H. El Khashab, “Real-time implementation of self-adaptive salp swarm optimization-based microgrid droop control,” *IEEE Access*, vol. 8, pp. 185738–185751, 2020, doi: 10.1109/ACCESS.2020.3030160.
- [48] M. A. Djema and M. Boudour, “Load Frequency Control Enhancement for an Islanded Multi-Area AC MicroGrid,” *2022 IEEE Int. Conf. Electr. Sci. Technol. Maghreb, Cist. 2022*, pp. 1–6, 2022, doi: 10.1109/CISTEM55808.2022.10044017.

- 
- 
- [49] L. Zhang, H. Zheng, Q. Hu, B. Su, and L. Lyu, "An Adaptive Droop Control Strategy for Islanded Microgrid Based on Improved Particle Swarm Optimization," *IEEE Access*, vol. 8, pp. 3579–3593, 2020, doi: 10.1109/ACCESS.2019.2960871.
- [50] W. Aribowo, H. Suryoatmojo, and F. A. Pamuji, "Optimalization Droop Control Based on Aquila Optimizer Algorithm For DC Microgrid," *2022 Int. Semin. Intell. Technol. Its Appl. Adv. Innov. Electr. Syst. Humanit. ISITIA 2022 - Proceeding*, pp. 460–465, 2022, doi: 10.1109/ISITIA56226.2022.9855330.
- [51] K. Yu, Q. Ai, S. Wang, J. Ni, and T. Lv, "Analysis and Optimization of Droop Controller for Microgrid System Based on Small-Signal Dynamic Model," *IEEE Trans. Smart Grid*, vol. 7, no. 2, pp. 695–705, 2016, doi: 10.1109/TSG.2015.2501316.
- [52] R. B. C. A. G. R. M. G. L. S. M. F. Z. Majumder, "Improvement of Stability and Load Sharing in an Autonomous Microgrid Using Supplementary Droop Control Loop," *IEEE Trans. POWER Syst.*, vol. 25, no. 1, pp. 796–808, 2010, doi: 10.14233/ajchem.2015.17888.
- [53] M. Goyal and A. Ghosh, "Microgrids interconnection to support mutually during any contingency," *Sustain. Energy, Grids Networks*, vol. 6, pp. 100–108, 2016, doi: 10.1016/j.segan.2016.02.006.
- [54] D. K. Dheer, Y. Gupta, and S. Doolla, "A Self-Adjusting Droop Control Strategy to Improve Reactive Power Sharing in Islanded Microgrid," *IEEE Trans. Sustain. Energy*, vol. 11, no. 3, pp. 1624–1635, 2020, doi: 10.1109/TSTE.2019.2933144.
- [55] M. Z. Khan, E. M. Ahmed, S. Habib, and Z. M. Ali, "Multi-objective Optimization Technique for Droop Controlled Distributed Generators in AC Islanded Microgrid," *Electr. Power Syst. Res.*, vol. 213, no. June, p. 108671, 2022, doi: 10.1016/j.epsr.2022.108671.
- [56] Y. Xia, M. Yu, P. Yang, Y. Peng, and W. Wei, "Generation-Storage Coordination for Islanded DC Microgrids Dominated by PV Generators," *IEEE Trans. Energy Convers.*, vol. 34, no. 1, pp. 130–138, 2019, doi: 10.1109/TEC.2018.2860247.
- [57] Q. Q. Zhang and R. J. Wai, "Distributed secondary control of islanded micro-grid based on adaptive fuzzy-neural-network-inherited total-sliding-mode control technique," *Int. J. Electr. Power Energy Syst.*, vol. 137, no. November 2021, p. 107792, 2022, doi: 10.1016/j.ijepes.2021.107792.
- [58] A. E. Moarref, M. Sedighizadeh, and M. Esmaili, "Multi-objective voltage and frequency regulation in autonomous microgrids using Pareto-based Big Bang-Big Crunch algorithm," *Control Eng. Pract.*, vol. 55, pp. 56–68, 2016, doi: 10.1016/j.conengprac.2016.06.011.
- [59] N. M. Dawoud, T. F. Megahed, and S. S. Kaddah, "Enhancing the performance of multi-microgrid with high penetration of renewable energy using modified droop control," *Electr. Power Syst. Res.*, vol. 201, no. February, p. 107538, 2021, doi: 10.1016/j.epsr.2021.107538.
- [60] M. E. T. Souza Junior and L. C. G. Freitas, "Power Electronics for Modern Sustainable Power Systems: Distributed Generation, Microgrids and Smart Grids—A Review," *Sustain.*, vol. 14, no. 6, 2022, doi: 10.3390/su14063597.

- 
- 
- [61] F. Blaabjerg, T. Dragicevic, and P. Davari, “Applications of power electronics,” *Electron.*, vol. 8, no. 4, 2019, doi: 10.3390/electronics8040465.
- [62] A. L. Bukar, C. W. Tan, and K. Y. Lau, “Optimal sizing of an autonomous photovoltaic/wind/battery/diesel generator microgrid using grasshopper optimization algorithm,” *Sol. Energy*, vol. 188, no. June, pp. 685–696, 2019, doi: 10.1016/j.solener.2019.06.050.
- [63] M. A. Hossain, H. R. Pota, W. Issa, and M. J. Hossain, “Overview of AC microgrid controls with inverter-interfaced generations,” *Energies*, vol. 10, no. 9, pp. 1–27, 2017, doi: 10.3390/en10091300.
- [64] E. Buraimoh, I. E. Davidson, and F. Martinez-Rodrigo, “Fault ride-through enhancement of grid supporting inverter-based microgrid using delayed signal cancellation algorithm secondary control,” *Energies*, vol. 12, no. 20, 2019, doi: 10.3390/en12203994.
- [65] R. Ortega, V. H. García, A. L. García-García, J. J. Rodríguez, V. Vásquez, and J. C. Sosa-Savedra, “Modeling and application of controllers for a photovoltaic inverter for operation in a microgrid,” *Sustain.*, vol. 13, no. 9, pp. 1–27, 2021, doi: 10.3390/su13095115.
- [66] S. Bacha, I. Munteanu, and A. I. Bratcu, *Introduction*, no. 9781447154778. 2014. doi: 10.1007/978-1-4471-5478-5\_1.
- [67] M. Systems, F. Mohammadi, G. Nazri, and M. Saif, “An Improved Droop-Based Control Strategy for,” no. 1, pp. 20–23, 2020.
- [68] A. M. Abouassy, D. E. A. Mansour, T. Asano, and T. F. Megahed, “Power Sharing Issues and Control Strategies in Islanded Microgrid: A Comparative Study,” *IEEE Conf. Power Electron. Renew. Energy, CPERE 2023*, 2023, doi: 10.1109/CPERE56564.2023.10119567.
- [69] M. H. Marzaki, M. Tajjudin, M. H. F. Rahiman, and R. Adnan, “Performance of FOPI with error filter based on controllers performance criterion (ISE, IAE and ITAE),” *2015 10th Asian Control Conf. Emerg. Control Tech. a Sustain. World, ASCC 2015*, pp. 5–10, 2015, doi: 10.1109/ASCC.2015.7244851.
- [70] A. Rashwan, A. Mikhaylov, T. Senjyu, M. Eslami, A. M. Hemeida, and D. S. M. Osheba, “Modified Droop Control for Microgrid Power-Sharing Stability Improvement,” *Sustain.*, vol. 15, no. 14, 2023, doi: 10.3390/su151411220.
- [71] R. M. Kareem, M. K. A.-Nussairi, R. Bayindir, “Analysis and Optimization of Droop Controller for Microgrid System based on Slime Mould Algorithm,” *Setubal, PORTUGAL: IEEE, 12th International Conference on Smart Grid (icSmartGrid)*, 2024, pp. 609–613. doi: 10.1109/icSmartGrid61824.2024.10578266.
- [72] S. Srivastava, G. Ravi, P. Tripathi, L. Roy, K. Sahay, S. Dongre, “Droop Control based Control technique and Advancements for Microgrid Stability- A Review,” in *2023 IEEE Renewable Energy and Sustainable E-Mobility Conference (RESEM)*, Bhopal, India: IEEE, 2023. doi: 10.1109/RESEM57584.2023.10236126.
- [73] U. B. Tayab, M. A. Bin Roslan, L. J. Hwai, and M. Kashif, “A review of droop control

- 
- 
- techniques for microgrid,” *Renew. Sustain. Energy Rev.*, vol. 76, no. March, pp. 717–727, 2017, doi: 10.1016/j.rser.2017.03.028.
- [74] P. Zafari, A. Zangeneh, M. Moradzadeh, A. Ghafouri, and M. A. Parazdeh, “Various Droop Control Strategies in Microgrids,” *Power Syst.*, pp. 527–554, 2020, doi: 10.1007/978-3-030-23723-3\_22.
- [75] B. K. Unnikrishnan, M. S. Johnson, and E. P. Cheriyan, “Small signal stability improvement of a microgrid by the optimised dynamic droop control method,” *IET Renew. Power Gener.*, vol. 14, no. 5, pp. 822–833, 2020, doi: 10.1049/iet-rpg.2019.0428.
- [76] E. Buraimoh, A. O. Aluko, O. E. Oni, and I. E. Davidson, “Decentralized Virtual Impedance-Conventional Droop Control for Power Sharing for Inverter-Based Distributed Energy Resources of a Microgrid,” *Energies*, vol. 15, no. 12, 2022, doi: 10.3390/en15124439.
- [77] A. Rashwan, “A Modified Adaptive Droop Control for Improved Load Sharing in Microgrids Considering DG Boundary Limits,” *Int. J. Appl. Energy Syst.*, vol. 6, no. 1, pp. 1–11, 2024, doi: 10.21608/ijaes.2023.215062.1018.
- [78] E. Rokrok and M. E. H. Golshan, “Adaptive voltage droop scheme for voltage source converters in an islanded multibus microgrid,” *IET Gener. Transm. Distrib.*, vol. 4, no. 5, pp. 562–578, 2010, doi: 10.1049/iet-gtd.2009.0146.
- [79] Z. Lyu, Q. Wei, Y. Zhang, J. Zhao, and E. Manla, “Adaptive virtual impedance droop control based on consensus control of reactive current,” *Energies*, vol. 11, no. 7, 2018, doi: 10.3390/en11071801.
- [80] X. Meng, J. Liu, and Z. Liu, “A Generalized Droop Control for Grid-Supporting Inverter Based on Comparison between Traditional Droop Control and Virtual Synchronous Generator Control,” *IEEE Trans. Power Electron.*, vol. 34, no. 6, pp. 5416–5438, 2019, doi: 10.1109/TPEL.2018.2868722.
- [81] T. Xu *et al.*, “Consensus active power sharing for islanded microgrids based on distributed angle droop control,” *IET Renew. Power Gener.*, vol. 15, no. 13, pp. 2826–2839, 2021, doi: 10.1049/rpg2.12210.
- [82] T. Xu, J. Zhou, H. Yang, P. Li, L. Yu, and X. Guo, “Consensus based distributed angle droop control for islands resynchronization,” *IEEE Power Energy Soc. Gen. Meet.*, vol. 2020-Augus, 2020, doi: 10.1109/PESGM41954.2020.9281421.
- [83] R. Majumder, A. Ghosh, G. Ledwich, and F. Zare, “Angle droop versus frequency droop in a voltage source converter based autonomous microgrid,” *2009 IEEE Power Energy Soc. Gen. Meet. PES '09*, 2009, doi: 10.1109/PES.2009.5275987.
- [84] M. S. Golsorkhi and D. D. C. Lu, “A control method for inverter-based islanded microgrids based on V-I droop characteristics,” *IEEE Trans. Power Deliv.*, vol. 30, no. 3, pp. 1196–1204, 2015, doi: 10.1109/TPWRD.2014.2357471.
- [85] T. A. Jumani, M. W. Mustafa, A. S. Alghamdi, M. M. Rasid, A. Alamgir, and A. B. Awan, “Swarm Intelligence-Based Optimization Techniques for Dynamic Response and Power Quality Enhancement of AC Microgrids: A Comprehensive Review,” *IEEE*

- 
- 
- Access*, vol. 8, pp. 75986–76001, 2020, doi: 10.1109/ACCESS.2020.2989133.
- [86] M. H. Nadimi-Shahraki, S. Taghian, and S. Mirjalili, “An improved grey wolf optimizer for solving engineering problems,” *Expert Syst. Appl.*, vol. 166, p. 113917, 2021, doi: 10.1016/j.eswa.2020.113917.
- [87] S. Li, H. Chen, M. Wang, A. A. Heidari, and S. Mirjalili, “Slime mould algorithm: A new method for stochastic optimization,” *Futur. Gener. Comput. Syst.*, vol. 111, pp. 300–323, 2020, doi: 10.1016/j.future.2020.03.055.
- [88] D. Wang, D. Tan, and L. Liu, “Particle swarm optimization algorithm: an overview,” *Soft Comput.*, vol. 22, no. 2, pp. 387–408, 2018, doi: 10.1007/s00500-016-2474-6.
- [89] S. Mirjalili, “SCA: A Sine Cosine Algorithm for solving optimization problems,” *Knowledge-Based Syst.*, vol. 96, pp. 120–133, 2016, doi: 10.1016/j.knosys.2015.12.022.
- [90] S. Ali, A. Bhargava, A. Saxena, and P. Kumar, “A Hybrid Marine Predator Sine Cosine Algorithm for Parameter Selection of Hybrid Active Power Filter,” *Mathematics*, vol. 11, no. 3, 2023, doi: 10.3390/math11030598.
- [91] L. Liu, H. Xu, B. Wang, and C. Ke, “Multi-Strategy Fusion of Sine Cosine and Arithmetic Hybrid Optimization Algorithm,” *Electron.*, vol. 12, no. 9, 2023, doi: 10.3390/electronics12091961.
- [92] A. B. Gabis, Y. Meraihi, S. Mirjalili, and A. Ramdane-Cherif, *A comprehensive survey of sine cosine algorithm: variants and applications*, vol. 54, no. 7. Springer Netherlands, 2021. doi: 10.1007/s10462-021-10026-y.
- [93] S. Mirjalili, “SCA: A Sine Cosine Algorithm for solving optimization problems,” *Knowledge-Based Syst.*, vol. 96, pp. 120–133, 2016, doi: 10.1016/j.knosys.2015.12.022.
- [94] J. Xue and B. Shen, “A novel swarm intelligence optimization approach: sparrow search algorithm,” *Syst. Sci. Control Eng.*, vol. 8, no. 1, pp. 22–34, 2020, doi: 10.1080/21642583.2019.1708830.
- [95] C. Ouyang, D. Zhu, and F. Wang, “A Learning Sparrow Search Algorithm,” *Comput. Intell. Neurosci.*, vol. 2021, 2021, doi: 10.1155/2021/3946958.
- [96] Z. Wang, J. Wang, D. Li, and D. Zhu, “A Multi-Strategy Sparrow Search Algorithm with Selective Ensemble,” *Electron.*, vol. 12, no. 11, 2023, doi: 10.3390/electronics12112505.
- [97] M. A. Awadallah, M. A. Al-Betar, I. A. Doush, S. N. Makhadmeh, and G. Al-Naymat, “Recent Versions and Applications of Sparrow Search Algorithm,” *Arch. Comput. Methods Eng.*, vol. 30, no. 5, pp. 2831–2858, 2023, doi: 10.1007/s11831-023-09887-z.



## الخلاصة

الشبكة الصغيرة هو نظام طاقة صغير مع وحدة توليد الموزعة (DG). يعد التحكم في التردد والجهود مراحل التشغيل المستقلة عن الشبكة. إنها مشكلة صعبة ومهمة لتوفير الموثوقية والاستقرار. وبالتالي، فإن مشكلة التحكم في التشغيل هي مشكلة رئيسية في الشبكة الصغيرة التي يجب معالجتها أثناء التشغيل. ومع ذلك، فإن اختلافات التحميل وعمليات التبديل بين الوضع الجزري وأتصال الشبكة تسبب التردد والفولتية في الانحراف عن قيمها الاسمية وتؤدي إلى اضطرابات في الشبكة الصغيرة والسلوك الديناميكي، والتي تستدعي تطوير طريقة تحكم مثالية. من بين هذه الطرق، يعد التحكم في التبدلي طريقة شائعة بسبب عدم وجود روابط اتصال حرجة بين العاكس المرتبط المتوازي لتنظيم وحدات DG داخل الشبكة الصغيرة. لسوء الحظ، هذه الإستراتيجية ليست دقيقة في الحفاظ على تردد النظام والجهود بالقرب من قيمها الاسمية. نتيجة لذلك، يجب تحديد قيم المعلمة بعناية باستخدام تقنيات التحسين. يهدف هذا العمل إلى تحسين وحدة التحكم في التبدلي استناداً إلى معلمات تحكم PI المحسنة للتحكم في تردد وجهد الشبكات الصغيرة في ظل ظروف مختلفة باستخدام ثلاثة خوارزميات تحسين ميتايورستية فعالة، SMA, SCA, SSA أخيراً، لتقييم فعالية استراتيجيات التحكم المقترحة، تتم مقارنة نتائج الدراسة مع أساليب التحكم التقليدية للتحكم في التبدلي. أظهرت نتائج المحاكاة التفوق الكبير للطرق المقترحة، بما في ذلك SMA، من حيث استقرار التردد، والاستجابة للجهود، وتوازن مشاركة الحمل، والاختزال، والتحسين في وقت التسوية ووقت الارتفاع. علاوة على ذلك، أثبتت قدرتها على تقليل التذبذبات وتعزيز دقة الاستجابة بناءً على مقاييس الخطأ مثل الخطأ المطلق للوقت المتكامل (ITAE)، وخطأ مربع الوقت المتكامل (ITSE)، والخطأ المطلق المتكامل (IAE)، وخطأ مربع متكامل (ISE). أظهرت طريقة SMA تفوقها في جميع الحالات التي تم اختبارها ومحاكاتها، والتي تبين وقت ارتفاع أسرع للوصول إلى الاستقرار (0.3956s)، وأدنى تجاوز لاختراق (0.2247%)، ووقت تسوية (0.497060) عند التبديل بين أوضاع التشغيل في الشبكات الصغيرة.



جمهورية العراق  
وزارة التعليم العالي والبحث العلمي  
جامعة ميسان / كلية الهندسة  
قسم الهندسة الكهربائية



## تحكم التدلي في الشبكات الصغيرة لتحسين الكفاءة والاستقرار

رسالة مقدمة إلى كلية الهندسة في جامعة ميسان كجزء من متطلبات الحصول على شهادة الماجستير في علوم الهندسة الكهربائية / كهرباء عام

إعداد الطالبة

رقية مجيد كريم

بكالوريوس هندسة كهربائية 2021

بإشراف

الأستاذ المساعد الدكتور محمد خلف جمعة